MODELING THE EFFECTS OF THE IMMUNE SYSTEM ON BONE FRACTURE HEALING

by

IMELDA TREJO LORENZO

Presented to the Faculty of the Graduate School of
The University of Texas at Arlington in Partial Fulfillment
of the Requirements
for the Degree of

DOCTOR OF PHILOSOPHY

THE UNIVERSITY OF TEXAS AT ARLINGTON
May 2019

ACKNOWLEDGEMENTS

First, I would like to thank the Concejo Nacional de Ciencia y Tecnología (CONACyT) and The University of Texas at Arlington (UTA) for financially supporting my PhD graduate program. This program finishes with the elaboration and submission of the present dissertation manuscripts. I want also to thank the Consejo de Ciencia, Tecnología e Innovacíon de Hidalgo, the Universidad Autónoma del Estado de Hidalgo (Mathematics and Health and Medicine Deparments) and the Collegio de Bachilleres Plantel Tasquillo who provide the documentations needed for the CONACyT application and for paying my flight tickets to join the UTA graduate program.

Second, I would like to express my gratitude to my advisor Dr. Hristo Kojouharov for guiding me through the PhD program and helping me to prepare for life after the doctorate. His advice and encouragement helped me to excel in my academics and research work. I wish to thank Dr. Benito Chen, Dr. Marco Brotto, Dr. Guojun Liao and Dr. Gaik Ambartsoumian for their interest in my research and for taking time to serve in my comprehensive committee and dissertation committee. I also would like to thank Dr. Benito Chen and Dr. Christopher Kribs for their help and support in all my four year graduate program. I want to extend my appreciation to all my mentors: Dr. Francisco Javier Solís, Dr. Raúl Felipe, Dr. Rúben Martínez Avedaño, Dr. Margarita Tetlalmatzi Montiel, Dr. Jaime Cruz Sampedro, and Dr.

Alicia Prieto how have shaped my abilities to do mathematics and have encouraged me during all my academic studies.

Next, I would like to thank Lona, Michel, Velvet, Laura, and Shanna for their time and assistance throughout the graduate program. Furthermore, I want to express my great gratitude to all my UTA friends, they made my PhD graduate program the most exciting, enjoyable, and value ever: Mehtap Lafci, Mayowa Olawoyin, Sita Charkrit, May Trieu, Talon Johnson, Ariel Bowman, Mary Gockenbach, Kiran Mainali, Julio Enciso, Susana Aguirre-Medel, Paola Sotelo, Enrique Barragan, Miguel Arellano, Maria García, Emel Bolat, Felicia Puerto, and all my other friends.

Finally, I am extremely grateful to my parents, sister, brother, and all my family for their sacrifice, encouragement, and patience. Without their love and help, I would not have gone this far.

April 26, 2019

ABSTRACT

MODELING THE EFFECTS OF THE IMMUNE SYSTEM ON BONE FRACTURE HEALING

Imelda Trejo Lorenzo, Ph.D.

The University of Texas at Arlington, 2019

Supervising Professor: Hristo V. Kojouharov

Bone fracture healing is a complex biological process that results in a full reconstruction of the bone [36]. However, it is not always an easy and successful process. Indeed, in some unfavorable conditions, the bone fracture healing fails with approximately 10% of fractures resulting in nonunion [49]. Furthermore, the risk of nonunion healing increases with age, severe trauma, and immune deficiency [29, 55]. In addition, clinical consequences of fractures include surgical management, prolonged hospitalization, and rehabilitation resulting in high socioeconomic costs [31]. A better understanding of bone healing would enable to find optimal conditions for successful outcomes and to develop strategies for fracture treatments under normal or pathological scenarios.

Immune cells and their released molecular factors play a key role for successful bone healing [29, 47]. During bone fracture healing, the immune system cells clear up debris and regulate tissue cellular functions: proliferation, differentiation, and tissue production [47]. However, the exact mechanisms and functions of the immune cells present at the fracture site are still not completely understood [49]. Prolonged and

chronic participation of the immune cells during the inflammation phase results in delayed union or nonunion healing, while depletion of them results in delayed bone formation [29, 47, 49]. Therefore, for successful bone healing, the participation of immune cells in the healing process must be brief and well regulated [47, 49].

In this work, several new mathematical models are presented that describe the process of bone fracture healing. The models incorporate complex interactions between immune cells and bone cells at the fracture site. The resulting systems of nonlinear ordinary differential equations are studied analytically and numerically. Mathematical conditions for successful bone fracture repairs are formulated. The models are used to numerically monitor the evolution of broken bones for different types of fractures and to explore possible treatments that can accelerate the bone fracture healing process.

TABLE OF CONTENTS

CHAPTER 1

INTRODUCTION

Bone fracture healing is a complex biological process that results in a full reconstruction of the bone [36]. This process is given through a sequence of events that involves the participation of different cell types and is strongly regulated by several molecular factors and mechanical stimuli [5, 8, 41, 43, 47, 48]. This chapter, the biological background of long bone fracture repair is described with an emphasis on the immune system regulations during the healing process.

1.1 Bone Fracture Healing Phases

The bone fracture healing process can be described in three characteristic phases: inflammatory, repair, and remodelling. Figure 1.1 describes the time-line of events occurring in each phase. During inflammation, necroses of cells results in the delivery of pro-inflammatory cytokines which activate and attract inflammatory immune cells, such as neutrophils and monocytes, to the injury site [38, 49, 12]. In response to their phagocytic activities these cells magnify pro-inflammatory production, leading to an acute inflammation [9, 38, 19]. Subsequently, monocytes differentiate into macrophages to down-regulate the inflammation and resolve it. Once this differentiation begins, the influx of inflammatory cells ceases and they die out [50]. During the resolution of inflammation, macrophages increase their population by migration and activate to their classical and alternative phenotypes accordingly to the cytokines stimuli [48, 40]. Classically activated macrophages release a high concentration of pro-inflammatory cytokines, including the tumor necrotic factor-α (TNF-α), and low

levels of anti-inflammatory cytokines in response to their engulfing functions [25]. Alternatively activated macrophages secrete high levels of the interleukin-10 (IL-10), transforming growth factor-β (TGF-β), and low levels of TNF-α, as they continue with the clearance of debris and the modulation of inflammation [25]. The TNF-α, Il-10, and TGF-β stimulate the migration of mesenchymal stem cells (MSCs) to the injury site and promote the differentiation and proliferation of the tissue forming cells: MSCs, fibroblasts, chondrocytes, and osteoblasts [11]. The correct modulation among the TNF-α, Il-10, and the TGF-β is essential to stimulate and secure the healing of a broken bone.

During the repair phase, migrating MSCs contribute to the delivery of IL-10, and proliferate or differentiate into fibroblasts, chondrocytes, and osteoblasts, according to different molecular and mechanical stimuli [37, 11, 6, 24]. Particularly, specific growth factors, such as the bone morphogenetic proteins (BMPs) and the TGF-β, activate and direct the differentiation of MSCs into osteoblasts and chondrocytes [6, 2, 56]. Fibroblasts and chondrocytes proliferate and release the fibrinous/cartilagenous extracellular matrix, which fills up the fracture gap and provides stability on the fracture [2, 13, 43], while osteoblasts proliferate and deposit the new bone, also called woven bone [2]. Bone deposit results from the mineralized collagen and other proteins delivered by the osteoblasts [43]. After bone mineralization, osteoblasts remain on the bone surface or differentiate into osteocytes which become part of the bone extracellular matrix [12, 18].

During the last phase of the bone fracture healing process, the fibrocartilage and the woven bone are constantly removed and replaced by a functional bone [14]. This process is referred to as bone remodeling and consists of a systematic tissue degradation and production by osteoclasts and osteoblasts, respectively. Bone

remodeling is a slow process that can take months to years until the bone tissue recovers completely its functionality [35].

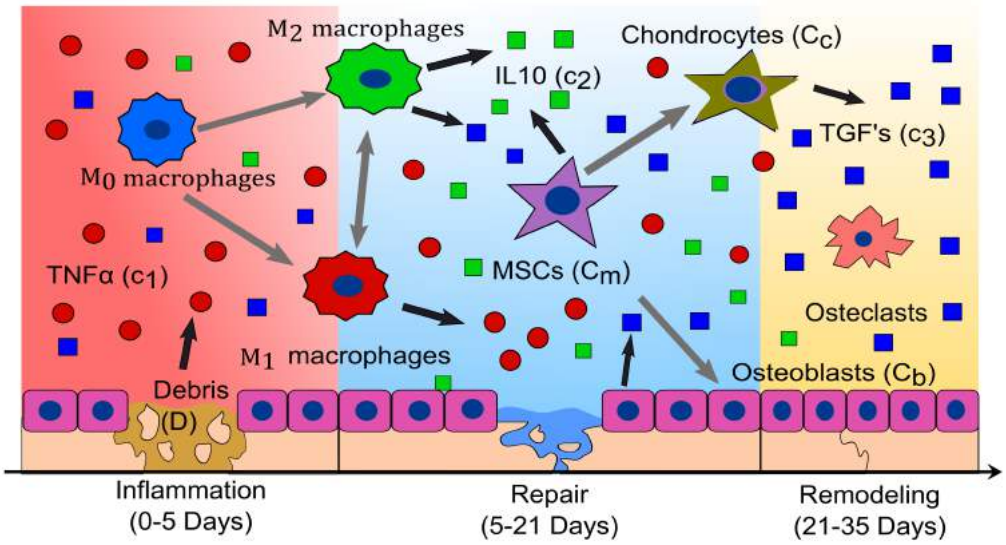

Figure 1.1. Inflammatory, repair, and remodeling phases of the bone fracture healing process. During the inflammatory phase, debris (D) activate the healing process by attracting macrophages M_0 to the injury site, which subsequently activate into their M_1 or M_2 phenotypes. Activated macrophages remove debris and secrete pro- and anti-inflammatory cytokines, such as the TNF-α (c_1) and the IL-10 (c_2), which regulate the inflammation and the cellular functions. During the repair phase, migrating mesenchymal stem cells (MSCs) up-regulate the IL-10 production, proliferate, and differentiate into osteoblasts (C_b) and chondrocytes (C_c). The MSCs differentiation is regulated by growth factors, such as the transforming growth factor-β (c_3). c_3 is synthesized by the M_2, C_b, and C_c. Chondrocyte and osteoblast cells synthesize the fibro/cartilage and woven bone, which closes the fracture gap. During the bone remodeling phase, osteoblasts and osteoclasts constantly remove and deposit new bone until the fracture is fully repaired.

1.1.1 Sequence of healing events

In a moderate fracture, acute inflammation is observed 24 hrs after the injury, which is also when TNF-α peaks, returning to its baseline levels within 72 hrs [35, 38].

Fibrinous/cartilaginous tissue production is observed in the first 3 days; it peaks in about 10 to 12 days, and its removal starts as early as 21 days [2]. The inflammation is considered resolved when debris is eliminated, activated macrophages emigrate to the lymphatic nods to die, and inactivated macrophages return to their normal density [50]. These events are observed two weeks after the beginning of the healing process [14, 15]. Approximately at 28 to 35 days, osteoclasts populate the injury site, and a substantial removal of the fibrocartilage is observed [14]. The fracture healing outcome is considered a delayed union if the fibrous/cartilaginous tissue is not removed completely in about 3 to 4 months after the injury, while it is considered a nonunion if no functional bone is obtained in 6 months after the trauma [22].

1.2 Immune System Responses after a Bone Fracture

The immune system consists of cellular and molecular components that work together to protect the body against infection. After a bone fracture, the immune system cells are the first lineage cells that activate the healing process [49]. Neutrophils, monocytes, and macrophages are the major contributor cells to the bone healing process as they engulf debris, regulate inflammation, and promote vascular and tissue formation through their secreted molecules profile [11, 48].

1.2.1 Immune system cells

Monocytes are precursor cells derived from the bone marrow. Monocytes circulate the body by moving into the bloodstream, and, after crossing the walls of capillaries, monocytes develop into macrophages [1, 54]. Neutrophils are the most common motile-type of phagocytes, short-lived cells that tend to attack bacteria [50]. Macrophages are resident tissue cells that, in response to injury, regulate inflammation and promote vascular and tissue formation [48]. Macrophages are

the most important immune cells present throughout all of the healing phases [47]. Macrophages are classified into classically and alternatively activated macrophages [48, 10, 43]. Classically activated macrophages release high levels of pro-inflammatory cytokines, including the TNF-α and the interleukin-1 (IL-1), which exhibit inhibitory and destructive properties in high concentrations [9, 48]. In contrast, alternatively activated macrophages are characterized with the secretion of the anti-inflammatory cytokines, such as the IL-10 and the TGF-β, which increase their phagocytic activities, mitigate the inflammatory responses, promote growth, and accelerate the fracture healing [48, 10, 31, 29]. Within the bone, macrophages are founded in the periousteum and endousteum [61]. Macrophages are also promising candidates for targets in immune-modulatory interventions [31, 48].

1.2.2 Regulatory molecules

The bone fracture healing process is strongly regulated by released molecular factors. These molecules can be categorized into two groups: cytokines and growth factors [11]. Cytokines work as chemotactic agents and mainly regulate the immune system responses, while growth factors promote proliferation and differentiation of the tissue forming cells [17].

1.2.2.1 Cytokines

Cytokines are proteins that mainly regulate the immune system cells [17]. They either have positive or negative effects on the cellular functions depending on the influence of other cytokines, concentration, and exposed time [5, 8, 41, 43]. Cytokines are functionally classified into pro-inflammatory and anti-inflammatory families.

Pro-inflammatory cytokines, such as the TNF-α, are mainly released by the inflammatory cells and activate the immune system defense to kill bacteria and fight

infections. Anti-inflammatory cytokines block the pro-inflammatory synthesis and activate the mesenchymal lineage cellular functions [29]. The IL-10 is one of the most potent anti-inflammatory molecules that inhibit the pro-inflammatory production [1, 29] and is mainly delivery by macrophages and MSCs [29].

The correct balance between the pro- and anti-inflammatory cytokines during fracture healing is necessary for successful fracture repair. High levels of TNF-α induce chronic inflammations, inhibits proliferation and differentiation of the tissue cells, and induces a gradual destruction of the cartilage and bone tissue [41]. However the absence of TNF-α results in nonunion or delayed nonunion [9, 38]. Furthermore, the TNF-α exhibits a dual effect on the MSCs, below to 15-20 ng/mL, it enhances MSCs' proliferation while, above of this concentration, inhibits MSCs' proliferation [4].

1.2.2.2 Growth factors

Growth factors are proteins that activate and promote cellular proliferation and differentiation [11]. The bone morphogenetic proteins (BMPs) and the TGF-β are the two major families that promote bone formation [6, 2, 56].

BMPs regulate growth of different cell types and potentially induce MSCs differentiation into chondrocytes and osteoblasts [11]. The main source of BMPs are MSCs, osteoblasts, and chondrocytes. TGF-β enhances proliferation of MSCs, chondrocytes, and osteoblasts. TGF-β also directs the MSCs differentiation into osteoblasts and chondrocytes [2]. Furthermore, TGF-β suppresses the pro-inflammatory cytokine productions [1] and is a potent chemotactic stimulator for MSCs and macrophages [11]. TGF-beta is released by the immune-system cells at the time of fracture and is synthesized by both osteoblasts and chondrocytes at specific times during the fracture healing process [2, 26].

1.3 Bone and Tissue Forming Cells

Bone fracture healing is given by a systematic tissue formation and degradation. Bellow, the functions of the most important bone cells involved in tissue formation are described.

1.3.1 Tissue forming cells

Mesenchymal stem cells (MSCs) are adult, nonhematopoietic, stem cells that have the ability to proliferate and differentiate into osteoblasts, chondrocytes, fibroblasts, and adipocytes, among other connective tissue, such as bone, cartilage, tendon, skeletal muscle, and adipose tissue, which makes them an attractive cell source for cell-based regenerative therapies [6, 58]. MSCs reside in specific environments located within the vicinity of vessel walls [58]. Within the bone tissue they are located in the perousteum, endosteum, and bone marrow [58, 61, 46].

Osteoblasts are derived from MSCs and are responsible for bone formation [12]. Osteoblasts have the ability to proliferate and differentiate into osteocytes [2]. They are located on the bone surface (osteon), where release collagen and other proteins which in a process of mineralization result in bone tissue [43]. After bone mineralization, osteoblasts remain on the bone surface or differentiate [12, 18].

Chondrocytes are derived from MSCs and synthesize cartilage. They have the ability to proliferate with a terminal stage. Fibroblasts secrete collagen fibers. Both fibroblasts and chondrocytes are residents of connective-cartilage tissue. During the bone fracture healing, chondrocytes and fibroblasts proliferate and secrete the fibro/cartilagenous tissue that supports bone formation [35, 13].

Osteoclasts remove bone by demineralizing it with acid and dissolving collagen with enzymes [12]. These cells originate from the bone marrow cells (from hematopoi-

etic precursor cells) similar to monocytes and machrophages. They are located on the bone surface.

1.3.2 Bone tissue types

Woven and lamellar bone are two types of bone tissue that differ in composition, organization, growth, and mechanical properties. Woven bone is quickly formed and poorly organized with a more or less random arrangement of collagen fibers and mineral crystals. Lamellar bone is slowly formed, organized in parallel layers or lamellae that make it stronger than woven bone [12]. During bone fracture healing, woven bone is firstly created and, then, through the bone remodeling process, is totally replaced by the lamellar bone [12, 14].

1.3.3 Bone tissue formation

There are two ways of bone tissue formation: intramembranous and endochondral ossification [12]. In intramembranous ossification, MSCs differentiate to osteoblasts which directly deposit bone [11]. In endochondral ossification, MSCs differentiate into chondrocytes which synthesize cartilage. This cartilage is mineralized through chondrocyte apoptosis, and subsequently osteoblasts penetrate the dead structure and generate bone [18].

1.3.4 Bone structure

Long bones are structured in different layers, from the outside to the inside: periosteum, cortical bone, endosteum, trabecullar, and bone marrow [12]. The periosteum is the boundary layer attached to the soft tissue. It provides a good blood supply to the bone and contains progenitor cells. The cortical bone consists of cylindrical structures of lamellar bone (also called osteon) [12]. The trabecullar

or cancellous bone consists of interconnected cuboid bones filled with bone marrow. The endosteum is a thin vascular membrane of connective tissue that lines the inner surface of the bone tissue and the medullary cavity where lies the bone marrow. Bone marrow is a tissue composed of blood vessels, nerves, and various types of cells, whose main function is to produce the basic blood cells.

CHAPTER 2

MODELING THE FUNDAMENTAL FUNCTIONS OF THE IMMUNE SYSTEM IN BONE FRACTURE HEALING

The most important effects of the immune system on bone fracture healing are observed during the inflammatory and repair phases of the healing process [27, 48, 47]. During the inflammatory phase, immune system cells modulate and resolve the inflammation by engulfing debris. During the repair phase immune system cells provide an optimal environment for the cellular proliferation, differentiation, and tissue production through their released molecules factors [36]. In this chapter the phagocytic and the pro-inflammatory regulatory effects of the immune system in the bone fracture healing are modeled. In order to mathematically represent and study the complex processes involved in bone fracture healing different modeling assumptions will be established.

2.1 Modeling Assumptions

The primary variables during the inflammatory and repair phases of the bone fracture healing process are debris (D), macrophages (M), MSCs (C_m), osteoblasts (C_b), TNF-α (c_1), fibrocartilage (m_c), and woven bone (m_b). The biological system interactions are depicted in Figure 2.1. In the flow diagram, the cells and cellular dynamics are represented by the circular shapes and solid arrows. The molecular concentrations and their production/decay are represented by the octagonal shapes and dashed arrows. The pro-inflammatory cytokines activation/inhibition effects on the cellular functions are represented by the dotted arrows. Removal of debris and

the negative effect among the variables are represented by the dot-ending dotted arrows.

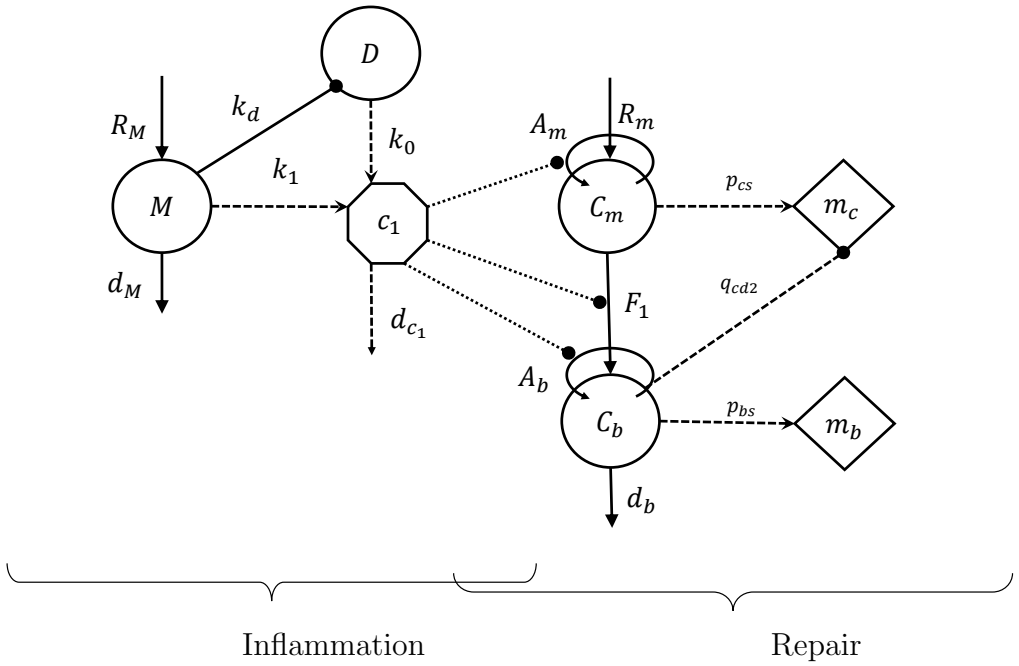

Figure 2.1. Flow diagram of the cellular and molecular dynamics during the inflammatory and repair phases of the bone fracture healing process .

It is assumed that the tissue cellular functions are regulated by c_1. It is also assumed that c_1 is delivered through cell necrosis and by the macrophages. It is further assumed that the repair process is governed by the production of m_c and m_b [2, 7], whose final levels are used to classify the outcome of the bone healing process. Additionally, it is assumed that debris D are proportional to the number of necrotic cells [27]. It is also assumed that macrophages M release c_1 and engulf debris. Additionally, the population of macrophages increases proportionally in size to the density of debris up to a maximal value of M_{max} [40]. The accumulation of

macrophages at the injury site is modeled by its recruitment due to inflammation, which is assumed to be proportional to the debris density.

Furthermore, it is assumed that the differentiation rates of MSCs into osteoblasts and osteoblasts into osteocytes are constant. MSCs synthesize the fibrocartilage, while osteoblasts synthesize the woven bone. It is also assumed that only the fibrocartilage is constantly removed by the osteoclasts, with the density of the osteoclasts being assumed proportional to the density of the osteoblasts [2]. In addition, it is assumed that the populations of the two tissue cells, C_m and C_b, experience logistic growth, where the growth rates decrease linearly as the populations' sizes approach a maximum value, K_{lm} and K_{lb}, imposed by the limited resources of the environment [2, 42]. It is also assumed that MSCs increase their population by migration proportionally to the debris density. However, it is assumed that there is no recruitment of osteoblasts.

2.2 Model Formulation

The inflammatory and repair phases of the bone fracture healing process are modeled with a mass-action system of nonlinear ordinary differential equations. All variables represent homogeneous quantities in a given volume. Following the outlined biological assumptions and the flow diagram given in Figure 2.1 yields the resulting system of equations:

$$\frac{dD}{dt} = -R_D M \tag{2.1}$$

$$\frac{dM}{dt} = R_M - d_M M \tag{2.2}$$

$$\frac{dc_1}{dt} = k_0 D + k_1 M - d_{c_1} c_1 \tag{2.3}$$

$$\frac{dC_m}{dt} = (R_m + A_m C_m)\left(1 - \frac{C_m}{K_{lm}}\right) - F_1 C_m \tag{2.4}$$

$$\frac{dC_b}{dt} = A_b C_b \left(1 - \frac{C_b}{K_{lb}}\right) + F_1 C_m - d_b C_b \tag{2.5}$$

$$\frac{dm_c}{dt} = (p_{cs} - q_{cd_1} m_c) C_m - q_{cd_2} m_c C_b \tag{2.6}$$

$$\frac{dm_b}{dt} = (p_{bs} - q_{bd} m_b) C_b \tag{2.7}$$

Equation (2.1) describes the rate of change with respect to time of the debris density, which decreases proportionally to M. The engulfing rate R_D is modeled by a Hill Type II function to represent the saturation of the phagocyte rate of macrophages [34, 39]:

$$R_D = k_d \times \frac{D}{a_{ed} + D}.$$

Equation (2.2) describes the rate of change with respect to time of the macrophages density. It increases because of migration and decreases by a constant emigration rate, d_M. It is assumed that M migrate to the injury site proportionally to D up to a maximal constant rate, k_{max}, [1, 25]:

$$R_M = k_{max} \left(1 - \frac{M}{M_{max}}\right) D.$$

Equations (2.3) describes the rate of change with respect to time of c_1. Here, k_0 and k_1 are the constant rates of the cytokine production and d_{c_1} is the cytokine constant decay rates. Equation (2.4) describes the rate of change with respect to time of C_m, which increases by cellular migration and division up to a constant-maximal carrying capacity, K_{lm}, and decreases by differentiation [2]. The migration rate of MSCs is modeled proportional to the debris density, $R_m = k_m D$, and the total MSCs proliferation rate is modeled by [51]:

$$A_m = k_{pm} \times \frac{a_{pm}^2 + a_{pm_1} c_1}{a_{pm}^2 + c_1^2},$$

where in the absence of inflammation, $c_1 = 0$, MSCs proliferate at a constant rate k_{pm}. However, when there is inflammation, $c_1 > 0$, the proliferation rate of MSCs

increases or decreases according to the concentration of c_1, i.e., high concentration levels of c_1 inhibit C_m proliferation, while low concentration levels of c_1 accelerate C_m proliferation. The differentiation rate of C_m is inhibited by c_1, which is modeled by the following function [27]:

$$F_1 = d_m \times \frac{a_{mb_1}}{a_{mb_1} + c_1}.$$

Equation (2.5) describes the rate of change with respect to time of C_b. It increases when MSCs differentiate into osteoblasts or when osteoblasts proliferate [2]. It decreases at a constant rate d_b when osteoblasts differentiate into osteocytes. The osteoblasts proliferation rate is inhibited by c_1, which is modeled by the following function [27]:

$$A_b = k_{pb} \times \frac{a_{pb}}{a_{pb} + c_1}.$$

Equations (2.6) and (2.7) describe the rate of change with respect to time of the fibrocartilage and woven bone, where p_{cs} and p_{bs} are the tissue constant synthesis rates, and q_{cd1}, q_{cd2}, and q_{bd} are the tissue degradation rates, respectively [2].

2.3 Qualitative Analysis

The analysis of Model (2.1)-(2.7) is done by finding the equilibria and their corresponding stability properties. An equilibrium is a state of the system where the variables do not change over time and can be found by setting the right-hand sides of the equations equal to zero [42]. Once the equilibria are identified, it is important to determine the behavior of the model near equilibria by analyzing their local stability properties. An equilibrium is locally stable if the system moves toward it when it is near the equilibrium, otherwise it is unstable [42]. Therefore, the equilibria provide the possible outcomes of the bone fracture healing process and their corresponding

stability properties define the conditions under which a particular healing result occurs.

An equilibrium point of the model is denoted by the vector form $E(D, M, c_1, C_m, C_b, m_c, m_b)$. The model has three biologically meaningful equilibria: $E_0(0, 0, 0, 0, 0, m^*_{c_0}, m^*_{b_0})$, $E_1(0, 0, 0, 0, K_{lb}(1 - d_b/k_{pb}), 0, p_{bs}/q_{bd})$, $E_2(0, 0, 0, C^*_m, C^*_b, m^*_c, p_{bs}/q_{bd})$. Their definitions, existence, and corresponding stability conditions are described in the following theorems. The existence of each equilibrium point arises from the fact that all biologically meaningful variables are nonnegative, and their stability analysis is conducted using the Jacobian of the system at each equilibrium point and finding its corresponding eigenvalues [42, 60].

Theorem 2.3.1. *Suppose that $m^*_{c_0} \geq 0$ and $m^*_{b_0} \geq 0$. Then $E_0(0, 0, 0, 0, 0, m^*_{c_0}, m^*_{b_0})$ exists for all the parameter values and E_0 belongs to the set $B = \{(0, 0, 0, 0, 0, m_c, m_b) : 0 \leq m_c \leq p_{cs}/q_{cd_1}, 0 \leq m_b \leq p_{bs}/q_{bd}\}$, which is a local attractor set of the solution set given by System (2.1)-(2.7) if and only if $k_{pm} \leq d_m$ and $k_{pb} \leq d_b$.*

Proof of Theorem 2.3.1. $E_0(0, 0, 0, 0, 0, m^*_{c_0}, m^*_{b_0})$ exists for all the parameter values, since its elements are nonnegative and do not depend on the parameters. Next, it will be proved that any solution of the System (2.1)-(2.7) with positive initial conditions is positive. The right-hand side functions of System (2.1)-(2.7) are continuous and bounded, since all model variables and parameters are positive. Hence, for each initial condition of the system, there is a unique solution [53]. Since zero is a solution of the System (2.1)-(2.7) and by uniqueness of solution then all the solutions of the system with positive initial condition are positive [53].

Next, it will be proved that the hyperplane $A = \{(0, 0, 0, 0, 0, m_c, m_b) : m_c \geq 0, m_b \geq 0\}$ is an attractor set of the solutions of the system (2.1)-(2.7). There

are two cases to consider based on the relation between the cells proliferation and differentiation rates.

First, let us examine the case when $k_{pm} < d_m$ and $k_{pb} < d_b$. The Jacobian matrix $J(E_0)$ is given by the following lower triangular block matrix

$$J(E_0) = \begin{pmatrix} J_1(E_0) & \mathbf{0} & \mathbf{0} \\ J_1^* & J_2(E_0) & \mathbf{0} \\ \mathbf{0} & J_2^* & J_3(E_0) \end{pmatrix},$$

where

$$J_1(E_0) = \begin{pmatrix} 0 & 0 & 0 \\ k_{max} & -d_M & 0 \\ k_0 & 0 & -d_{c_1} \end{pmatrix}, \quad J_2(E_0) = \begin{pmatrix} -d_m + k_{pm} & 0 \\ d_m & -d_b + k_{pb} \end{pmatrix},$$

$$J_3(E_0) = \begin{pmatrix} 0 & 0 \\ 0 & 0 \end{pmatrix},$$

and J_1^*, J_2^* are non zero submatrices. Therefore the corresponding characteristic polynomial associated with $J(E_0)$ is given by the product of the characteristic polynomials associated with each submatrix [52]:

$$p(\lambda) = \lambda^3 (\lambda + d_M)(\lambda + d_{c_1})(\lambda + d_m - k_{pm})(\lambda + d_b - k_{pb})$$

Therefore, the eigenvalues of $J(E_0)$ are negative for the variables M, c_1, C_m, and C_b and are equal to zero for D, m_c, and m_b. Since $D'(t) \leq 0$ for all the variables in the system (2.1)-(2.7) and $(D^*, 0, 0, 0, 0, m_c, m_b)$ with $D^* \neq 0$ is not an equilibrium point, then the solutions of the system (2.1)-(2.5) are attracted to the set $A = \{(0, 0, 0, 0, 0, m_c, m_b) : m_c \geq 0, m_b \geq 0\}$. Equations (2.6) and (2.7) imply that $m_c' \leq 0$ and $m_b' \leq 0$ for all $m_c > p_{cs}/q_{cd_1}$ and $m_b > p_{bs}/q_{bd}$. Therefore, set B is a local attractor set of A [53].

Next, let us consider the case when $k_{pm} = d_m$ and $d_b = k_{pb}$. Here, the eigenvalues of $J(E_0)$ are the same as above except those associated with C_m and C_b, which are equal to zero. Therefore, in this case, considering the second order approximations of the right hand sides of Equations (2.4) and (2.5), instead of just the first order approximations, and using similar arguments as above, proves that the set B is a local attractor set of A. □

It is important to note that the System (2.4)-(2.5) is well-posedness, since for any non-negative initial condition, the solution of the system exists, is unique, and remains within the state space, i.e., $D \geq 0$, $M \geq 0$, $c_1 \geq 0$, $C_m \geq 0$, $C_b \geq 0$, $m_c \geq 0$ and $m_b \geq 0$, see the proof of Theorem 2.3.1.

Theorem 2.3.2. *The equilibrium* $E_1(0, 0, 0, 0, K_{lb}(1 - d_b/k_{pb}), 0, p_{bs}/q_{bd})$ *exists when* $k_{pb} > d_b$, *and it is locally stable if and only if* $d_m \geq k_{pm}$.

Proof of Theorem 2.3.2. E_1 is well defined since by hypothesis all its elements are nonnegative. Next, the Jacobian matrix corresponding to E_1 is given by the following lower triangular block matrix:

$$J(E_1) = \begin{pmatrix} J_1(E_1) & \mathbf{0} & \mathbf{0} \\ J_1^* & J_2(E_1) & \mathbf{0} \\ \mathbf{0} & J_2^* & J_3(E_1) \end{pmatrix},$$

where $J_1(E_1)$ has the same expression as $J_1(E_0)$ defined in Theorem 2.3.1, J_1^* and J_2^* are nonzero sub-matrices and

$$J_2(E_1) = \begin{pmatrix} -d_m + k_{pm} & 0 \\ d_m & d_b - k_{pb} \end{pmatrix},$$

$$J_3(E_1) = \begin{pmatrix} -q_{cd_2} K_{lb}(1 - \frac{d_b}{k_{pb}}) & 0 \\ 0 & -q_{bd} K_{lb}(1 - \frac{d_b}{k_{pb}}) \end{pmatrix}.$$

Since $d_m - k_{pm} \geq 0$ and $k_{pb} > d_b$ and all the eigenvalues of $J_1(E_0)$ are non-positive values, then all the eigenvalues of $J(E_1)$ are all negative except the eigenvalues associated with D and C_m when $k_{pm} = d_m$, which are equal to zero. Therefore, by applying similar arguments provided in the proof of Theorem 2.3.1 when the eigenvalues are zero, it implies that E_1 is a locally stable node. □

Theorem 2.3.3. *Suppose that $k_{pm} > d_m$. Then the equilibrium $E_2(0, 0, 0, 0, 0, c_2^*, C_m^*, C_b^*, m_c^*, p_{bs}/q_{bd})$, where $C_m^* = K_{lm}(1 - d_m/k_{pm})$, $m_c^* = p_{cs}C_m^*/(q_{cd1}C_m^* + q_{cd2}C_b^*)$, and $C_b^* = K_{lb}(k_{pb} - d_b + \sqrt{(k_{pb} - d_b)^2 + 4k_{pb}d_m C_m^*/K_{lb}})/2k_{pb}$, exists and is locally stable.*

Proof of Theorem 2.3.3. From the definition of E_2 and the hypothesis, $k_{pm} > d_m$, it is easy to see that all the elements of E_2 are nonnegative. Nets, the Jacobian matrix corresponding to E_2 is given by the following lower triangular block matrix:

$$J(E_2) = \begin{pmatrix} J_1(E_2) & \mathbf{0} & \mathbf{0} \\ J_1^* & J_2(E_2) & \mathbf{0} \\ \mathbf{0} & J_2^* & J_3(E_2) \end{pmatrix},$$

where $J_1(E_2)$ has the same expression as $J_1(E_0)$ defined in Theorem 2.3.1, J_2^* and J_2^* are nonzero submatrices, and

$$J_2(E_2) = \begin{pmatrix} d_m - k_{mb} & 0 \\ d_m & -\sqrt{(d_b - k_{pb})^2 + 4\frac{k_{bp}d_m C_m^*}{K_{lb}}} \end{pmatrix},$$

$$J_3(E_2) = \begin{pmatrix} -q_{cd_1}C_m^* - q_{cd_2}C_b^* & 0 \\ 0 & -q_{bd}C_b^* \end{pmatrix}.$$

Since $k_{pm} > d_m$, and all equilibrium variables and parameter values are positive, then all the eigenvalues of $J_1(E_2)$, $J_2(E_2)$, $J_3(E_2)$ are negative except for the eigenvalue associated to D which is equal to zero. Following the same arguments applied in the proof of Theorem 2.3.1 for the eigenvalue equals to zero, it can be concluded that E_2 is locally stable. □

The existence conditions for the three equilibria are summarized in Table 2.1, and their stability conditions and the all possible resulting set of equilibria are summarized in Table 2.2. From Theorems 2.3.1-2.3.1, the existence condition for E_0 requires that the steady state tissue densities to be either zero or any positive number. For E_1, the existence condition arises from the requirement that the steady state density of C_b must be greater than zero, which implies that the proliferation rate of osteoblasts must be greater than their differentiation rate, i.e., $k_{pb} > d_b$.

Similarly for E_2, the existence condition arises from the requirement that the steady state density for C_m must be greater than zero, which implies that the proliferation rate of MSCs must be greater than their differentiation rate, i.e., $k_{pm} > d_m$.

Table 2.1. Existence conditions for the equilibrium points and their biological meaning.

Equilibria	**Conditions**	**Meaning**
$E_0\left(0,0,0,0,0,m^*_{c_0},m^*_{b_0}\right)$	$m^*_{c_0},m^*_{b_0}\geq 0$	nonunion
$E_1\left(0,0,0,0,K_{lb}(1-\frac{d_b}{k_{pb}}),0,\frac{p_{bs}}{q_{bd}}\right)$	$k_{pb}>d_b$	successful healing
$E_2\left(0,0,0,C^*_m,C^*_b,m^*_c,\frac{p_{bs}}{q_{bd}}\right)$	$k_{pm}>d_m$	nonunion or delayed union

E_0 is stable when $k_{pm} \leq d_m$ and $k_{pb} \leq d_b$ (see Theorem 2.3.1), which implies that the differentiation rates of the MSCs and osteoblasts are greater than or equal to their proliferation rates, respectively. The steady-state E_0 represents a nonunion. In this case, the inflammation is resolved since the first five entries of E_0 are zero; however, the repair process has failed since the osteoblasts and osteoclasts have died out before the beginning of the remodeling process. Hence, the tissue densities, $m^*_{c_0}$ and $m^*_{b_0}$, can be any two positive values smaller than their maximal densities, p_{cs}/q_{cd1} and p_{bs}/q_{bd}, respectively (see Theorem 2.3.1).

E_1 is stable when $k_{pm} \leq d_m$ and $k_{pb} > d_b$ (see Theorem 2.3.2). The steady-state E_1 represents a successful repair of the bone fracture; where the inflammation is resolved, the fibrocartilage is completely removed from the repair site, and the woven bone has achieved its maximal density. In this case, osteoblasts proliferate faster than they differentiate while MSCs have the opposite behavior.

E_2 is stable when $k_{pm} > d_m$ (see Theorem 2.3.3). The steady-state E_2 represents a nonunion or delayed union, where the inflammation is resolved but the osteoclasts have failed to degrade the cartilage in a timely fashion.

Table 2.2. Stability conditions for the equilibrium points.

Equilibria	**Stability Conditions**	**Stability**
E_0	$k_{pm} \leq d_m$, $k_{pb} \leq d_b$	E_0 belongs to an attracting local set
E_0, E_1	$k_{pm} \leq d_m$, $k_{pb} > d_b$	E_0 unstable; E_1 locally stable
E_0, E_2	$k_{pm} > d_m$, $k_{pb} \leq d_b$	E_0 unstable; E_2 locally stable
E_0, E_1, E_2	$k_{pm} > d_m$, $k_{pb} > d_b$	E_0 and E_1 unstable; E_2 locally stable

2.4 Numerical Results

The proposed new model (2.1) - (2.7) is used to study the importance of macrophages during the inflammatory and repair phases of the bone fracture healing process, which occur within the first 21 days after trauma [27, 64]. It is also used to investigate the evolution of a broken bone under normal and pathological conditions. Table 5.1 summarizes the baseline parameter values and units for the numerical simulations. These values are estimated in a qualitative manner from data in other studies [39, 40, 63, 2, 24, 27]. Some of those from [27, 55] were also rescaled to account for the different mathematical expressions of the proliferation and differentiation rates of the tissue cells. All parameter values are based on murine experiments with healthy mice having a moderate fracture (a broken long bone with a gap size less

than 3mm) [2, 24]. However, the bone fracture healing process for humans involves the same cells, cytokines, and qualitative dynamics, differing only in the number of cells, concentrations, and the length of time it takes for a full recovery [20].

First, a set of numerical simulations is presented to support the theoretical results (successful and nonunion equilibria) and to numerically monitor the healing progression of a moderate fracture in normal conditions. Next, the mathematical model is used to investigate the effects of macrophages during the bone fracture repair. Then, another set of numerical simulations is performed to analyze the inflammatory effects in bone healing for different types of fractures. Finally, a set of numerical simulations is presented to explore various cellular treatments under numerous pathological conditions.

2.4.1 Different outcomes of the bone fracture healing process

A set of numerical simulations is presented to support the theoretical results. According to the qualitative analysis of the model, there are three equilibria: E_0, E_1 and E_2, where their stability conditions are determined by the tissue cells' proliferation and differentiation rates, k_{pm}, k_{pb}, d_m and d_b, respectively. The following parameter values are used: $k_{pm} = 0.5$, $d_m = 1$, $k_{pb} = 0.2202$, and $d_b = 0.3$, to demonstrate the stability of E_0, since then $k_{pm} < d_m$ and $k_{pb} < d_b$. The stability of E_1 is demonstrated using the following parameter values: $d_m = 1$, $k_{pm} = 0.5$, $k_{pb} = 0.2202$, and $d_b = 0.15$, since then $k_{pm} \leq d_m$ and $k_{pb} > d_b$. Finally, the following parameter values are used: $k_{pm} = 0.5$ and $d_m = 0.1$, to demonstrate the stability of E_2, since then $k_{pm} > d_m$. Different time-periods are used in Figures 2.2-2.4 to better demonstrate the qualitative behavior of the system under different stability conditions.

Figure 2.2 shows the qualitative behavior of E_1 for the macrophages, debris, and TNF-α densities, with the inflammation being resolved in about 40 days. Since at this time, macrophages density is near zero.

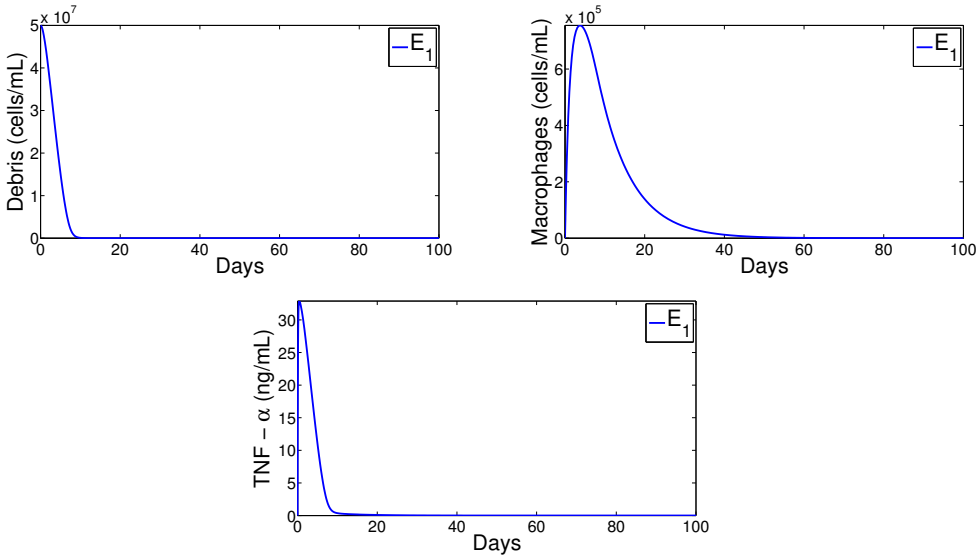

Figure 2.2. Cellular and molecular evolution of the resolution of the inflammation in normal conditions.

Figure 2.3 shows the qualitative behaviors of E_1 for the MSCs, osteoblasts, cartilage, and bone densities. Here, the MSCs density decays to zero over time, while the osteoblasts maintain a constant density below their carrying capacity $K_{lb} = 1 \times 10^6$. In addition, the bottom plots of Figure 2.3 show that the cartilage is eventually degraded by the osteoclasts, and the bone achieves its maximum density of 1 ng/mL. Therefore, E_1 exhibits the temporal progression of a successful bone fracture healing.

Figure 2.4 shows the qualitative evolution for the MSCs, osteoblasts, cartilage, and bone densities for E_0 (solid lines) and E_2 (dotted lines). Since the temporal evolution of macrophages, debris, and cytokines densities in E_0 and E_2 are similar to those for E_1 showed in Figure 2.2, then they are omitted here. It can be observed

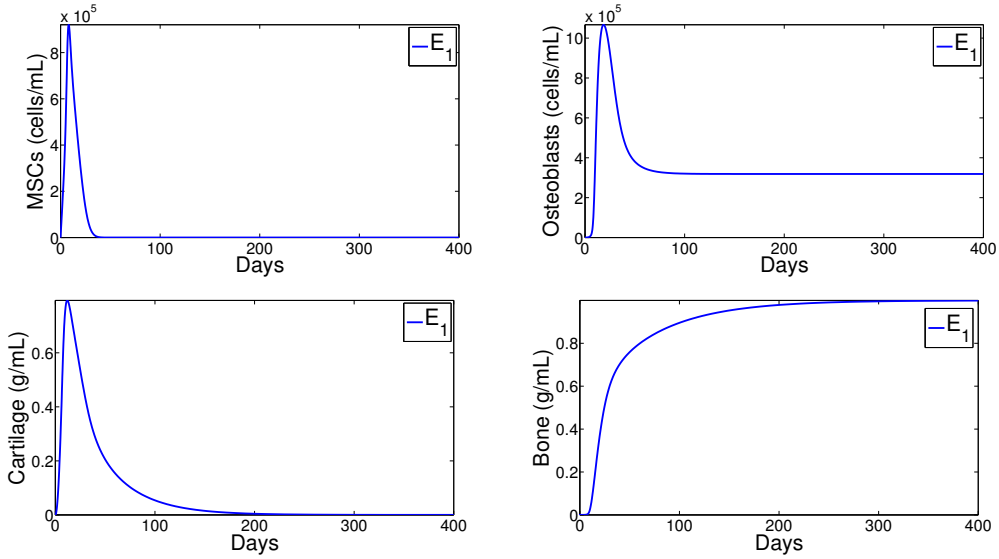

Figure 2.3. Cellular and molecular evolution of the repair process in a successful fracture healing.

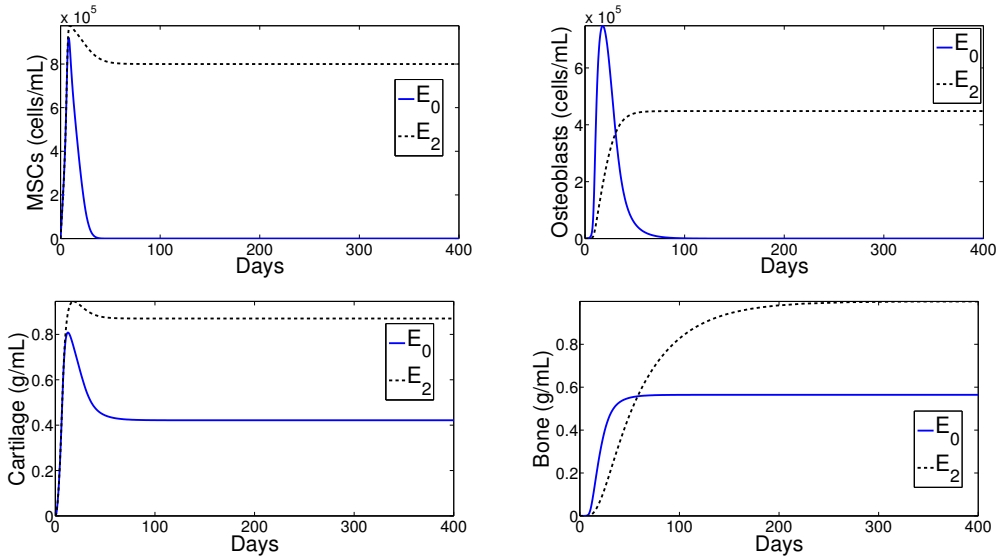

Figure 2.4. Cellular and molecular evolution of the repair process in a nonunion fracture healing.

in Figure 2.4 that the two cellular densities in E_0, MSCs and osteoblasts, decay to zero over time, with the osteoclasts failing to degrade the cartilage, which results in nonunion. Mathematically, this case occurs when osteoblasts proliferate at a

rate lower than their differentiation rate, i.e., $k_{pb} < d_b$. In practice, this scenario is commonly observed in advanced-age patients whose MSCs and osteoblast cells decrease their capability to proliferate and differentiate [31]. On the other hand, the two cells and the two tissues in E_2 remain at positive constant values (Figure 2.4), but the final fracture healing outcome is still a nonunion. Here, the osteoclasts again fail to degrade the cartilage [31], even though the bone has achieved its maximum density of 1 ng/mL. Therefore, in this case, migration of osteoclasts must be enhanced through surgical interventions in order to achieve a successful bone repair [2].

2.4.2 Importance of macrophages during the bone fracture healing process

Next, the mathematical model is used to investigate the effects of macrophages during the inflammatory and repair phases of the bone fracture healing process. The major contribution of macrophages to fracture healing is through their phagocytic function and their regulation of the tissue cellular functions, which is modeled with the c_1. Therefore, the values of the parameter k_d, representing the phagocytic rate of macrophages, and k_1, representing the secretion rates of c_1 by M are varied in the numerical simulations as compared to their base values from Table 5.1.

Figure 2.5 shows that macrophages have drastic effects on the short-term tissue dynamics during the healing process. Because of the faster phagocytic rate (dashed-doted lines) of macrophages, the fibrocartilage formation is less, and its degradation started earlier, while woven bone doubles in about 1 week. In contrast, with a slower phagocytic rate (dashed lines) of macrophages, the fibrocartilage experiences an increase during the second week and beyond, while the woven bone hardly formed.

Figure 2.6 shows that macrophages promote the production of the fibrocartilage after the second week and beyond, while macrophages lightly inhibit the woven bone production during the second week.

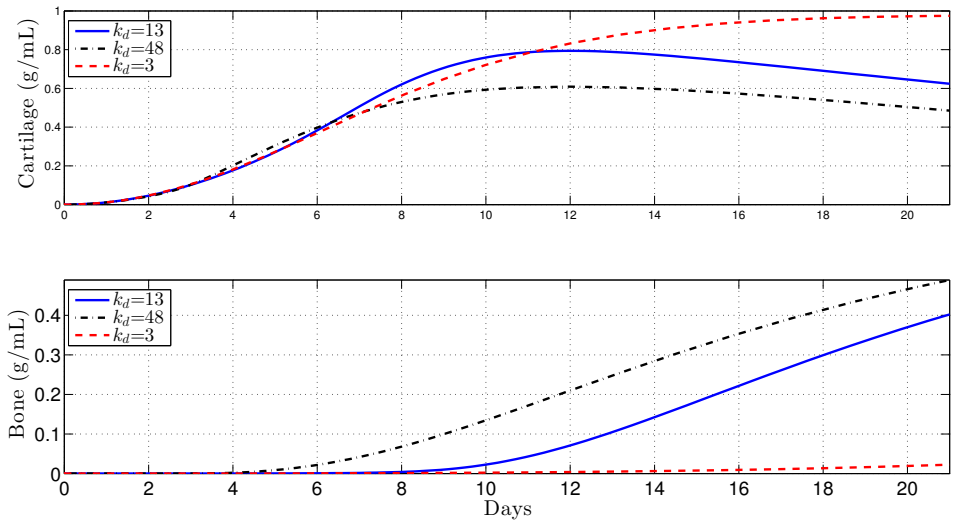

Figure 2.5. Tissues evolution for different phagocytic rates: baseline phagocytic rate (solid line), $k_d = 13$; faster phagocytic rate (dashed-doted line), $k_d = 48$; slower phagocytic rate (dashed line), $k_d = 3$.

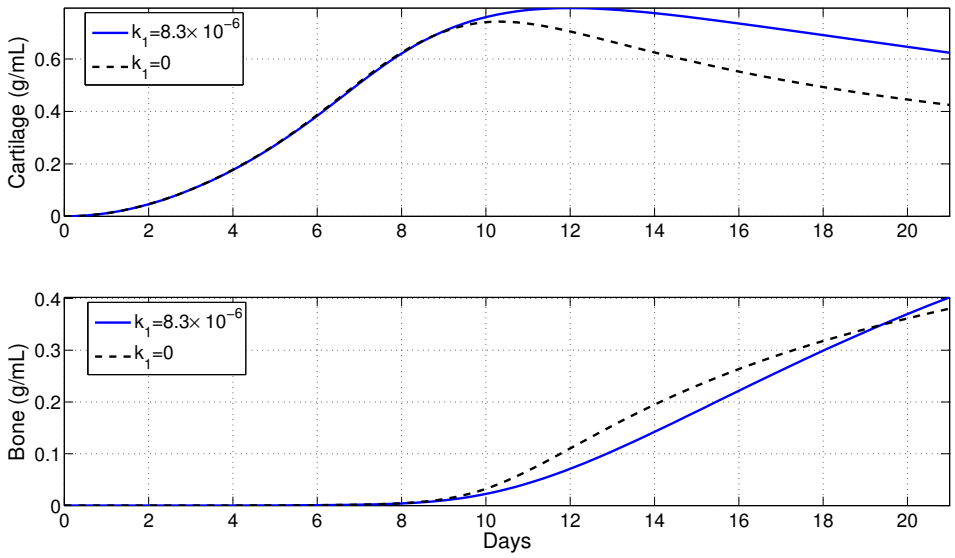

Figure 2.6. Tissues evolution when the regulatory effect of macrophages through c_1 is modeled in the healing process (solid line), $k_1 = 8.3 \times 10^{-6}$, and when they do not contribute to the healing process (dashed line), $k_1 = 0$.

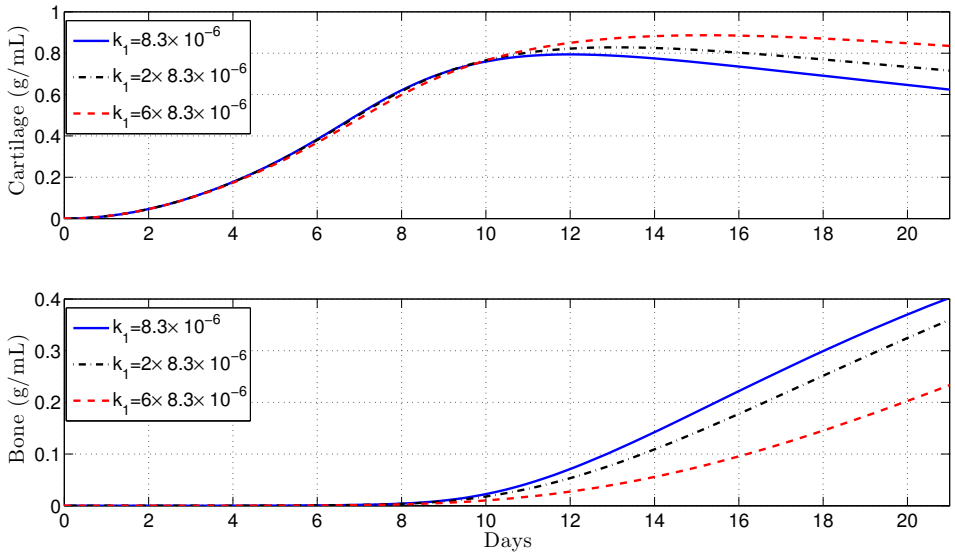

Figure 2.7. Tissues evolution for different c_1 production rates by macrophages: baseline production rate (solid line), $k_1 = 8.3 \times 10^{-6}$; doubling the production rate (dashed-doted line), $k_1 = 2 \times 8.3 \times 10^{-6}$; increasing six times the production rate (dashed line), $k_1 = 6 \times 8.3 \times 10^{-6}$.

Figure 2.7 shows that macrophages have drastic negative effects on the bone healing as they increase their c_1 production rate: less removal of the fibrocartilage and less bone production are observed after the second week and beyond, when k_1 is increased by two and six times its base line parameter value.

2.4.3 Evolution of the healing process for different types of fractures

In this section, the model is used to monitor the evolution of a successful repair (Table 5.1) for different types of fractures. In healthy individuals, simple, moderate, and severe fractures are correlated with the debris densities [32, 23]. Therefore, the initial debris concentration is set to $D(0) = 5 \times 10^5$, $D(0) = 5 \times 10^7$, and $D(0) = 5 \times 10^8$, for a simple, moderate, and severe fracture, respectively.

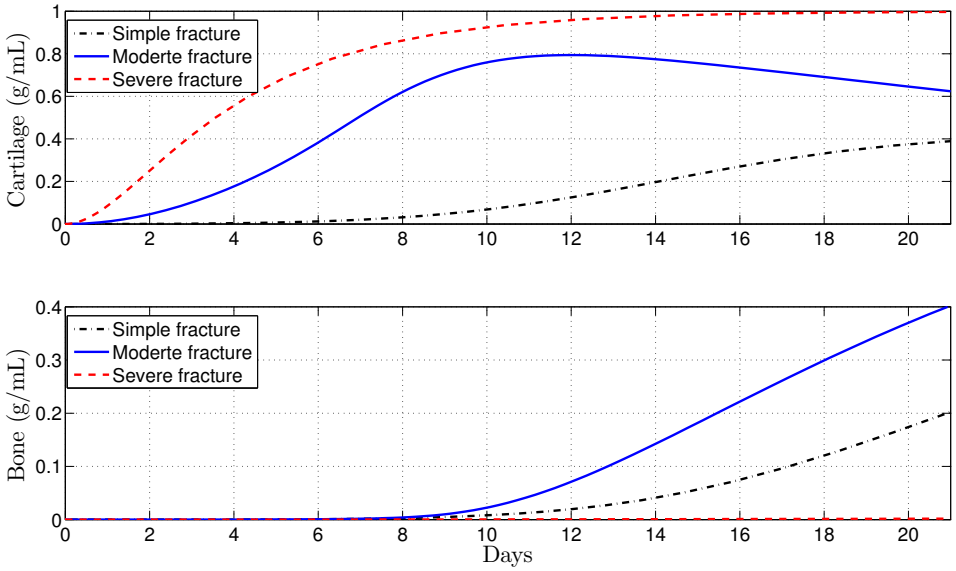

Figure 2.8. Tissues evolution of a successful repair for different types of fractures.

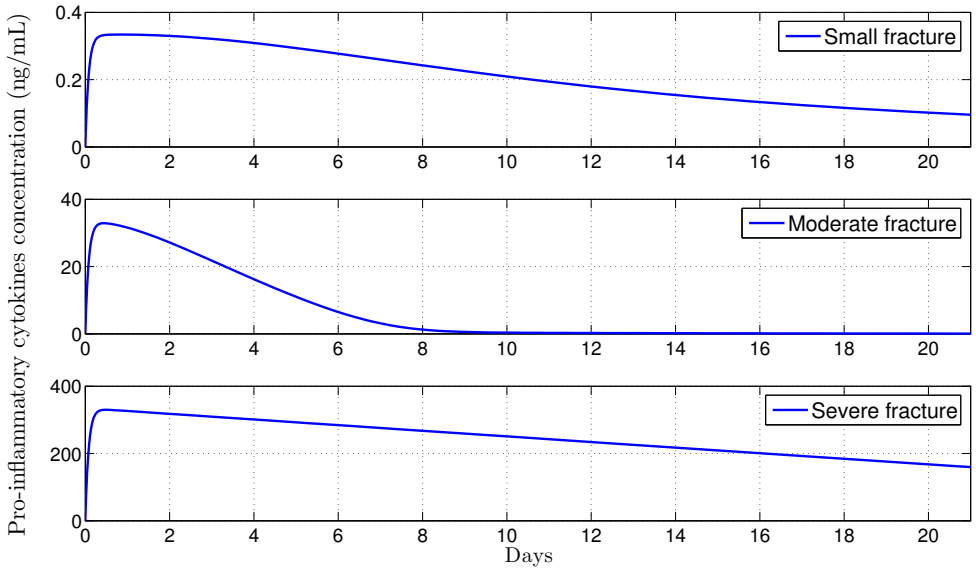

Figure 2.9. Concentration of inflammatory cytokines present in small, moderate, and severe fractures.

Figure 2.8 shows that the tissue production is a slow process for a simple fracture, since both the cartilage and bone densities are less than the corresponding tissue densities for moderate and severe fractures. A slow healing process is commonly observed in micro-crack healing [32]. Furthermore, there is less cartilage formation over time in simple fractures [23]. For a moderate fracture, the maximal production of the cartilage is observed around 10 days followed by a significant degradation, while the bone tissue production occurs after the first week. For a severe fracture, Figure 2.8 shows that there is a delay in the two tissues production compared with those given by moderate fractures, with the peak of the cartilage and bone productions observed at around day 16.

From Figure 2.9, it can be observed that the peak of inflammatory cytokines concentration increases as debris densities increases. Furthermore, high concentration of inflammatory cytokines leads to delayed healing, as it is observed in severe fractures. Therefore the healing time of a broken bone is determined by the inflammatory cytokines concentrations.

2.4.3.1 Cellular therapeutic interventions under immune-compromised conditions

Additions of MSCs to the injury site through injection and/or transplantation have been used in practice to stimulate and augment bone fracture healing [29]. Another cellular intervention is the scaffold implants, where macrophages and MSCs are co-cultured together [31]. In this section, the Model (2.1)-(2.7) is used to explore these possible therapeutic treatments to accelerate the healing of a broken bone under normal and pathological conditions such as severe fractures, advanced age, and senile osteoporosis [31]. The parameter values used in the numerical simulations that explore these possible therapeutic treatments are the same as in Subsection 2.4.3.

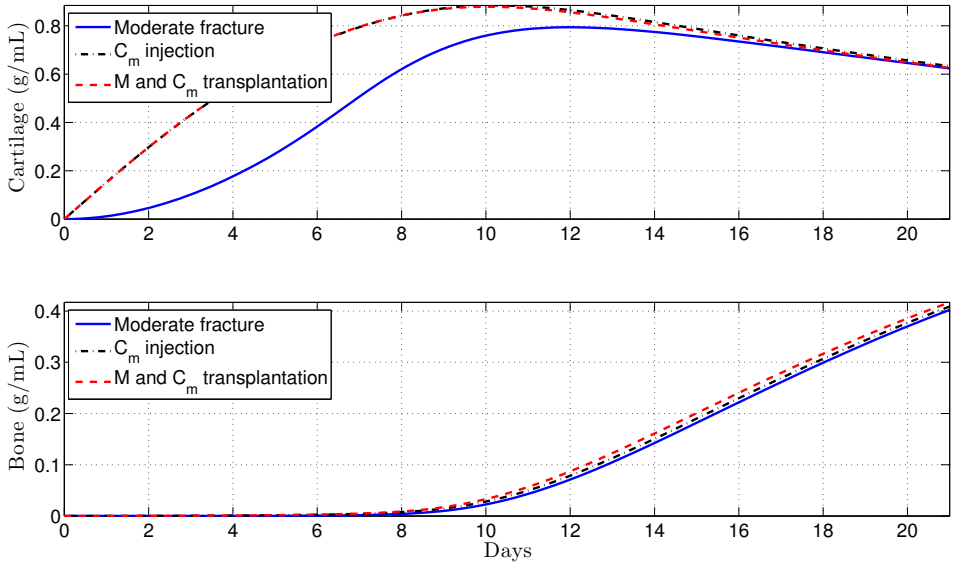

Figure 2.10. Tissues evolution in a moderate fracture without therapeutic innervation (solid line) and with MSCs injection (dashed-dotted line) and with MSCs and macrophages transplantation (dashed line).

First, for healthy individuals with moderate and severe fractures the debris values are $D(0) = 5 \times 10^7$ and $D(0) = 5 \times 10^8$, respectively. Second, the following parameter values are used: $k_d = 3$ and $k_1 = 9 \times 10^{-6}$ to simulate bone fracture healing in aging individuals, since in this case, the macrophages phagocytic rate decreases, and there is an increase of pro-inflammatory cytokine synthesis by the macrophages [19, 31]. Finally, $c_1(0) = 100$, $k_{pm} = 0.2$, $d_m = 0.5$, $k_{pb} = 0.16$, and $d_b = 0.15$ are used to simulate the healing process for a senile osteoporotic fracture, since in this case, a high level of pro-inflammatory cytokines is observed, and the MSCs and osteoblast functions decrease [31]. The MSCs injection are simulated by setting $C_m(0) = 5 \times 10^4$. The MSCs and macrophages transplantation are simulated by setting $C_m(0) = 5 \times 10^5$ and $M(0) = 2 \times 10^5$.

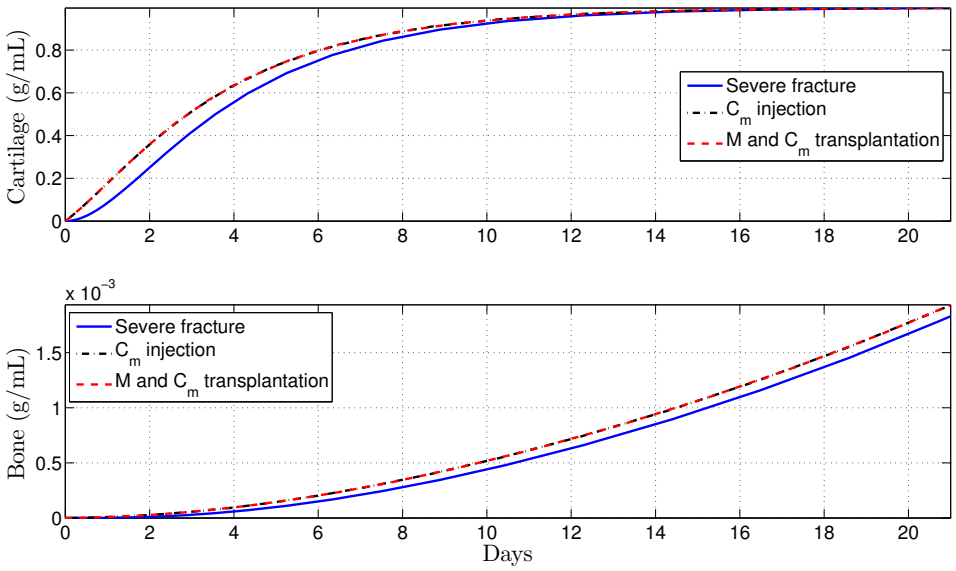

Figure 2.11. Tissues evolution in a severe fracture without therapeutic innervation (solid line) and with MSCs injection (dashed-dotted line) and with MSCs and macrophages transplantation (dashed line).

Figures 2.10, 2.11, 2.12, and 2.13 show that the two cellular interventions increase both tissue productions. Furthermore, those interventions result in larger improvements in aging fractures, see Figure 2.12. However, there is no bigger difference between the two therapeutic interventions, the MSCs injection and the MSCs and macrophages transplantation.

2.5 Summary of the Results

In this Chapter 2, a new mathematical model was formulated to gain a better understanding of the most fundamental functions of the immune system during the bone fracture healing process: phagocytosis and the delivery of pro-inflammatory cytokines.

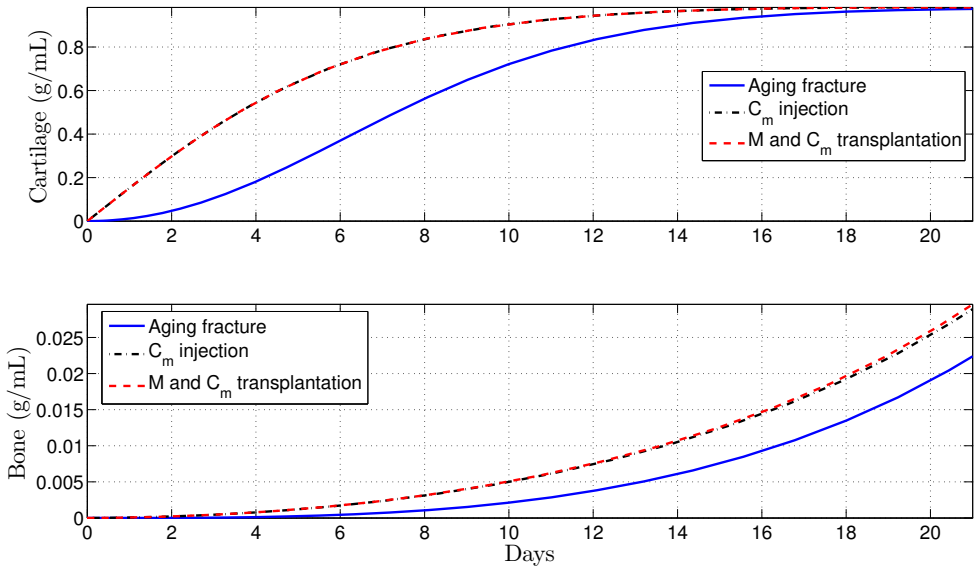

Figure 2.12. Tissues evolution in an aging fracture without therapeutic innervation (solid line), with MSCs injection (dashed-dotted line) and with MSCs injection (dashed-dotted line) and with MSCs and macrophages transplantation (dashed line).

The mathematical analysis revealed that there are three feasible fracture healing outcomes. Two of the outcomes represent a nonunion healing: one is the case when the cells deactivate or die out before the healing process finishes up and the other is the case when the tissue cells remain constant but the osteoclasts fail to completely remove the cartilage. The third outcome represents a successful healing, where the osteoblasts and osteoclasts are constantly producing and removing the woven bone. The mathematical analysis also revealed that a success of bone healing is achieved when the MSCs mitotic rate is less than the osteogenic differentiation rate and osteoblasts proliferation rate is bigger than their apoptotic rate. Furthermore, the numerical simulations showed that the phagocytic functions of the immune system cells strongly regulate the short-term tissue evolution during the healing process. If the phagocytic rate of the macrophages is diminishing, then less tissue

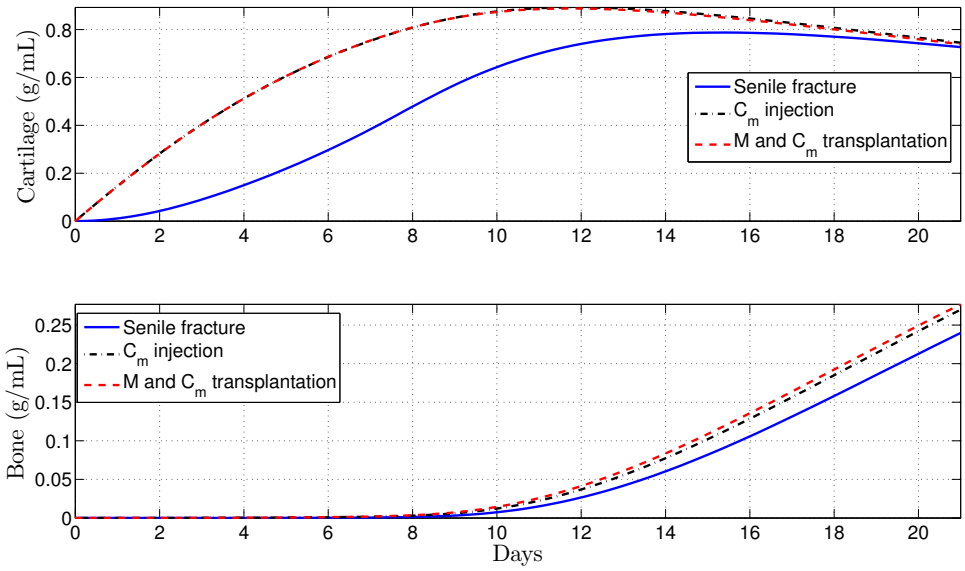

Figure 2.13. Tissues evolution in a senile fracture without therapeutic innervation (solid line) and and with MSCs injection (dashed-dotted line) and with MSCs and macrophages transplantation (dashed line).

productions is observed over time. Furthermore, that high concentration levels of pro-inflammatory cytokines negatively affect the healing time of a fracture. It was also found that the administration of growth factors improve the healing process in a dose-dependant manner in moderate fractures and always improve the healing in severe fractures. Furthermore, that the administration of growth factors exhibited the most improvement treatments during the healing of a broken bone compare to the anti-inflammatory cytokines administration. In addition, the injection and transplantation of MSCs and macrophages to the injury site at the beginning of the healing process accelerate the healing time.

CHAPTER 3

MODELING THE MACROPHAGE-MEDIATED INFLAMMATION INVOLVED IN THE BONE FRACTURE HEALING PROCESS

In this chapter, the mathematical model (2.1)-(2.7) is extended to separately incorporate the two different phenotypes of macrophages: classically and alternatively activated macrophages, as they have distinct functions during the healing process [10, 43, 48]. Classically activated macrophages release high levels of pro-inflammatory cytokines, including the TNF-α and IL-1, which exhibit inhibitory and destructive properties in high concentrations [9, 48]. In contrast, alternatively activated macrophages are characterized with the secretion of the anti-inflammatory cytokines, such as the IL-10 and TGF-β, which increase their phagocytic activities, mitigate the inflammatory responses, promote growth, and accelerate the fracture healing [10, 29, 31, 48]. This extension leads to a more realistic model by incorporating the different phagocytic rates and the separate production of the pro- and anti-inflammatory cytokines by the two types of macrophages [10, 33].

The model can be used to investigate the anti-inflammatory regulatory effects of the immune system during bone fracture healing. The model can also be used to investigate potential therapeutic treatments based on the use of anti-inflammatory cytokines, stem cells, and macrophages, suggesting possible ways to guide clinical experiments and bone tissue engineering strategies [10, 48].

3.1 Modeling Assumptions

The modeling assumptions follow the assumptions provided in Chapter 2 with the incorporation of further details on the macrophages and the pro- and anti-inflammatory, described below. The macrophages density is modeled separately as undifferentiated macrophages (M_0), classical macrophages (M_1), and alternative macrophages (M_2). It is also included a generic anti-inflammatory cytokines (c_2), which is delivered by the M_2, C_m, and C_b. The biological system interactions are depicted in Figure 3.1. In the flow diagram, the cells and cellular dynamics are represented by the circular shapes and solid arrows. The molecular concentrations and their production/decay are represented by the octagonal shapes and dashed arrows. The pro- and anti-inflammatory cytokines activation/inhibition effects on the cellular functions are represented by the dotted arrows. Removal of debris and the negative effect among the variables are represented by the dot-ending dotted arrows.

It is assumed that the cellular functions are regulated by c_1, such as the TNF-α, and c_2, such as a combination of the IL-10 and the TGF-β. It is also assumed that c_1 is delivered through cell necrosis and by the classically activated macrophages, while c_2 is delivered by the alternatively activated macrophages, MSCs, and osteoblasts. It is also assumed that unactivated macrophages M_0 do not release cytokines and do not engulf debris. Additionally, the population of M_0 increases proportionally in size to the density of debris up to a maximal value of M_{max} [40]. The only source of activated macrophages, M_1 and M_2, is M_0. Even though both phenotypes of activated macrophages have the ability to release both pro- and anti-inflammatory cytokines, it is assumed that only M_1 deliver c_1 and M_2 deliver c_2, as those are the major cytokines for each phenotype [39]. M_0 activate to M_1 under the c_1 stimulus, while they activate to M_2 under the c_2 stimulus. M_1 and M_2 macrophages do not

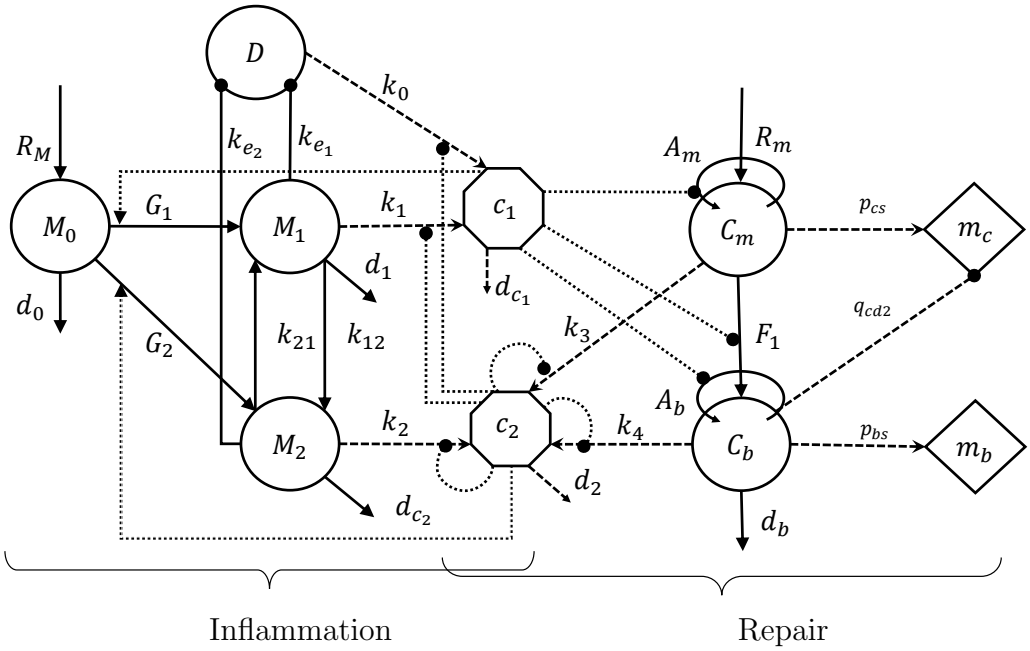

Figure 3.1. Flow diagram of the cellular and molecular dynamics during the inflammatory and repair phases of the bone fracture healing process.

de-differentiate back to the M_0 macrophages [63]; and are able to switch phenotypes at a constant rate [59].

3.2 Model Formulation

The inflammatory and repair phases of the bone fracture healing process are modeled with a mass-action system of nonlinear ordinary differential equations. All variables represent homogeneous quantities in a given volume. Following the outlined biological assumptions and the flow diagram given in Figure 3.1 yields the resulting system of equations:

$$\frac{dD}{dt} = -R_D(k_{e_1}M_1 + k_{e_2}M_2) \tag{3.1}$$

$$\frac{dM_0}{dt} = R_M - G_1M_0 - G_2M_0 - d_0M_0 \tag{3.2}$$

$$\frac{dM_1}{dt} = G_1 M_0 + k_{21} M_2 - k_{12} M_1 - d_1 M_1 \tag{3.3}$$

$$\frac{dM_2}{dt} = G_2 M_0 + k_{12} M_1 - k_{21} M_2 - d_2 M_2 \tag{3.4}$$

$$\frac{dc_1}{dt} = H_1(k_0 D + k_1 M_1) - d_{c_1} c_1 \tag{3.5}$$

$$\frac{dc_2}{dt} = H_2(k_2 M_2 + k_3 C_m + k_4 C_b) - d_{c_2} c_2 \tag{3.6}$$

$$\frac{dC_m}{dt} = (R_m + A_m C_m)\left(1 - \frac{C_m}{K_{lm}}\right) - F_1 C_m \tag{3.7}$$

$$\frac{dC_b}{dt} = A_b C_b \left(1 - \frac{C_b}{K_{lb}}\right) + F_1 C_m - d_b C_b \tag{3.8}$$

$$\frac{dm_c}{dt} = (p_{cs} - q_{cd_1} m_c) C_m - q_{cd_2} m_c C_b \tag{3.9}$$

$$\frac{dm_b}{dt} = (p_{bs} - q_{bd} m_b) C_b. \tag{3.10}$$

Equation (3.1) describes the rate of change with respect to time of the debris density, which decreases proportionally to M_1 and M_2. Equation (3.2) describes the rate of change with respect to time of the undifferentiated macrophages density. It increases because of migration and decreases by differentiating into M_1 and M_2 or by a constant emigration rate. It is assumed that M_0 migrate to the injury site proportionally to D up to a maximal constant rate, k_{max}, [1, 25]:

$$R_M = k_{max}\left(1 - \frac{M}{M_{max}}\right) D,$$

where $M = M_0 + M_1 + M_2$. The differentiation rates of M_0 into M_1 and M_2 are stimulated by the cytokines accordingly to a Hill Type II equations, respectively [59]:

$$G_1 = k_{01} \times \frac{c_1}{a_{01} + c_1}, \quad G_2 = k_{02} \times \frac{c_2}{a_{02} + c_2}.$$

Equation (3.3) describes the rate of change with respect to time of M_1, which increases when M_0 activate to M_1 and M_2 shift phenotype; and decreases by emigration and when M_1 shift phenotype. Similarly, Equation (3.4) describes the rate of change with respect to time of M_2. Equations (3.5) and (3.6) describes the rate of change with

respect to time of c_1 and c_2. Here, k_0, k_1, k_2, k_3, and k_4 are the constant rates of the cytokine productions and d_{c_1} and d_{c_2} are the cytokine constant decay rates. The inhibitory effects of the anti-inflammatory cytokines to the c_1 and c_2 production rates are modeled by the following functions [59]:

$$H_1 = \frac{a_{12}}{a_{12} + c_2}, \quad H_2 = \frac{a_{22}}{a_{22} + c_2}.$$

The equations (3.7)-(3.10) were introduced and described in Section 2.2.

3.3 Qualitative Analysis

The analysis of model is done by finding the equilibria and their corresponding stability properties. An equilibrium point of the model is denoted by the vector form $E\,(D, M_0, M_1, M_2, c_1, c_2, C_m, C_b, m_c, m_b)$ and it is found by setting the right-hand sides of the equations (3.1)-(3.10) equal to zero [42]. The model has three biologically meaningful equilibria: $E_0(0,0,0,0,0,0,0,0,m^*_{c_0}, m^*_{b_0})$, $E_1(0,0,0,0,0,c^*_2,0,C^*_b,0,p_{bs}/q_{bd})$, $E_2(0,0,0,0,0,c^*_2,C^*_m,C^*_b,m^*_c,p_{bs}/q_{bd})$. Their definitions, existence, and corresponding stability conditions are stated and proved below. The analysis is conducted using the Jacobian of the system at each equilibrium point, and finding its corresponding eigenvalues [42, 53].

Theorem 3.3.1. *The* $E_0(0,0,0,0,0,0,0,0,m^*_{c_0}, m^*_{b_0})$ *belongs to the set* $B = \{(0,0,0,0,0,0,0,0,m_c,m_b) : 0 \le m_c \le p_{cs}/q_{cd_1}, 0 \le m_b \le p_{bs}/q_{bd}\}$, *which is a local attractor set of the solution set given by System (3.1)-(3.10) if and only if* $k_{pm} \le d_m$ *and* $k_{pb} \le d_b$.

Proof of Theorem 3.3.1. The right-hand side functions of System (3.1)-(3.10) are continuous and bounded, since all model variables and parameters are positive. Hence, for each initial condition of the system, there is a unique solution [53]. Then,

as zero is a solution of the System (3.1)-(3.10) and by uniqueness of solution, all the solutions of the system with positive initial condition are positive [53].

Next, it will be proved that the hyperplane $A = \{(0,0,0,0,0,0,0,0,m_c,m_b) : m_c \geq 0, m_b \geq 0\}$ is an attractor set of the solutions of the system (3.1)-(3.10). There are two cases to consider based on the relation between the cells proliferation and differentiation rates.

First, let us examine the case when $k_{pm} < d_m$ and $k_{pm} < d_b$. The Jacobian matrix $J(E_0)$ is given by the following lower triangular block matrix

$$J(E_0) = \begin{pmatrix} J_1(E_0) & \mathbf{0} & \mathbf{0} \\ * & J_2(E_0) & \mathbf{0} \\ \mathbf{0} & * & J_3(E_0) \end{pmatrix},$$

where

$$J_1(E_0) = \begin{pmatrix} 0 & 0 & \mathbf{0} & 0 \\ k_{max} & -d_0 & \mathbf{0} & 0 \\ \mathbf{0} & \mathbf{0} & J_{11} & 0 \\ k_0 & 0 & * & -d_{c_1} \end{pmatrix}, \quad J_{11} = \begin{pmatrix} -d_1 - k_{12} & k_{21} \\ k_{12} & -d_2 - k_{21} \end{pmatrix}$$

$$J_2(E_0) = \begin{pmatrix} -d_{c_2} & k_3 & k_4 \\ 0 & -d_m + k_{pm} & 0 \\ 0 & d_m & -d_b + k_{pb} \end{pmatrix}, \quad J_3(E_0) = \begin{pmatrix} 0 & 0 \\ 0 & 0 \end{pmatrix}.$$

Therefore the corresponding characteristic polynomial associated with $J(E_0)$ is given by the product of the characteristic polynomials associated with each submatrix [52]:

$$p(\lambda) = \lambda^3 (\lambda + d_0)(\lambda + d_{c_1})(\lambda + d_{c_2})(\lambda + d_m - k_{pm})(\lambda + d_b - k_{pm})(\lambda^2 + a\lambda + b),$$

where $a = d_1 + d_2 + k_{12} + k_{21}$ and $b = k_{12}d_2 + k_{21}d_1 + d_1d_2$. The polynomial factor of order two of $p(\lambda)$ has the following two roots: $(-a \pm \sqrt{a^2 - 4b})/2$, which are

negative since $a^2 - 4b = (d_1 - d_2 + k_{12} - k_{21})^2 + 4k_{12}k_{21} > 0$ and $b > 0$. Therefore, the eigenvalues of $J(E_0)$ are negative for the variables M_0, M_1, M_2, c_1, c_2, C_m, and C_b, and are equal to zero for D, m_c, and m_b. Since $D'(t) \leq 0$ for all the variables in the system (3.1)-(3.10) and $(D^*, 0, 0, 0, 0, 0, 0, 0, 0, m_c, m_b)$ with $D^* \neq 0$ is not an equilibrium point, then the solutions of the system (3.1)-(3.8) are attracted to the set $A = \{(0, 0, 0, 0, 0, 0, 0, 0, 0, m_c, m_b) : m_c \geq 0, m_b \geq 0\}$. Equations (3.9) and (3.10) imply that $m_c' \leq 0$ and $m_b' \leq 0$ for all $m_c > p_{cs}/q_{cd_1}$ and $m_b > p_{bs}/q_{bd}$. Therefore, the set B is a local attractor set of A [53].

Next, let us consider the case when $k_{pm} = d_m$ and $d_b = k_{pb}$. Here, the eigenvalues of $J(E_0)$ are the same as above except those associated with C_m and C_b, which are equal to zero. Therefore, in this case, by considering the second order approximations of the right hand sides of Equations (3.7) and (3.8), instead of just the first order approximations, and using similar arguments as above, proves that the set B is a local attractor set of A. □

Theorem 3.3.2. *The equilibrium* $E_1(0, 0, 0, 0, 0, c_2^*, 0, C_b^*, 0, p_{bs}/q_{bd})$, *where*

$$C_b^* = K_{lb}(1 - d_b/k_{pb}), \quad c_2^* = a_{22}(-1 + \sqrt{1 + 4k_4 C_{b_1}^*/a_{22}d_{c_2}})/2,$$

exits when $k_{pb} > d_b$ *and is locally stable if and only if* $d_m \geq k_{pm}$.

Proof of Theorem 3.3.2. The Jacobian matrix corresponding to the point E_1 is given by the following lower triangular block matrix:

$$J(E_1) = \begin{pmatrix} J_1(E_1) & \mathbf{0} & \mathbf{0} \\ * & J_2(E_1) & \mathbf{0} \\ \mathbf{0} & * & J_3(E_1) \end{pmatrix},$$

where

$$J_1(E_1) = \begin{pmatrix} 0 & 0 & \mathbf{0} & 0 \\ k_{max} & -d_0 - G_2^* & \mathbf{0} & 0 \\ \mathbf{0} & * & J_{11} & \mathbf{0} \\ k_0 H_1^* & 0 & * & -d_{c_1} \end{pmatrix},$$

$$J_2(E_2) = \begin{pmatrix} -d_{c_2}\left(1 + \frac{c_{2_1}^*}{a_{22}+c_{2_1}^*}\right) & k_3 H_2^* & k_4 H_2^* \\ 0 & -d_m + k_{pm} & 0 \\ 0 & d_m & d_b - k_{pb} \end{pmatrix},$$

$$J_3(E_1) = \begin{pmatrix} -q_{cd_2} K_{lb}(1 - \frac{d_b}{k_{pb}}) & 0 \\ 0 & -q_{bd} K_{lb}(1 - \frac{d_b}{k_{pb}}) \end{pmatrix},$$

$G_2^* = \frac{k_{02} c_2^*}{a_{02}+c_2^*}$, $H_1^* = \frac{a_{12}}{a_{12}+c_2^*}$, $H_2^* = \frac{a_{22}}{a_{22}+c_2^*}$ and J_{11} is defined as in Theorem 3.3.1. Since all the eigenvalues of J_{11} are negative (Theorem 3.3.1) and $d_m - k_{pm} \geq 0$ and $k_{pb} > d_b$, then the eigenvalues of $J(E_1)$ are negative except the eigenvalues associated with D and C_m when $k_{pm} = d_m$, which are equal to zero. Therefore, E_1 is a locally stable node, since $D' \leq 0$ for all the variables of the system (3.1)-(3.10) and $C_m' \leq 0$ when $k_{pm} = d_m$. □

Theorem 3.3.3. *The equilibrium $E_2(0, 0, 0, 0, 0, c_2^*, C_m^*, C_b^*, m_c^*, p_{bs}/q_{bd})$ is locally stable if and only if $k_{pm} > d_m$, where $C_m^* = K_{lm}(1 - d_m/k_{pm})$, $C_b^* = K_{lb}(k_{pb} - d_b + \sqrt{(k_{pb} - d_b)^2 + 4k_{pb} d_m C_m^*/K_{lb}})/2k_{pb}$, $c_2^* = a_{22}(-1+\sqrt{1 + 4(k_3 C_m^* + k_4 C_b^*)/a_{22} d_{c_2}})/2$, and $m_c^* = p_{cs} C_m^*/(q_{cd1} C_m^* + q_{cd2} C_b^*)$.*

Proof of Theorem 3.3.3. The Jacobian matrix corresponding to the point E_2 is given by the following lower triangular block matrix:

$$J(E_2) = \begin{pmatrix} J_1(E_2) & \mathbf{0} & \mathbf{0} \\ * & J_2(E_2) & \mathbf{0} \\ \mathbf{0} & * & J_3(E_2) \end{pmatrix},$$

where $J_1(E_2)$ has the same expression as $J_1(E_1)$ defined in Theorem 3.3.2, but with the steady state variables defined by Theorem 3.3.3 and

$$J_2(E_2) = \begin{pmatrix} -d_{c_2}\left(1+\frac{c_2^*}{a_{22}+c_2^*}\right) & k_3H_2^* & k_4H_2^* \\ 0 & d_m - k_{mb} & 0 \\ 0 & d_m & -\sqrt{(d_b-k_{pb})^2 + 4\frac{k_{bp}d_mC_m^*}{K_{lb}}} \end{pmatrix},$$

$$J_3(E_2) = \begin{pmatrix} -q_{cd_1}C_m^* - q_{cd_2}C_b^* & 0 \\ 0 & -q_{bd}C_b^* \end{pmatrix},$$

$G_2^* = \frac{k_{02}c_2^*}{a_{02}+c_2^*}$, $H_1^* = \frac{a_{12}}{a_{12}+c_2^*}$, $H_2^* = \frac{a_{22}}{a_{22}+c_2^*}$ and J_{11} is defined in Theorem 3.3.1. Since all the eigenvalues of J_{11} are negative (Theorem 2.3.1) and $k_{pm} > d_m$, and all equilibrium variables and parameter values are positive, then all the eigenvalues of $J_1(E_2)$, $J_2(E_2)$, $J_3(E_2)$ are negative except for the eigenvalue associated to D which is equal to zero. Therefore, since $D' \leq 0$ for all the variable system, then E_2 is locally stable. □

In summary, the mathematical analysis of Model (3.1)-(3.10) revels that the number of equilibria and their corresponding existence and stability conditions are the same as Model (2.1)-(2.7), with the appropriate set of variables.

3.4 Numerical Results

The proposed new model (3.1)-(3.10) is used to study the importance of macrophages during the inflammatory and repair phases of the bone fracture healing process. First, a set of numerical simulation results is presented to compare the models (2.1)-(2.7) and (3.1)-(3.1). Second, a set of numerical simulations is performed to analyze the effects of different concentrations of anti-inflammatory cytokines on the fracture healing under numerous pathological conditions.

3.4.1 Comparison of Model (2.1)-(2.7) and Model (3.1)-(3.10)

The model (2.1)-(2.7) takes into account the regulatory effects of the immune system given by its phagocytes, M, and their released pro-inflammatory cytokines, c_1. The present mathematical model (3.1)-(3.10) extend the model (2.1)-(2.7) by incorporating the ability of the immune system to regulate the inflammation by its anti-inflammatory cytokines, c_2, production. Therefore, the two different phenotypes of macrophages M_1 and M_2 were separately incorporated in the model as c_1 is mainly delivery by M_1 and c_2 is mainly delivered by the M_2. The models (2.1)-(2.7) and (3.1)-(3.10) are compared to demonstrate the importance of the immune system as inflammatory-mediators involved in the bone fracture healing process. The same parameter values are used in both models (Table 5.1), with $k_{e_1} = 1$, $k_{e_2} = 2$, $k_{01} = 0.55$, $k_{01} = 0.55$, $k_{01} = 0.55 \times 10^{-6}$, $k_3 = 8 \times 10^{-6}$, $q_{bd} = 5 \times 10^{-8}$, and $d_M = 0.121$. Figure

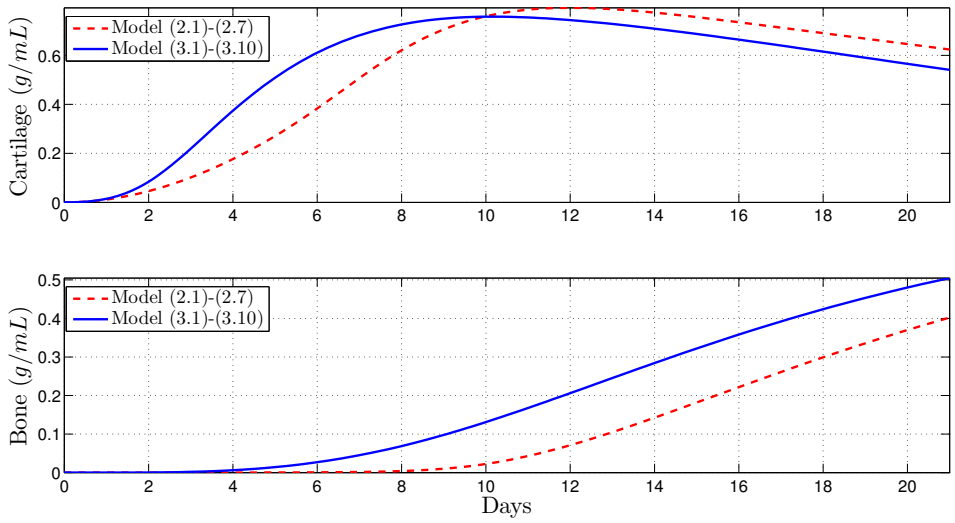

Figure 3.2. Comparison of tissues evolution in Model (2.1) - (2.7) and Model (3.1) - (3.10).

3.2 shows the numerical evolutions of the tissues' production when $D(0) = 5 \times 10^7$. In all simulations, we refer to fibrocartilage and woven bone as cartilage and bone, respectively. More cartilage production m_c and less bone production m_b is observed when the c_2 is not incorporated, model (2.1)-(2.7). Moreover, the model (3.1)-(3.10) is much more realistic as the m_b production is observed in the first week according to the experimental data.

3.4.2 Importance of macrophages during the bone fracture healing process

In this section, the mathematical model is used to investigate the regulatory effects of macrophages through their two phenotypes, M_1 and M_2, which deliver separately the pro- and anti-inflammatory cytokines. Therefore, the values of the parameters k_i, representing the secretion rates of c_i by M_i, $i = 1, 2$, are varied in the numerical simulations as compared to their base values from Table 5.1.

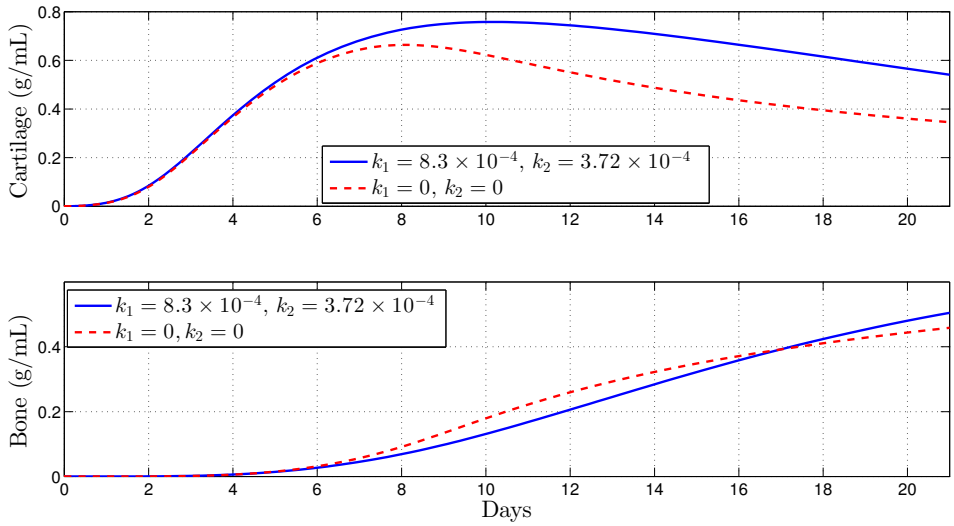

Figure 3.3. Tissues evolution when macrophages contribute to the healing process (solid line), $k_1, k_2 \neq 0$, and when they do not contribute to the healing process (dashed line), $k_1 = k_2 = 0$.

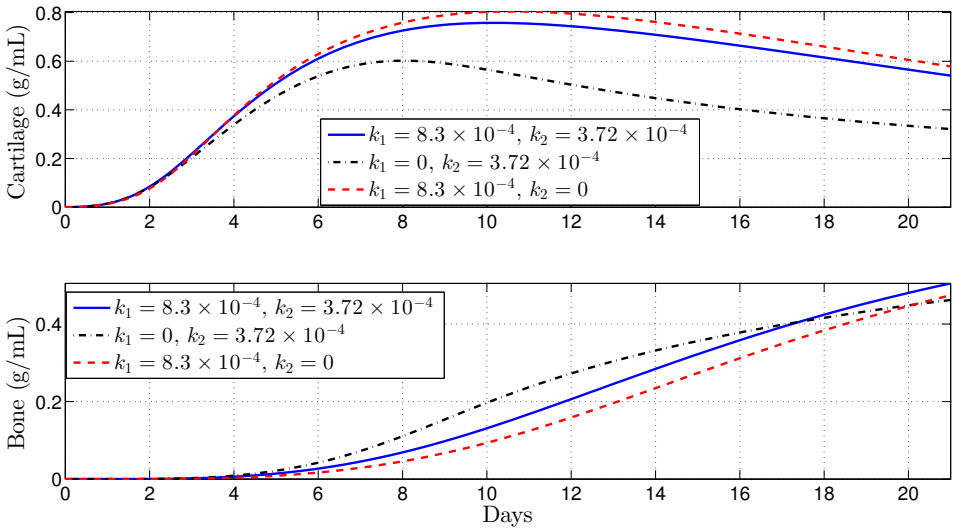

Figure 3.4. Tissues evolution when the alternatively activated macrophages, M_2, do not contribute to the healing process (dashed line), $k_2 = 0$, and when the classically activated macrophages, M_1, do not contribute to the healing process (dotted line), $k_1 = 0$.

Figure 3.3 shows that macrophages have a drastic effect on the short-term tissue dynamics during the healing process. In the presence of M_1 and M_2, fibrocartilage formation experiences an additional steady increase during the second week and beyond, while woven bone barely increases its density in the second week. The simulations presented in Figure 3.4 demonstrate the individual effects of the different phenotypes of macrophages and show that the alternatively activated macrophages M_2 have a more dominant contribution to the tissues production as compared to the classically activated macrophages M_1.

3.4.3 Immune-modulation therapeutic treatments of bone fractures

Treatments based on anti-inflammatory cytokines, such as the cytokine-specific agents that block the pro-inflammatory cytokines productions, have exhibited promis-

ing clinical results and have led to intense orthopedic research activities [9, 16, 18, 29, 38, 44, 49, 62]. In this section, a set of numerical simulations is presented to investigate the effect of the administrations of anti-inflammatory cytokines during the bone fracture healing process in healthy individuals and also in immune-compromised patients.

In healthy individuals, the administration of anti-inflammatory drugs is implemented for simple, two moderate, and severe fractures: $D(0) = 5\times10^6$, $D(0) = 2\times10^7$, $D(0) = 5 \times 10^7$, and $D(0) = 5 \times 10^8$, respectively. First, the administration of anti-inflammatory cytokines is done by increasing the initial concentration of c_2: $c_2(0) = 0$, 10 and 100 ng/mL. Second, anti-inflammatory cytokines is continuously administrate. It is modeled by increasing the anti-inflammatory cytokines production rate of the M_2, i.e., $k_2 = 3.72 \times 10^{-4}$, $2 \times 3.72 \times 10^{-4}$, $6 \times 3.72 \times 10^{-4}$ ng/mL.

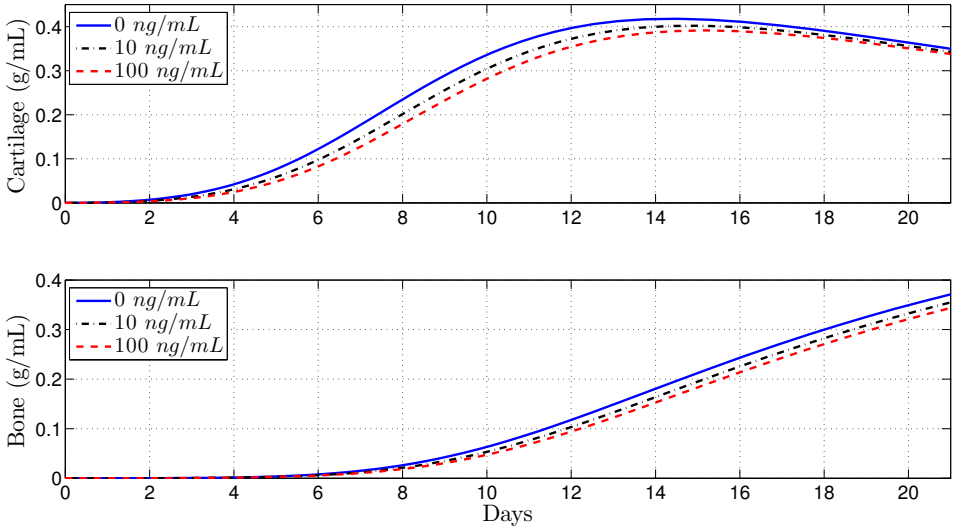

Figure 3.5. Tissues evolution in a simple fracture under different initial anti-inflammatory cytokines concentrations, $D(0) = 5 \times 10^6$.

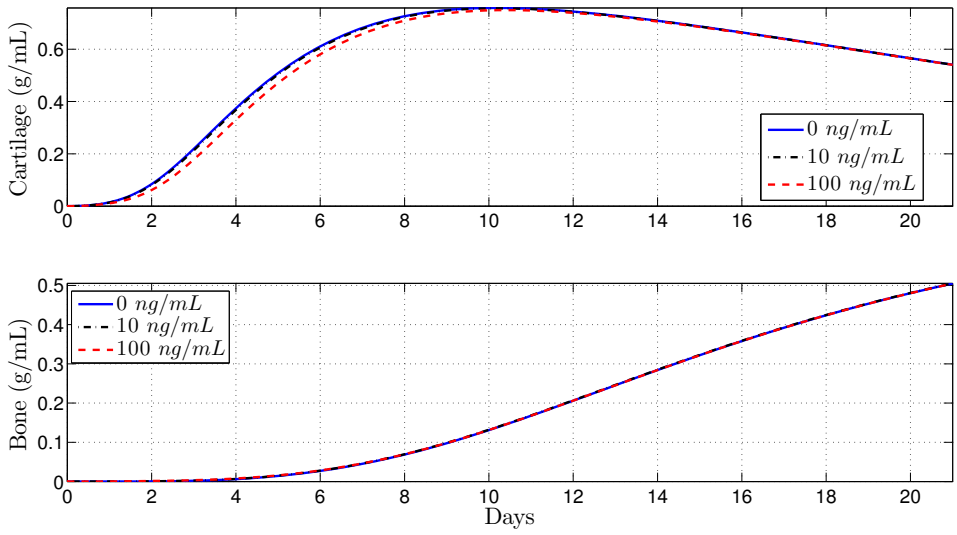

Figure 3.6. Tissues evolution in a moderate fracture under different initial anti-inflammatory cytokines concentrations, $D(0) = 5 \times 10^7$.

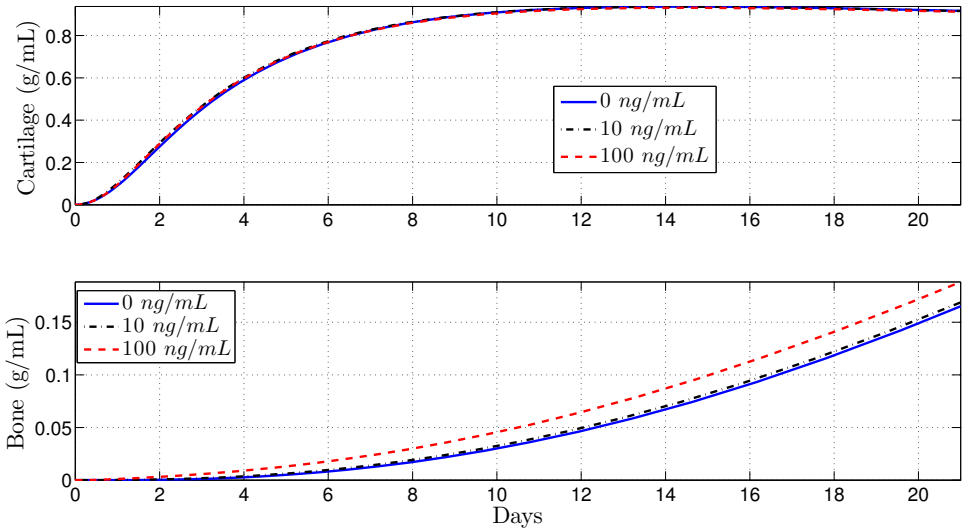

Figure 3.7. Tissues evolution in a severe fracture under different initial anti-inflammatory cytokines concentrations $D(0) = 5 \times 10^8$.

Figure 3.5 shows that in the simple fracture the administration of anti- inflammatory drugs at the beginning of the healing process inhibits the two tissue's

production. Figures 3.6 shows that the administration of c_2 at the beginning of the healing process in a moderate fractures, $D(0) = 5 \times 10^7$, does not lead to any drastic change in the two tissue's production. Figures 3.7 shows that the administration of c_2 at the beginning of the healing process in the severe fractures, $D(0) = 5 \times 10^8$, enhances the production of bone, while the cartilage production does not experience any change.

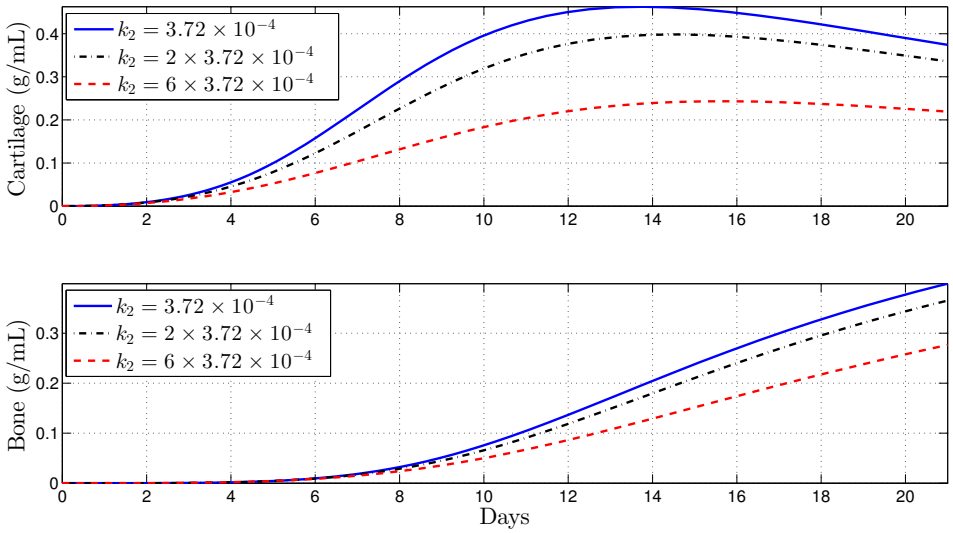

Figure 3.8. Tissues evolution in a simple fracture under a continuous administration of anti-inflammatory cytokines: $k_2 = 3.72 \times 10^{-4}$ (solid line), $k_2 = 2 \times 3.72 \times 10^{-4}$ (dotted-dashed line), $k_2 = 6 \times 3.72 \times 10^{-4}$ (dashed line).

Figure 3.8 shows that in the simple fracture the continuous administration of anti-inflammatory drugs drastically inhibit the two tissue's production. Figures 3.9 shows that the excessive administration of c_2 in a moderate fractures $D(0) = 2 \times 10^7$ inhibit the two tissue's production. Figures 3.10 shows that the administration of c_2 in the moderate fractures with $D(0) = 5 \times 10^7$ improves the bone tissue evolution while enhance a fast removal of the cartilage tissue. Figures 3.11 shows that the

administration of c_2 in the severe fractures enhances the production of bone, while the cartilage production does not change at all. Therefore, the administration of anti-inflammatory cytokines, c_2, has a negative effect in simple fracture, improves the tissue evolution in moderate fractures in a dose-dependent manner, and always improve the tissues evolution in severe fractures. In all the cases, the best anti-inflammatory administration strategy is the continuous administration rather than one administration at the begging of the healing process.

Next, the model is used to implement the administration of anti-inflammatory drugs under different pathological conditions. First, the following parameter values are used: $k_{e_1} = k_{e_2} = 0.5$ and $k_1 = 9 \times 10^{-3}$ to simulate bone fracture healing in aging individuals, since in this case, the macrophages phagocytic rate decreases and there is an increase of pro-inflammatory cytokine synthesis by M_1 [19, 31]. Second, $k_1 = 9 \times 10^{-3}$, $k_{pm} = 0.2$, $d_m = 0.5$, $k_{pb} = 0.16$, and $d_b = 0.15$ are used to simulate the

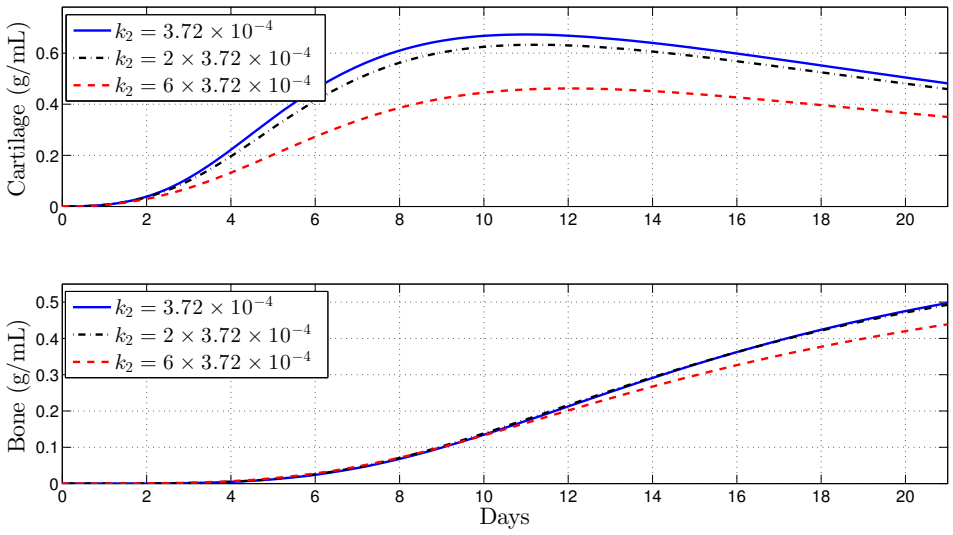

Figure 3.9. Tissues evolution in a moderate fracture, $D(0) = 2 \times 10^7$ under a continuous administration of anti-inflammatory cytokines: $k_2 = 3.72 \times 10^{-4}$ (solid line), $k_2 = 2 \times 3.72 \times 10^{-4}$ (dotted-dashed line), $k_2 = 6 \times 3.72 \times 10^{-4}$ (dashed line).

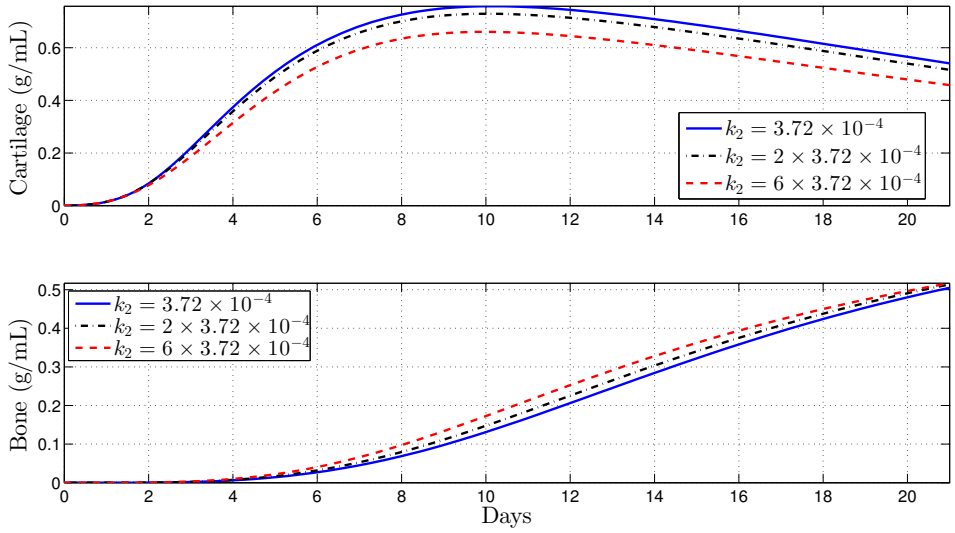

Figure 3.10. Tissues evolution in a moderate fracture, $D(0) = 5 \times 10^7$, under a continuous administration of anti-inflammatory cytokines: $k_2 = 3.72 \times 10^{-4}$ (solid line), $k_2 = 2 \times 3.72 \times 10^{-4}$ (dotted-dashed line), $k_2 = 6 \times 3.72 \times 10^{-4}$ (dashed line).

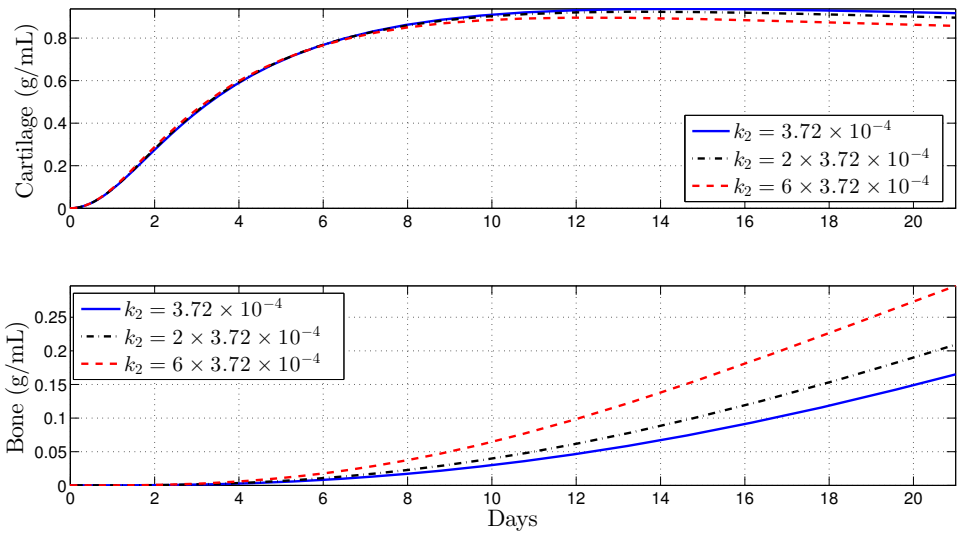

Figure 3.11. Tissues evolution in a severe fracture under a continuous administration of anti-inflammatory cytokines: $k_2 = 3.72 \times 10^{-4}$ (solid line), $k_2 = 2 \times 3.72 \times 10^{-4}$ (dotted-dashed line), $k_2 = 6 \times 3.72 \times 10^{-4}$ (dashed line).

healing process for a senile osteoporotic fracture, since in this case a high level of pro-inflammatory cytokines is observed and the MSCs and osteoblast functions decrease [31]. In both cases the the administration of anti-inflammatory drugs is modeled by increasing the anti-inflammatory cytokines production rate given by M_2, k_2. Figure 3.12 and 3.13 show that the administration of anti-inflammatory cytokines under the above two different pathological conditions always improve tissue's productions.

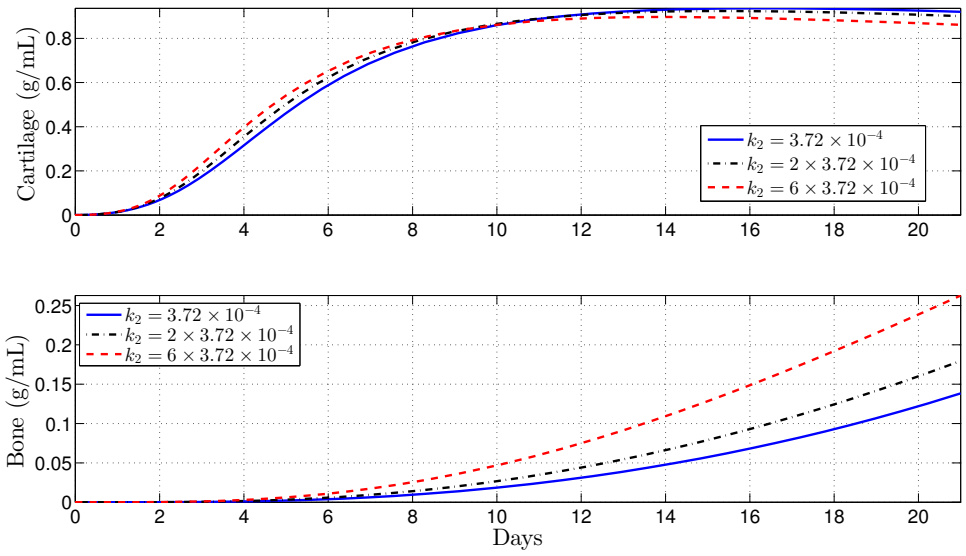

Figure 3.12. Tissues evolution in an advanced age fracture under different anti-inflammatory cytokines concentration.

3.5 Summary of the Results

In this chapter a new mathematical model was introduced to mathematically and numerically study the macrophage-mediated inflammation involved in the early stages of the bone fracture healing process: inflammatory and repair phases. The new model is an extension of the model developed in Chapter 2. Classically and

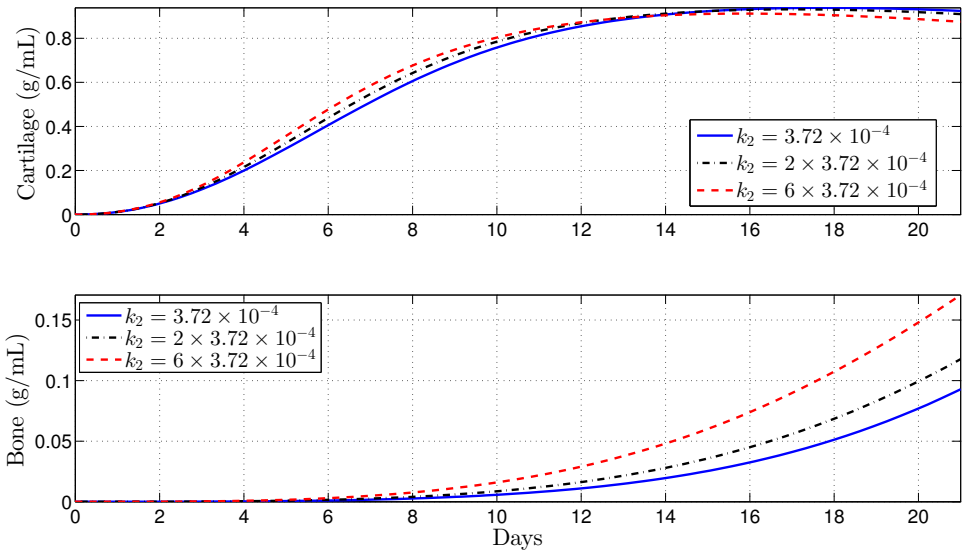

Figure 3.13. Tissues evolution in a senile osteoporotic fracture under different anti-inflammatory cytokines concentrations.

alternatively activated macrophages were incorporated in the model to study their capabilities to modulate and resolve the inflammation through their delivered pro- and anti-inflammatory cytokines. The resolution of the inflammation was assumed to be initiated with the activation of the macrophages into their classical phenotype. The classically activated macrophages deliver the pro-inflammatory cytokines, such as TNF-α, as they engulf debris. Then the alternatively activated macrophages, MSCs, and osteoblasts modulate the inflammation by releasing the anti-inflammatory cytokines, such as IL-10 and TGF-β. Finally, the alternatively activated macrophages remove the remaining debris. The new model also incorporated the different engulfing rates of activated macrophages, allowing a better understanding of the interplay between macrophages and tissue cells during the bone fracture healing process.

The mathematical analysis of Model (3.1)-(3.10) revels that the number of equilibria and their corresponding existence and stability conditions are the same as Model (2.1)-(2.7), with the appropriate set of variables.

The new model was used to study numerically the importance of macrophages during the early stages of tissue productions. It revealed that macrophages significantly improve the tissue productions with alternatively activated macrophages having the main affect on the process. Then, the model was also used to monitor the progression of the healing of a broken bone and to predict its final outcome under different types of treatments. In particular, the administration of anti-inflammatory drugs to improve the bone fracture healing process was numerically simulated. It was found that the administration of anti-inflammatory cytokines fails to accelerate the healing process in simple fractures, while it accelerates the healing process in moderate fractures depending on the cytokine concentrations, and always improves the healing process in severe fractures. Such results have been also clinically observed when corticosteroids and nonsteroidal anti-inflammatory drugs (NSAIDs) are administered in bone fractures [38].

Therefore, based on the model findings, the concentration of debris must be carefully considered when administering anti-inflammatory drugs to enhance the fracture healing process [23].

CHAPTER 4

MODELING THE EFFECTS OF THE IMMUNE SYSTEM ON BONE FRACTURE HEALING

In this chapter the model (3.1)-(3.10) is extended by incorporating the chondrocytes and the growth factors. This extension leads to a more realistic model by incorporating the two distinct functions of MSCs and chondrocytes during the healing process: chondrocytes synthesize the cartilage [12] and the TGF-β, and MSCs release the IL-10 but not the TGF-β [11, 26]. Moreover, the MSCs differentiation into chondrocytes or osteoblasts is stimulated by growth factors [6, 26, 56]. Furthermore, this extension allows improvements in modeling the immune system functions during the bone fracture healing process. Both the immune system and the MSCs modulate the inflammation [29, 27] by the anti-inflammatory cytokine production [28, 49]. Both the immune cells, and the osteoblasts and chondrocytes release the growth factors [11]. Growth factors also suppress the pro-inflammatory cytokine production [1], and regulate the MSCs differentiation [3, 26].

4.1 Modeling Assumptions

The modeling assumptions follow the assumptions provided in Chapters 2 and 3 with the incorporation of the chondrocytes (C_c) and a generic growth factor (c_3), such as the TGF-β. The biological system interactions are depicted in Figure 4.1. In the flow diagram, the cells and cellular dynamics are represented by the circular shapes and solid arrows. The molecular concentrations and their production/decay are represented by the octagonal shapes and dashed arrows. Growth factors, pro- and

anti-inflammatory cytokines activation/inhibition effects on the cellular functions are represented by the dotted arrows. Removal of debris and the negative effect among the variables are represented by the dot-ending dotted arrows. It is assumed that the chondrocytes are derived from MSCs, proliferate, deposit the fibrocartilage, and die [12]. C_c experience a logistic growth, and hypertrophic chodrocytes (necrotic chondrocytes) are replaced by osteoblasts [2, 12]. It is assumed that the chondrocyte replacement is regulated by the growth factor c_3 [2]. It is also assume that the c_3 activate and regulate the C_m differentiation into C_b and C_c [26, 11]. It is assume that the c_3 is delivered by alternative activated macrophages, osteoblasts, and chondrocytes [11]. It is also assume that the anti-inflammatory cytokines c_2 is delivered by the M_2 and the C_m, and both c_2 and c_3 inhibit the c_1 production [1, 29].

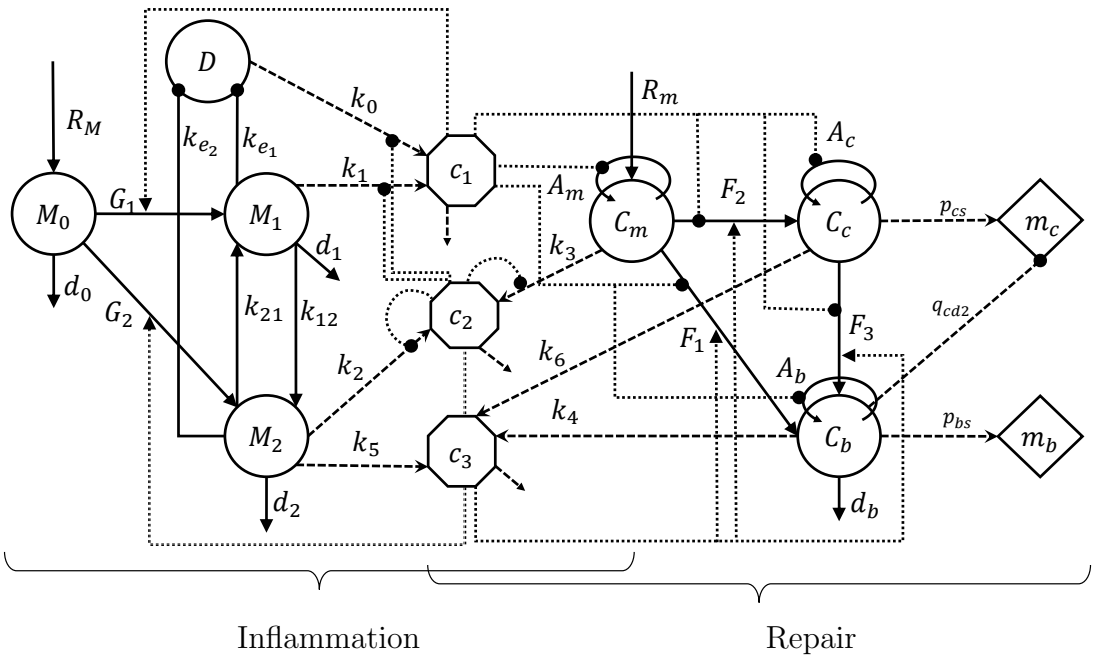

Figure 4.1. Flow diagram of the cellular and molecular dynamics during the inflammatory and repair phases of the bone fracture healing process.

4.2 Model Formulation

Following the outlined biological assumptions and the flow diagram given in Figure 4.1 by using a mass-action system yields the resulting system of equations:

$$\frac{dD}{dt} = -R_D(k_{e_1}M_1 + k_{e_2}M_2) \tag{4.1}$$

$$\frac{dM_0}{dt} = R_M - G_1M_0 - G_2M_0 - d_0M_0 \tag{4.2}$$

$$\frac{dM_1}{dt} = G_1M_0 + k_{21}M_2 - k_{12}M_1 - d_1M_1 \tag{4.3}$$

$$\frac{dM_2}{dt} = G_2M_0 + k_{12}M_1 - k_{21}M_2 - d_2M_2 \tag{4.4}$$

$$\frac{dc_1}{dt} = H_1(k_0D + k_1M_1) - d_{c_1}c_1 \tag{4.5}$$

$$\frac{dc_2}{dt} = H_2(k_2M_2 + k_3C_m) - d_{c_2}c_2 \tag{4.6}$$

$$\frac{dc_3}{dt} = H_3(k_4C_b + k_5M_2 + k_6C_c) - d_{c_3}c_3 \tag{4.7}$$

$$\frac{dC_m}{dt} = (R_m + A_mC_m)\left(1 - \frac{C_m}{K_{lm}}\right) - F_1C_m - F_2C_m \tag{4.8}$$

$$\frac{dC_c}{dt} = A_cC_c\left(1 - \frac{C_c}{K_{lc}}\right) + F_2C_m - F_3C_c \tag{4.9}$$

$$\frac{dC_b}{dt} = A_bC_b\left(1 - \frac{C_b}{K_{lb}}\right) + F_1C_m + F_3C_c - d_bC_b \tag{4.10}$$

$$\frac{dm_c}{dt} = (p_{cs} - q_{cd_1}m_c)C_c - q_{cd_2}m_cC_b \tag{4.11}$$

$$\frac{dm_b}{dt} = (p_{bs} - q_{bd}m_b)C_b. \tag{4.12}$$

Equation (4.7) describes the rate of change with respect to time of c_3. It increases by the M_2, C_c, and C_b production and it decreases by degradation. The production of c_3 is modeled with the following equation [2]:

$$H_3 = \frac{c_3}{c_3 + a_{33}}.$$

Equation (4.9) describes the rate of change with respect to time of C_c. It increases when MSCs differentiate into chondrocytes or when chondrocytes proliferate, and it decreases by apoptosis. Necrosis of C_c is regulated by the c_1 and c_3 as follow [2]:

$$F_3 = d_c \times \frac{a_{cb_1}}{a_{cb_1} + c_1} \times \frac{c_3}{a_{cb} + c_3}.$$

Chondrocyte replacement is modeled with the $F_3 C_c$ term, which is incorporated in the Equation (4.10). The differentiation rates of C_m into C_b and C_c is activated by the c_3 and regulated by c_1 accordingly to the following functions [2, 27]:

$$F_1 = d_m \times \frac{a_{mb_1}}{a_{mb_1} + c_1} \times \frac{c_3}{a_{mb} + c_3}, \quad F_2 = d_{mc} \times \frac{a_{mc_1}}{a_{mc_1} + c_1} \times \frac{c_3}{a_{mc} + c_3}.$$

The differentiation term of C_m into C_c, i.e., $F_2 C_m$, is also incorporated in the Equation (4.8). The remaining equations and terms of Model (4.1)-(4.12) are explaining in Chapters 2 and 3.

4.3 Qualitative Analysis

The analysis of model is done by finding the equilibria and their corresponding stability properties. An equilibrium point of the model is denoted by the vector form $E\,(D, M_0, M_1, M_2, c_1, c_2, c_3, C_m, C_c, C_b, m_c, m_b)$ and it is found by setting the right-hand sides of the equations (4.8) - (4.12) equal to zero [42]. The model has eleven equilibria: $E_0(0,0,0,0,0,0,0,0,,0,0,m^*_{c_0}, m^*_{b_0})$, $E_1(0,0,0,0,0,0,0,0,0,0,K_{lb}(1-d_b/k_{pb}),0,p_{bs}/q_{bd})$, $E_2(0,0,0,0,0,0,0,0,0,K_{lc},0,p_{cs}/q_{cd_1},m^*_{b_0})$, $E_3(0,0,0,0,0,0,0,0,0,K_{lc}, K_{lb}(1-d_b/k_{pb}),m^*_c,p_{bs}/q_{bd})$, $E_4(0,0,0,0,0,c^*_2,0,K_{lm},0,0,m^*_{c_0},m^*_{b_0})$, $E_5(0,0,0,0,0,c^*_2, 0,K_{lm},0,K_{lb}(1-d_b/k_{pb}),0,p_{bs}/q_{bd})$, $E_6(0,0,0,0,0,c^*_2,0,K_{lm},K_{lc},0,p_{cs}/q_{cd1},m^*_{b_0})$, E_7 $(0,0,0,0,0,c^*_2,0,K_{lm},K_{lc},K_{lb}(1-d_b/k_{pb}),m^*_c,p_{bs}/q_{bd})$, $E_8(0,0,0,0,0,0,c^*_3,0,0,K_{lb}(1-d_b/k_{pb}),0,p_{bs}/q_{bd})$, $E_9(0,0,0,0,0,0,0,c^*_3,0,C^*_c,C^*_b,m^*_c,p_{bs}/q_{bd})$, $E_{10}(0,0,0,0,0,0,c^*_2,c^*_3,C^*_m, C^*_c,C^*_b,m^*_c,p_{bs}/q_{bd})$.

Their definitions, existence, and corresponding stability conditions are stated and proved below. The analysis is conducted using the Jacobian of the system at each equilibrium point, and finding its corresponding eigenvalues [42, 53].

Theorem 4.3.1. *Suppose that* $m_{c_0}^* \geq 0$, $m_{c_0}^* \geq 0$, $c_2^* = a_{22}(-1+\sqrt{1+4k_3K_{lm}/a_{22}d_{c_2}})/2$, *and* $m_c^* = p_{cs}K_{lc}/(q_{cd1}K_{lc}+q_{cd2}K_{lb}(1-d_b/k_{pb}))$. *Then the* $E_0(0,0,0,0,0,0,0,0,0,0, m_{c_0}^*, m_{b_0}^*)$, $E_2(0,0,0,0,0,0,0,0,0,K_{lc},0,p_{cs}/q_{cd_1},m_{b_0}^*)$, *and* $E_4(0,0,0,0,0,0,c_2^*,0,K_{lm},0,0, m_{c_0}^*, m_{b_0}^*)$ *exist for all the parameter values, and the* $E_1(0,0,0,0,0,0,0,0,0,0,K_{lb}(1-d_b/k_{pb}),0,p_{bs}/q_{bd})$, $E_3(0,0,0,0,0,0,0,0,0,K_{lc},K_{lb}(1-d_b/k_{pb}),m_c^*,p_{bs}/q_{bd})$, *and* $E_5(0,0,0,0,0,c_2^*,0,K_{lm},0,K_{lb}(1-d_b/k_{pb}),0,p_{bs}/q_{bd})$ *exist when* $k_{pb} > d_b$. *Furthermore, the* E_i, $i = 0,1,2,3,4,5$, *are unstable.*

Proof of Theorem 4.3.1. From the hypotheses all the steady state variables of each E_i, $i = 0,1,2,3,4,5$, are non-negative. Hence all of them exist. The Jacobian matrix of $J(E_i)$, $i = 0,1,2,3,4,5$, is given by the following lower triangular block matrix:

$$J(E_i) = \begin{pmatrix} J_1(E_i) & \mathbf{0} & \mathbf{0} \\ * & J_2(E_i) & \mathbf{0} \\ \mathbf{0} & * & J_3(E_i) \end{pmatrix},$$

where $J_1(E_i)$ is equal to $J_1(E_0)$ defined in Theorem 3.3.1, $J_3(E_i)$ is a two by two triangular matrix, similar to those defined in Chapter 3, and

$$J_2(E_i) = \begin{pmatrix} * & 0 & * & 0 & 0 \\ 0 & * & 0 & 0 & 0 \\ 0 & * & k_{pm} & 0 & 0 \\ 0 & * & 0 & * & 0 \\ 0 & * & 0 & 0 & * \end{pmatrix} \quad or \quad J_2(E_j) = \begin{pmatrix} * & 0 & * & 0 & 0 \\ 0 & * & 0 & 0 & 0 \\ 0 & * & * & 0 & 0 \\ 0 & * & 0 & k_{pc} & 0 \\ 0 & * & 0 & 0 & * \end{pmatrix}$$

for $i = 0,1,2,3$ and $j = 4,5$. Hence, $J_2(E_i)$, $i = 0,1,2,3,4,5$ has at least one positive eigenvalue. Therefore, E_i is unstable, for all $i = 0,1,2,3,4,5$ [42]. □

Theorem 4.3.2. *The* $E_6(0,0,0,0,0,c_2^*,0,K_{lm},K_{lc},0,p_{cs}/q_{cd1},m_{b_0}^*)$ *, where* $c_2^* = a_{22}(-1+\sqrt{1+4k_3K_{lm}/a_{22}d_{c_2}})/2$ *exists for all the parameter values and it belongs to the set* $B = \{(0,0,0,0,0,0,0,0,0,0,p_{cs}/q_{cd_1},m_b) : 0 \leq m_b \leq p_{bs}/q_{bd}\}$*, which is a local attractor set of the solution set given by System (4.1)-(4.12) if and only if* $k_{pb} \leq d_b$ *and* $k_6K_{lc}/d_{c_3} < a_{33}$*.*

Proof of Theorem 4.3.2. The proof is similar to the presented proof provided in Theorem 3.3.1 by using the follow matrices and the corresponding value of c_2^*:

$$J(E_2) = \begin{pmatrix} J_1(E_2) & \mathbf{0} & \mathbf{0} \\ * & J_2(E_2) & \mathbf{0} \\ \mathbf{0} & * & J_3(E_2) \end{pmatrix},$$

where $J_1(E_2)$ is equal to $J_1(E_0)$ defined in Theorem 3.3.1, and

$$J_2(E_2) = \begin{pmatrix} -d_{c_2}\left(1+\frac{c_{22}^*}{c_{22}^*+a_{22}}\right) & 0 & k_3H_2* & 0 & 0 \\ 0 & -d_{c_3}+k_6K_{lc}/a_{33} & 0 & 0 & 0 \\ 0 & * & -k_{pm} & 0 & 0 \\ 0 & * & 0 & -k_{cp} & 0 \\ 0 & * & 0 & 0 & -d_b+k_{pb} \end{pmatrix},$$

$$J_3(E_2) = \begin{pmatrix} -q_{cd_1}K_{lc} & 0 \\ 0 & 0 \end{pmatrix}.$$

□

Theorem 4.3.3. *The* $E_7(0,0,0,0,0,c_2^*,0,K_{lm},K_{lc},C_b^*,m_c^*,p_{bs}/q_{bd})$*, where* $C_b^* = K_{lb}(1-d_b/k_{pb})$*, and* $c_2^* = a_{22}(-1+\sqrt{1+4k_3K_{lm}/a_{22}d_{c_2}})/2$ *exists when* $k_{pb} > d_b$ *and it is stable when* $(k_4C_b^*+k_6K_{lc})/d_{c_3} > a_{33}$*.*

Proof of Theorem 4.3.3. The proof is similar to the proof presented in Theorem 3.3.2 by using the bellow matrix:

$$J_2(E_7) = \begin{pmatrix} -d_{c_2}\left(1+\frac{c_2^*}{c_2^*+a_{22}}\right) & 0 & k_3H_2^* & 0 & 0 \\ 0 & -d_{c_3}+\frac{k_4C_b^*+k_6K_{lc}}{a_{33}} & 0 & 0 & 0 \\ 0 & * & -k_{pm} & 0 & 0 \\ 0 & * & 0 & -k_{pc} & 0 \\ 0 & * & 0 & 0 & -d_b+k_{pb} \end{pmatrix}.$$

□

Theorem 4.3.4. *The* $E_8(0,0,0,0,0,0,c_3^*,0,0,C_b^*,0,p_{bs}/q_{bd})$*, where* $C_b^* = K_{lb}(1 - d_b/k_{pb})$*,* $c_3^* = k_4C_b^*/d_{c_3} - a_{33}$ *exists when* $k_{pb} > d_b$ *and* $k_4C_b^*/d_{c_3} > a_{33}$*. Furthermore,* E_8 *is stable if and only if* $d_m > k_{pb}$*,* $d_c > k_{pc}$*, and* $c_3^* > max\{a_{mb}k_{pm}/(d_m - k_{pm}), a_{cb}k_{pc}/(d_c - k_{pc})\}$*.*

Proof of Theorem 4.3.4. The proof is similar to the proof given in Theorem 3.3.2 by using the bellow matrix:

$$J_2(E_8) = \begin{pmatrix} -d_{c_2} & 0 & k_3 & 0 & 0 \\ 0 & -d_{c_3}\left(\frac{a_{33}}{c_3^*+a_{33}}\right) & 0 & 0 & * \\ 0 & 0 & k_{pm}-F_1^* & 0 & 0 \\ 0 & 0 & F_2^* & k_{pc}-F_3^* & 0 \\ 0 & 0 & F_1^* & F_3^* & -d_b+k_{pb} \end{pmatrix},$$

where F_i^* are values of the function F_i at c_3^*, $i = 1, 2, 3$. □

We were not be able to determine the stability conditions for the equilibria E_9 and E_{10} due to the complexity on the Jacobian Matrices given by $c_3 \neq 0$. However in Section 4.5 the model (4.1)-(4.12) is simplified by only consider the interaction among the c_3, C_m, C_b. These model simplification leads a better understanding on the

regulatory effects of c_3 during bone fracture repair, and allows to study the stability conditions for the equilibria when $c_3 \neq 0$ and at least two forming cells, i.e. C_m, C_c or C_b, are not zero, that are similar to the states of E_9 and E_{10}. Table 4.3 summarizes the existence and stability conditions for the equilibrium E_i, $i = 0, \ldots, 8$, of Model (4.1)-(4.12).

Equilibria	**Existence**	**Stability**
$E_0, \cdots, E_5$	$m^*_{c_0}, m^*_{b_0} \geq 0$	unstable
E_6	always	$k_{pb} < d_b$, $k_6 K_{lc}/d_{c_3} < a_{33}$
E_7	$k_{pb} > d_b$	$k_4 C^*_b + k_6 K_{lc}/d_{c_3} > a_{33}$
E_8	$k_{pb} > d_b$, $k_4 C^*_b/d_{c_3} > a_{33}$	$c^*_3 > \max\{a_{mb}k_{pm}/(d_m - k_{pm}), a_{cb}k_{pc}/(d_c - k_{pc})\}$

The steady-states E_0 and E_4 exist when the two tissue densities are non-negative values, i.e., $m^*_{c_0}, m^*_{b_0} \geq 0$. These equilibria represent a nonunion healing. Since in both cases, the inflammation is resolved since the first five entries of E_0 and E_4 are zero; however, the repair process has failed since the chondrocytes, osteoblasts, and osteoclasts have died out before the beginning of the remodeling process. Hence, the tissue densities, $m^*_{c_0}$ and $m^*_{b_0}$, can be any two positive values smaller than their maximal densities, p_{cs}/q_{cd1} and p_{bs}/q_{bd}, respectively (see Theorem 4.3.1).

The steady-states E_1, E_5, and E_8 exist when the proliferation rate of the osteoblasts is bigger than their differentiation rate, i.e., $k_{pb} > d_b$ (see Theorems 4.3.1 and 4.3.4). Furthermore, it is also required that the growth factor production rate over the growth factor degradation rate is bigger than the half saturation of the growth factor, i.e., $k_4 C^*_b/d_{c_3} > a_{33}$, for the existence of E_8, and $m^*_{c_0}, m^*_{b_0} \geq 0$ for the existence of E_1 and E_5. The three equilibria, E_1, E_5, and E_8, represent potential successful outcomes of the bone fracture healing process. Since in these cases, the inflammation is resolved, the fibrocartilage is completely removed from the repair

site, and the woven bone has achieved its maximal density. However in the equilibria E_1 and E_5 the growth factor concentration are degraded completely, while in E_8 it remains in a positive concentration. Since in healthy individuals, the concentration of growth factors within the bone is positive [2], the steady-state E_1 and E_5 represent an unsuccessful repair, while the E_8 represents a successful outcome. According to the stability condition of E_8, a broken bone with positive osteoblast and growth factor densities, will eventually evolve to a successful healing outcome, i.e., E_8, when the differentiation rate of the MSCs into the osteoblasts is bigger than the MSCs proliferation rate, i.e., $d_m > k_{pm}$, and the apoptotic rate of the chondrocytes is bigger than chondrocyte proliferation rate, i.e., $d_c > k_{pc}$, and the growth factor concentration is above to the concentration quantity: $\max\{a_{mb}k_{pm}/(d_m - k_{pm}), a_{cb}k_{pc}/(d_c - k_{pc})\}$.

The steady-states E_2 exists when $m^*_{b_0} > 0$, and E_6 exists for all parameter values (see Theorems 4.3.1 and 4.3.2). These two equilibria represent a nonunion healing. Since in both cases, the inflammation is resolved; however, the repair process has failed since the osteoblasts, and osteoclasts have died out before the beginning of the remodeling process, and the chondrocyte has achieved its maximal density. Hence, the woven bone density, $m^*_{b_0}$, can be any positive values smaller than their maximal densities, p_{bs}/q_{bd}, and the fibrocartilage achieves its maximal density, p_{cs}/q_{cd1}.

The equilibria E_3, E_7, E_9, and E_{10} represent delayed union or no-union outcomes. Since in this case the inflammation is resolved; however the osteoblasts and hence the osteoclasts have fail to remove the cartilage density. Furthermore, these equilibria describe the endochondral ossification, where both the fibrocartilage and woven bone are constantly produced by the chondrocytes and osteoblasts, respectively.

4.4 Numerical Results

The proposed new model (4.1)-(4.12) is used to study the importance of macrophages during the inflammatory and repair phases of the bone fracture healing process, which occur within the first 21 days after trauma [27, 64]. It is also used to investigate the evolution of a broken bone under normal and pathological conditions and to investigate the effects of different concentrations of growth factors on the fracture healing under numerous pathological conditions.

4.4.1 Comparison of Model (4.1)-(4.12) with existing models

Several mathematical models have been developed to have a better understanding of the bone fracture healing process. However, none of them have incorporated the debris density and the immune system functions during the the bone fracture healing process [13, 32]. In this section the model (4.1)-(4.12) is used to demonstrate the importance of the immune system during the inflammatory and repair phases of bone fracture healing process.

First, to demonstrate the importance of the immune system during the bone fracture healing process the initial conditions of the model (4.1)-(4.12) for the debris density is set to $D(0) = 0$ and $D(0) = 5 \times 10^7$. When $D(0) = 0$, the model (4.1)-(4.12) does not incorporate the immune system variables: macrophages and their synthesized molecular factors. Hence the model (4.1)-(4.12) is reduced to the proposed model developed in [2].

Figure 4.2 shows the numerical evolutions of the tissues' production for the Model (4.1)-(4.12) when $D(0) = 0$ (dashed lines) and when $D(0) = 5 \times 10^7$ (solid lines), with both $C_m(0) = 1000$, $c_3(0) = 20$, and the other initial conditions are set to be equal to zero. The production of cartilage m_c and bone m_b given by the present model with $D(0) = 5 \times 10^7$ is much more realistic than the production given

by the same model with $D(0) = 0$, since, according to the experimental data, the cartilage production peaks to its maximal density about 10-12 days after trauma and a significant bone tissue production is observed after the second week [45].

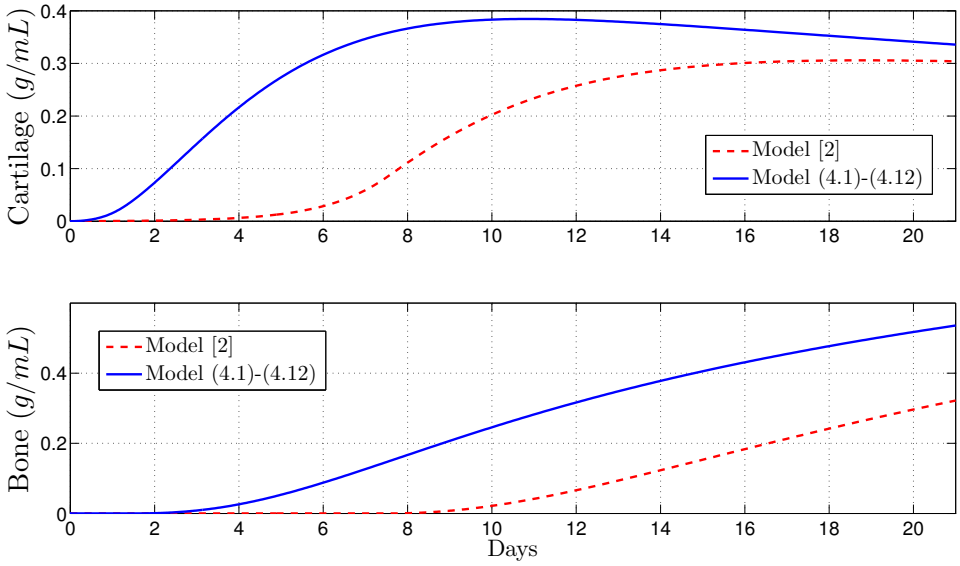

Figure 4.2. Comparison of tissues evolution for Model (4.1)-(4.12) when the immune system and debris are modeled (solid lines) and when the immune system and debris are not modeled (dashed lines).

Second, the models (3.1)-(3.10) and (4.1)-(4.12) are compared, both models incorporate the immune system functions during the bone fracture healing process. However, the model (4.1)-(4.12) carefully incorporate the c_3 and the C_c, where c_3 activate and direct the differentiation of C_m into C_b, and C_c. Furthermore, C_c synthesize the m_c. In addition, the incorporation of c_3 allows to carefully model the immune system molecular productions during the bone repair process: the pro- and anti-inflammatory cytokines, and growth factors. The same parameter values are used in both models (Table 5.1).

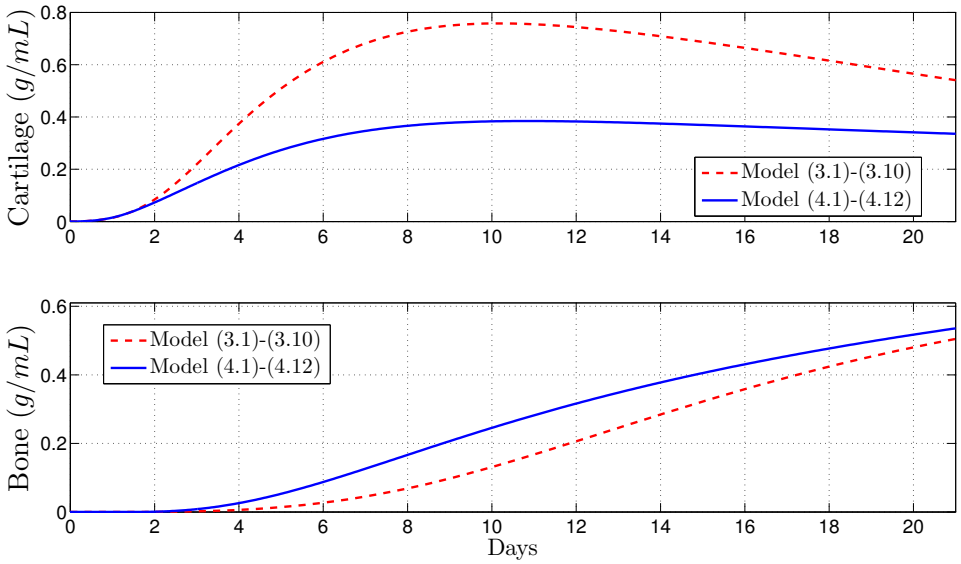

Figure 4.3. Comparison of tissues evolution in Model (3.1)-(3.10) and Model (4.1)-(4.12).

Figure 4.3 shows the numerical evolution of the tissues' production of the two compared models. There is less and slower fibrocartilage formation in model (4.1)-(4.12) than in Model (3.1)-(3.10). In model (4.1)-(4.12), there is more bone tissue production after the first week, than in Model (3.1)-(3.10). Therefore, the model (4.1)-(4.12) reveals that the chondrocytes formation is also a slow process.

4.4.2 Importance of macrophages during the bone fracture healing process

In this section, the mathematical model is used to investigate the effects of macrophages during the inflammatory and repair phases of the bone fracture healing process. The major contribution of macrophages to fracture healing is through their phagocytic capabilities and from their delivered molecular factors: pro and anti-inflammatory cytokines and the TFG-β at the repair site. Therefore, the values of

the parameters k_i, representing the secretion rates of c_i by M_i, $i = 1, 2, 5$, are varied in the numerical simulations as compared to their base values from Table 5.1.

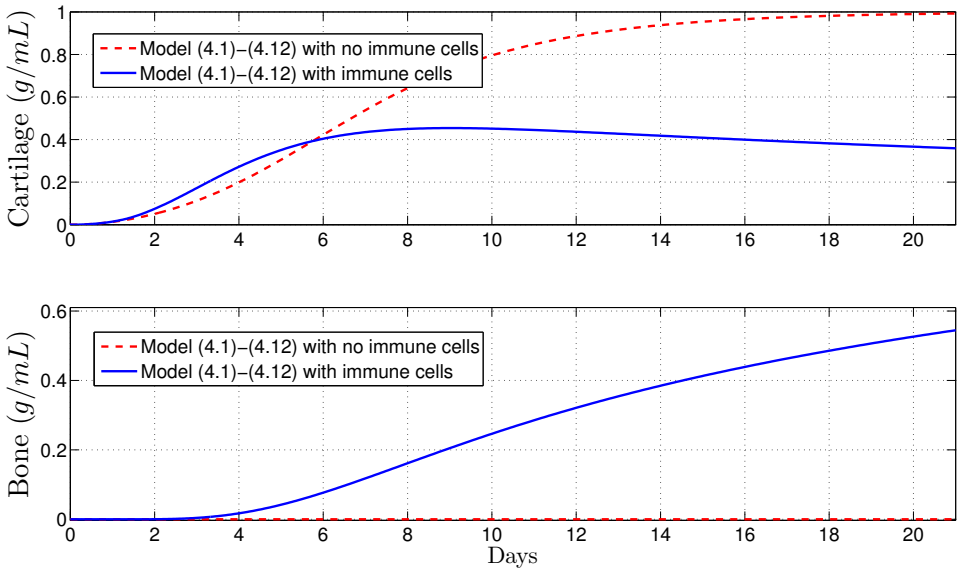

Figure 4.4. Tissues evolution when macrophages contribute to the healing process (solid line), $k_{max} = 0.015$, and when they do not contribute to the healing process (dashed line), $k_{max} = 0$.

Figure 4.4 shows that macrophages determine the successful fracture healing outcome. In the absence of macrophages there is no woven bone formation, while only fibrocartilage formation is observed. Furthermore, the fibrocartilage experiences an additional steady, doubling its density after the second week and beyond. Figure 4.5 shows that macrophages have a drastic effect on the short-term tissue dynamics during the healing process. In the presence of M_1 and M_2, fibrocartilage formation is less than doubles in about 1 week, while woven bone experiences an additional steady increase during the same period and beyond. The simulations presented in Figure 4.6 demonstrate the individual effects of the different phenotypes of macrophages and show

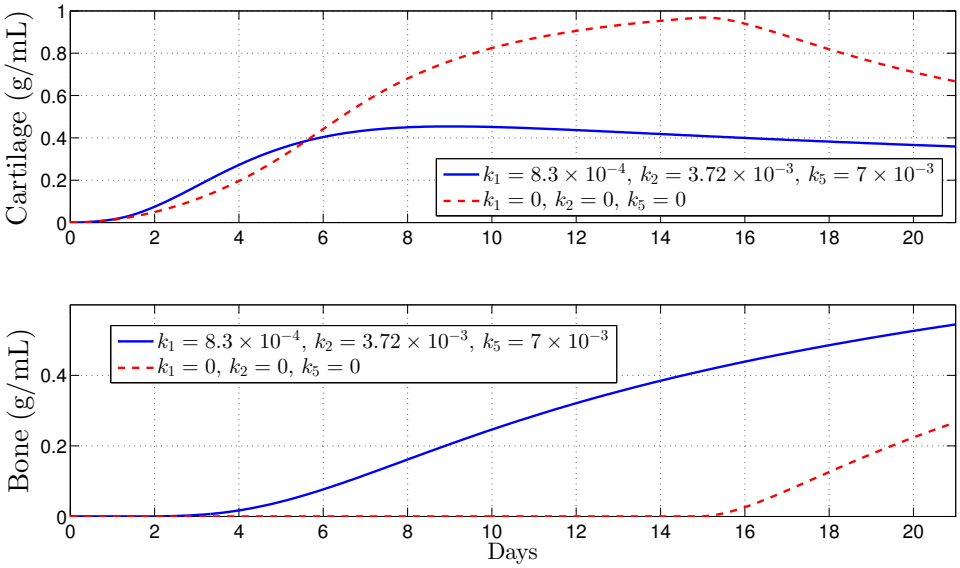

Figure 4.5. Tissues evolution when macrophages contribute to the healing process (solid line), $k_1, k_2, k_5 \neq 0$, and when they do not contribute to the healing process (dashed line), $k_1 = k_2 = k_5 = 0$.

that the alternatively activated macrophages M_2 have a more dominant contribution to the tissues production as compared to the classically activated macrophages M_1.

4.4.3 Administration of anti-inflammatory cytokines and growth factors during the healing of a broken bone

Treatments based on growth factors have exhibited promising clinical results to enhance bone fracture healing process [9, 16, 18, 29, 38, 44, 62, 49]. In this section, a set of numerical simulations is presented to investigate the effect of the administrations of growth factors during the healing process in healthy individuals. In healthy individuals, the administration of growth factor drugs is implemented for a moderate and severe fractures, $D(0) = 5 \times 10^7$ and $D(0) = 5 \times 10^8$, respectively.

Figure 4.7 shows that the administration of c_2 in the severe fractures poorly enhance the bone production while the cartilage production does not change. Similar

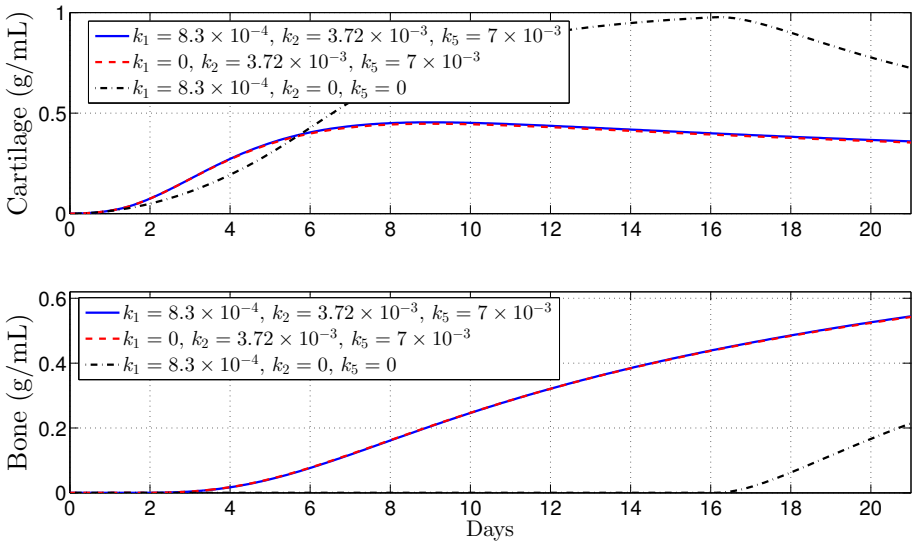

Figure 4.6. Tissues evolution when the alternatively activated macrophages, M_2, do not contribute to the healing process (dashed line), $k_2 = 0$, and when the classically activated macrophages, M_1, do not contribute to the healing process (dotted line), $k_1 = 0$.

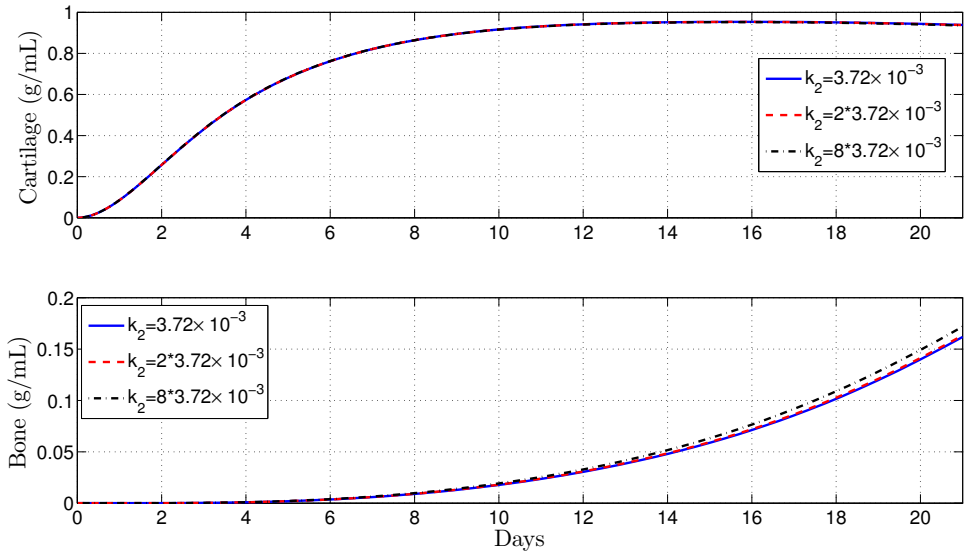

Figure 4.7. Tissues evolution in a severe fracture under different anti-inflammatory cytokines administration, $D(0) = 5 \times 10^8$.

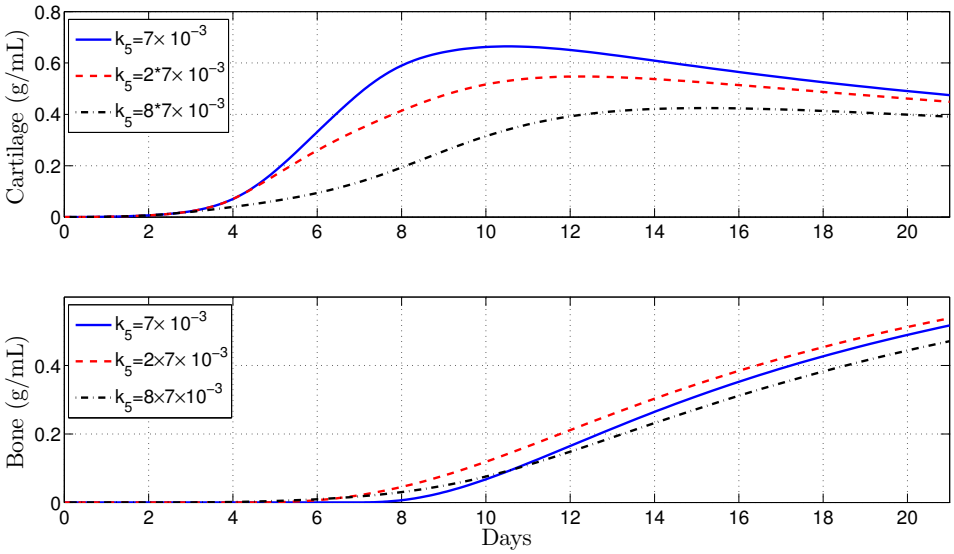

Figure 4.8. Tissues evolution in a moderate fracture under different growth factor concentration, $D(0) = 5 \times 10^7$.

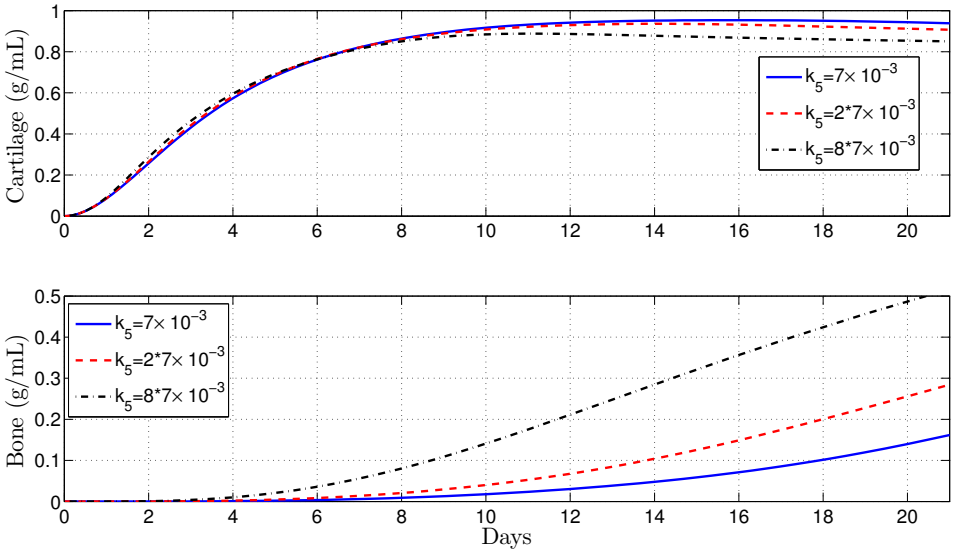

Figure 4.9. Tissues evolution in a severe fracture under different growth factor concentration, $D(0) = 5 \times 10^8$.

results were obtained for a small and moderate fractures under the administration of c_2. Figure 4.8 shows that the administration of c_3 in a moderate fracture slows down the cartilage productions and improves the bone evolution but in a dose-dependent manner. Figure 4.9 shows that the administration of c_3 in a severe fracture improves the bone tissue production and barely stimulate the removal of the cartilage.

4.5 Mechanism of the Osteogenic Cell Differentiation

In this section the Model (4.1)-(4.12) is reduced by considering only the dynamics among the mesenchymal stem cells (C_m), osteoblasts (C_b), and the transforming growth factor-β (c_3). This model simplification leads to have a better understanding of the regulatory effects of the c_3 directing the differentiation of the C_m into C_b. The modeling reduction is as follow:

$$\frac{dC_m}{dt} = k_{pm}C_m\left(1-\frac{C_m}{K_{lm}}\right) - d_m c_3 C_m \tag{4.13}$$

$$\frac{dC_b}{dt} = k_{pb}C_b\left(1-\frac{C_b}{K_{lb}}\right) + d_m c_3 C_m - d_b C_b \tag{4.14}$$

$$\frac{dc_3}{dt} = k_4 C_b - d_{c_3} c_3, \tag{4.15}$$

where the differentiation rate of the C_m into C_b is modeled with a linear function with respect to c_3, i.e., $F_1 = d_m c_3$, and the c_3 production rate is modeled with a constant rate, i.e., $H_3 = k_4$.

4.5.1 Qualitative Analysis

The analysis of model (4.13)-(4.15) is done by finding the equilibria and their corresponding stability properties. An equilibrium point of the model is denoted by the vector form $E(C_m^*, C_b^*, c_3^*)$ and it is found by setting the right-hand sides of the equations (4.13)-(4.15) equal to zero [42]. The model has four biologically

meaningful equilibria: $E_0(0,0,0)$, $E_1(K_{lm},0,0)$, $E_2(0,C_b^*,c_3^*)$, and $E_3(C_{m_3}^*,C_{b_3}^*,c_{33}^*)$. Their definitions, existence, and corresponding stability conditions are described in the following theorems. The existence of each equilibrium point arises from the fact that all biologically meaningful variables are nonnegative, and their stability analysis is conducted using the Jacobian of the system at each equilibrium point and finding its corresponding eigenvalues [42, 60]. Table 4.1 summarizes the equilibria and their corresponding stability conditions.

Table 4.1. Existence and stability conditions for the equilibrium points.

Equilibrium Points	**Existence Conditions**	**Local Stability**
$E_0(0,0,0)$	always	unstable
$E_1(K_{lm},0,0)$	always	$d_b > k_{pb} + K_{lm}\frac{d_m k_4}{d_{c_3}}$
$E_2(0,C_{b_2}^*,c_{32}^*)$	$d_b < k_{pb}$	$d_b < k_{pb}\left(1-\frac{k_{pm}d_{c_3}}{d_m k_4 K_{lb}}\right)$
$E_3(C_{m_3}^*,C_{b_3}^*,c_{33}^*)$	$k_{pb}\left(1-\frac{k_{pm}d_{c_3}}{d_m k_4 K_{lb}}\right) < d_b < k_{pb} + K_{lm}\frac{d_m k_4}{d_{c_3}}$	$b_1 b_2 - b_3 > 0$

Theorem 4.5.1. *The equilibria $E_0(0,0,0)$ exists for all the parameters and it is unstable.*

Proof of Theorem 4.5.1. The elements of E_0 are non-negative for all the model parameters, hence E_0 always exists. The Jacobian matrix $J(E_0)$ is given by the following sub-triangular matrix:

$$J(E_0) = \begin{pmatrix} k_{pm} & 0 & 0 \\ 0 & k_{pb}-d_b & 0 \\ 0 & k_4 & -d_{c_3} \end{pmatrix}.$$

Since the eigenvalue $\lambda_{C_m} = k_{pm} > 0$, then E_0 is unstable [42]. □

Theorem 4.5.2. *The $E_1(K_{lm},0,0)$ exists for all the parameters and is locally stable if $d_b > k_{pb} + d_m k_4 K_{lm}/d_{c_3}$.*

Proof of Theorem 4.5.2. The E_1 exists for all the parameters of the model since their elements are non-negative. The Jacobian matrix $J(E_1)$ is as follows:

$$J(E_1) = \begin{pmatrix} -k_{pm} & 0 & -d_m K_{lm} \\ 0 & k_{pb} - d_b & d_m K_{lm} \\ 0 & k_4 & -d_{c_3} \end{pmatrix}.$$

Hence the characteristic polynomial of $J(E_1)$ is given by $p(\lambda) = (\lambda + k_{pm})(\lambda^2 + a_1\lambda + a_0)$, where $a_1 = d_{c_3} + (d_b - k_{pb})$ and $a_0 = d_{c_3}(d_b - k_{pb}) - d_m k_4 K_{lm}$. By hypothesis $d_b - k_{pb} > d_m k_4 K_{lm}/d_{c_3} > 0$ therefore $a_0 > 0$ and $a_1 > 0$. By the Routh-Hurwitz criteria, $n = 2$, the roots of $\lambda^2 + a_1\lambda + a_0$ are negative or have negative real part. These imply that E_1 is locally stable [42]. □

Theorem 4.5.3. *The $E_2(0, C_b^*, c_3^*)$ exists if $k_{pb} > d_b$ and it is stable if and only if $k_{pb} > d_b + d_{c_3} k_{pb} k_{pm}/d_m k_4 K_{lb}$, where*

$$C_b^* = K_{lb}(1 - d_b/k_{pb}), \quad \textit{and} \quad c_3^* = k_4 C_b^*/d_{c_3}.$$

Proof of Theorem 4.5.3. By hypothesis $k_{pb} > d_b$, hence C_b^* and c_3^* are positive and then E_2 is well defined. The Jacobian matrix $J(E_2)$ is given by the following triangular matrix:

$$J(E_2) = \begin{pmatrix} k_{pm} - d_m c_3^* & 0 & 0 \\ d_m c_3^* & -k_{pb} + d_b & 0 \\ 0 & k_4 & -d_{c_3} \end{pmatrix}.$$

Since $k_{pm} - d_m c_3^* = \left(d_{c_3} k_{pb} k_{pm} - d_m k_4 K_{lb}(k_{pb} - d_b)\right)/d_{c_3} k_{pb}$, then, by hypothesis, it implies that $k_{pm} - d_m c_3^* < 0$. Hence all the eigenvalues of $J(E_2)$ are negative values. Therefore, E_2 is locally stable [42]. □

Theorem 4.5.4. *The $E_3(C_{m_3}^*, C_{b_3}^*, c_{33}^*)$ exists if $k_{pb}\left(1 - k_{pm} d_{c_3}/d_m k_4 K_{lb}\right) < d_b < k_{pb} + K_{lm} d_m k_4/d_{c_3}$, and is defined as follow*

$$C_{m_3}^* = \frac{k_{pm}}{\Delta}\left(\frac{k_{pb}}{K_{lb}} + \frac{d_m k_4 (d_b - k_{pb})}{k_{pm} d_{c_3}}\right), \quad C_{b_3}^* = \frac{k_{pm}}{\Delta}\left(\frac{d_m k_4}{d_{c_3}} + \frac{k_{pb} - d_b}{K_{lm}}\right),$$

$$c_{33}^* = \frac{k_4 k_{pm}}{d_{c_3}\,\Delta}\left(\frac{d_m k_4}{d_{c_3}} + \frac{k_{pb} - d_b}{K_{lm}}\right), \quad \Delta = \left(\frac{d_m k_4}{d_{c_3}}\right)^2 + \frac{k_{pm} k_{pb}}{K_{lm} K_{lb}}.$$

Furthermore, E_3 is locally stable if $b_1 b_2 - b_3 > 0$, is unstable if $b_1 b_2 - b_3 < 0$, and is locally a center if $b_1 b_2 - b_3 = 0$, where b_1, b_2, b_3 are defined as follow:

$$b_1 = \frac{k_{pm} C_{m_3}^*}{K_{lm}} + \frac{k_{pb} C_{b_3}^*}{K_{lb}} + \frac{d_m k_4 C_{m_3}^*}{d_{c_3}} + d_{c_3}, \quad b_3 = d_{c_3} \Delta C_{m_3}^* C_{b_3}^*,$$

$$b_2 = \frac{k_{pm} C_{m_3}^*}{K_{lm}}\left(\frac{k_{pb} C_{b_3}^*}{K_{lb}} + \frac{d_m k_4 C_{m_3}^*}{d_{c_3}} + d_{c_3}\right) + d_{c_3}\frac{k_{pb} C_{b_3}^*}{K_{lb}}.$$

Proof of Theorem 4.5.4. For the first statement of the theorem, notice that the $C_{m_3}^*$ and $C_{b_3}^*$ are monotonic functions with respect to the parameter d_b. Therefore, $C_{m_3}^* > C_{m_3}^*\left(k_{pb}(1 - k_{pm} d_{c_3}/d_m k_4 K_{lb})\right) = 0$, and $C_{b_3}^* > C_{b_3}^*\left(k_{pb} + K_{lm} d_m k_4/d_{c_3}\right) = 0$ for all d_b in the interval $I = \left(k_{pb}\left(1 - k_{pm} d_{c_3}/d_m k_4 K_{lb}\right), k_{pb} + K_{lm} d_m k_4/d_{c_3}\right)$. Therefore, $C_{m_3}^* > 0$ and $C_{b_3}^* > 0$ in I. This also implies that $c_3^* > 0$ in I. Hence E_3 is well defined and $E_3 \neq E_i$, $i = 0, 1, 2$. Next, for the second statement of the theorem, the Jacobian matrix $J(E_3)$ is given by the following matrix:

$$J(E_3) = \begin{pmatrix} -k_{pm} C_{m_3}^*/K_{lm} & 0 & -d_m C_{m_3}^* \\ d_m k_4 C_{b_3}^* d_{c_3} & -(k_{pb} C_{b_3}^*/K_{lb} + d_m k_4 C_{m_3}^*/d_{c_3}) & d_m C_{m_3}^* \\ 0 & k_4 & -d_{c_3} \end{pmatrix}.$$

Hence the polynomial characteristic of $J(E_3)$ is given by $p(\lambda) = \lambda^3 + b_1\lambda^2 + b_2\lambda + b_3$, where b_1, b_2, and b_3 are defined in the theorem. From the fact that $C_{m_3}^* > 0$ and $C_{b_3}^* > 0$, it can be concluded that each $b_i > 0$, $i = 0, 1, 2$. Therefore, when $b_1 b_2 - b_3 > 0$ by Routh-Hurwitz criteria, $n = 3$, the roots of $p(\lambda)$ are negative or have negative real part. Hence E_3 is locally stable.

Next, suppose that $b_1 b_2 - b_3 < 0$, it will be proved that E_3 is unstable. By the Descartes' rule of sign, the polynomial $p(\lambda)$ does not has positive roots, since $b_i > 0$, $i = 0, 1, 2$. Therefore, all the roots of $p(\lambda)$ are negative or complex. If all of them are

negative, then E_3 is stable, and then by Routh-Hurwitz criteria, $b_1b_2 - b_3 > 0$, that contradicts the hypothesis. Therefore, $p(\lambda)$ has a negative root, $-b$, and two complex conjugate roots, $\mu \pm iw$, since $p(\lambda)$ is of degree three. Notice that $b > 0$ and $\mu > 0$. Since, if $\mu < 0$ then E_3 is stable, and then by Routh-Hurwitz criteria $b_1b_2 - b_3 > 0$. This also contradicts the hypothesis. Therefore, $\mu > 0$, and hence E_3 is unstable.

Finally, if $b_1b_2 - b_3 = 0$, the $J(E_3)$ has one negative root and two purely imaginary roots given by: $-b_1$ and $\pm i\sqrt{b_2}$. Therefore, E_3 is locally a center. □

The following corollary provides a sufficient condition to guaranty the stability of E_3.

Corollary 4.5.5. *The $E_3(C_m, C_b, c_3)$ defined in Theorem 4.5.4 is locally stable when*

$$\frac{d_m k_4}{d_{c_3}} \leq \sqrt{2\frac{k_{pm}k_{pb}}{K_{lm}K_{lb}}}.$$

Proof of Corollary 4.5.5. From the Theorem 4.5.4, it is enough to prove that $b_1b_2 - b_3 > 0$. From the definition of each b_i, $i = 1, 2, 3$, it follows that

$$\begin{aligned} b_1b_2 - b_3 \;\; = & -\frac{C_bC_md_m^2k_4^2}{d_{c_3}} + \frac{2C_bC_md_{c_3}k_{pb}k_{pm}}{K_{lb}K_{lm}} + \frac{C_m^3d_m^2k_4^2k_{pm}}{d_{c_3}^2K_{lm}} + \frac{2C_bC_m^2d_mk_4k_{pb}k_{pm}}{d_{c_3}K_{lb}K_{lm}} \\ & + \frac{C_bC_md_mk_4k_{pb}}{K_{lb}} + \frac{C_m^3d_mk_4k_{pm}^2}{d_{c_3}K_{lm}^2} + \frac{2C_m^2d_mk_4k_{pm}}{K_{lm}} + \frac{C_b^2C_mk_{pb}^2k_{pm}}{K_{lb}^2K_{lm}} \\ & + \frac{C_b^2d_{c_3}k_{pb}^2}{K_{lb}^2} + \frac{C_bC_m^2k_{pb}k_{pm}^2}{K_{lb}K_{lm}^2} + \frac{C_bd_{c_3}^2k_{pb}}{K_{lb}} + \frac{C_m^2d_{c_3}k_{pm}^2}{K_{lm}^2} + \frac{C_md_{c_3}^2k_{pm}}{K_{lm}}. \end{aligned} \tag{4.16}$$

Since $C_m > 0$ and $C_b > 0$ then

$$b_1b_2 - b_3 > -\frac{C_bC_md_m^2k_4^2}{d_{c_3}} + \frac{2C_bC_md_{c_3}k_{pb}k_{pm}}{K_{lb}K_{lm}} = d_{c_3}C_bC_m\left(2\frac{k_{pb}k_{pm}}{K_{lb}K_{lm}} - \frac{d_m^2k_4^2}{d_{c_3}^2}\right),$$

which from the hypothesis follows that $b_1b_2 - b_3 > 0$. □

The following lemma establishes the number of equilibria of the model (4.13)-(4.15), and their corresponding stability properties. The proof of the lemma follows from the Theorems 4.5.1-4.5.4.

Lemma 4.5.6. *The number of equilibria of the model (4.13)-(4.15) and their stability properties are stated as follow:*

1. *there are two equilibria given by E_0 and E_1 when $d_b > k_{pb} + K_{lm}d_m k_4/d_{c_3}$. In this case, the E_0 is unstable, and E_1 is locally stable.*
2. *there are three equilibria given by E_0, E_1, and E_3 when $k_{pb} < d_b < k_{pb} + K_{lm}d_m k_4/d_{c_3}$. In this case, the E_0 and E_1 are unstable, and E_3 is locally stable if $b_1 b_2 - b_3 > 0$.*
3. *there are four equilibria given by E_0, E_1, E_2, and E_3 when $k_{pb}\,(1 - k_{pm}d_{c_3}/d_m k_4 K_{lb}) < d_b < k_{pb}$. In this case, the E_0, E_1, and E_2, are unstable, and E_3 is locally stable if $b_1 b_2 - b_3 > 0$.*
4. *there are three equilibria given by E_0, E_1, E_2 when $d_b < k_{pb}\,(1 - k_{pm}d_{c_3}/d_m k_4 K_{lb})$. In this case, the E_0 and E_1 are unstable, and E_2 is locally stable.*

Notice that from Lemma 4.5.6, the number of equilibria and their corresponding stability changes as the parameter d_b changes. When the stability of an equilibrium point E^* changes in a neighborhood of a parameter μ, the parameter μ is called bifurcation, and it is said that the system undergoes to a bifurcation at (E^*, μ) [60]. Therefore, the stability of the system (4.13)-(4.15) can be explained by looking at the bifurcation of each equilibria with respect to the parameter d_b. Two cases can be distinguished: (I) the case when $b_1 b_2 - b_3 > 0$ and (II) the case when $b_1 b_2 - b_3 < 0$.

For the case I, from the Lemma 4.5.6, there are two values of d_b where the system (4.13)-(4.15) undergoes to a bifurcation: (E_1, d_1) and (E_2, d_2), where $d_1 = k_{pb} + K_{lm}d_m k_4/d_{c_3}$ and $d_2 = k_{pb}\,(1 - k_{pm}d_{c_3}/d_m k_4 K_{lb})$. Notice that d_2 exists only when $k_{pm}d_{c_3} < d_m k_4 K_{lb}$. Figure 4.10 shows the bifurcation diagrams for the steady state of the variables C_m^* and C_b^* of the equilibria E_1 (red lines), E_2 (blue lines) and E_3 (dark lines). The variables for the E_0 are omitted since E_0 is unstable for all d_b values. System (4.13)-(4.15) undergoes to a bifurcation at (E_1, d_1), since $J(E_1)$ has

an eigenvalue equal to zero at $d_b = d_1$, and E_1 is stable when $d_b > d_1$ (red solid line from the Figure 4.10), and it is unstable when $d_b < d_1$ (red dashed line from the Figure 4.10). Results that follow from Lemma 4.5.6 and from the proof of Theorem 4.5.2. System (4.13)-(4.15) undergoes to a bifurcation at (E_2, d_2), since $J(E_2)$ has an eigenvalue equal to zero, when $d_b = d_2$, and E_2 is stable when $d_b < d_2$ (blue solid line at the Figure 4.10), and it is unstable when $d_b > d_2$ (blue dashed line at the Figure 4.10). Results that follow from Lemma 4.5.6 and from the proof of Theorem 4.5.2.

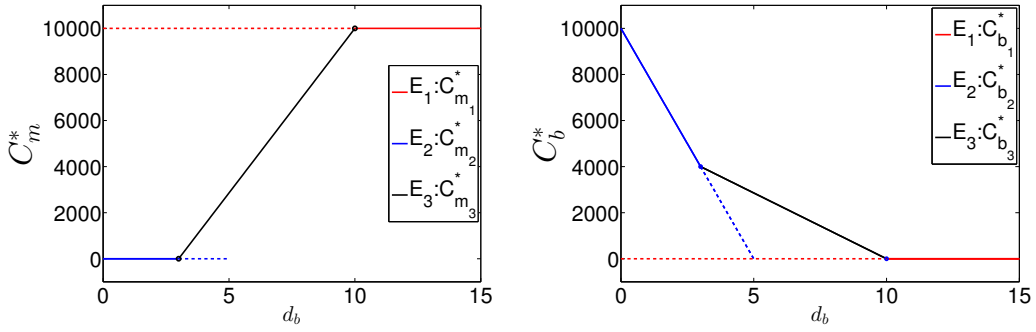

Figure 4.10. Bifurcation diagram when $k_{pm}d_{c_3} < d_m k_4 K_{lb}$ and $b_1 b_2 - b_3 > 0$: the y-axes exhibits the steady state for the MSCs and osteoblasts densities, C_m^* and C_b^*. The x-axis correspond to the values of the parameter d_b. Solid lines (stable), dashed lines (unstable). E_1 exists for all d_b, E_2 exists when $d_b < k_{pb}$, and E_3 exists when $d_1 < d_b < d_2$. E_1 changes stability at d_1 and E_2 changes stability at d_2.

For the case II, when $b_1 b_2 - b_3 < 0$, the stability of E_3 changes with respect to d_b, where d_b is defined in the interval $I = (k_{pb}\,(1 - k_{pm}d_{c_3}/d_m k_4 K_{lb})\,, k_{pb} + K_{lm}d_m k_4/d_{c_3})$. Let us introduce the concept of Hopf-bifurcation to show that the stability of E_3 changes with respect to d_b. The system (4.13)-(4.15) undergoes to a Hopf-bifurcation at (E_3, d_b), if $J(E_3)$ has a purely imaginary eigenvalue at d_b, and the stability of E_3 changes in a neighborhood of d_b (the imaginary part of the complex eigenvalue of $J(E_3)$ smoothly crosses the imaginary axes in a neighborhood of d_b) [60]. Due to the

complexity of the of the expressions of E_3 and $J(E_3)$ with respect to d_b for any value of d_b in I, we do not provide a theoretical proof of the existence of the Hopf-bifurcation at (E_3, d_3), where d_3 is a positive root of $b_1b_2-b_3$, i.e., $b_1b_2-b_3(d_3)=0$. However from the explicit expression of $b_1b_2-b_3$ given in Equation (4.16) and from the Theorem 4.5.4, it is easy to show that at d_3, $J(E_3)$ has purely imaginary eigenvalues and the stability of E_3 changes in a neighborhood of d_3, as is described below. From the definition of E_3, the equation $b_1b_2-b_3$ defines a polynomial of degree three with respect to d_b when all the parameters are fixed and d_b varies in I. Therefore, from the definition of $C^*_{m_3}$ and $C^*_{b_3}$, it follows that $C^*_{m_3}(k_{pb}+K_{lm}d_mk_4/d_{c_3})=K_{lm}$ and $C^*_{b_3}(k_{pb}+K_{lm}d_mk_4/d_{c_3})=0$. Hence, in a neighborhood of $k_{pb}+K_{lm}d_mk_4/d_{c_3}$ the polynomial $b_1b_2-b_3$ is positive. Therefore, $b_1b_2-b_3<0$ and $b_1b_2-b_3>0$ in I, which implies that there exists a value d_3 of d_b such that $(b_1b_2-b_3)(d_3)=0$. Hence from Theorem 4.5.4, $J(E_3)$ has purely conjugate imaginary eigenvalue at d_3. Furthermore, it is also expected that E_3 changes stability near to d_3 since E_3 is unstable at d_b such that $b_1b_2-b_3<0$ and E_3 is stable at d_b such that $b_1b_2-b_3>0$, ensuring that d_b belongs in I, see Theorem 4.5.4. Figure 4.11 shows the bifurcation diagram for the equilibria E_3, the plots were obtained from the xpp-auto software, see Appendix for the codes and parameter values. For these particular set of parameter values, the system undergoes to a Hopf-bifurcation at two different values of d_b, ($d_b=0.4078$ and $d_b=0.4641$). Hence E_3 changes stability in I, when $b_1b_2-b_3<0$.

4.5.2 Numerical simulations

In this subsection a set of numerical simulations is presented to support the theoretical results. Accordingly to the qualitative analysis of the Model (4.13)-(4.15), there are four equilibria: E_0, E_1, E_2, and E_3 where their stability conditions are determined by the bifurcation parameters: $d_1=k_{pb}+K_{lm}d_mk_4/d_{c_3}$,

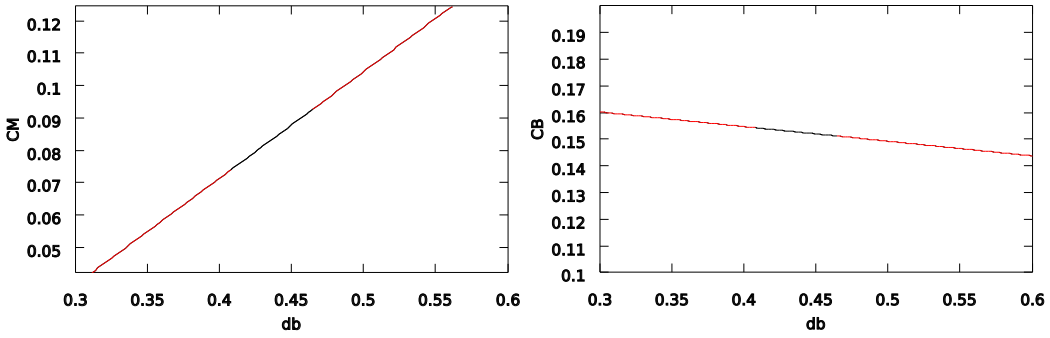

Figure 4.11. Bifurcation diagram when $k_{pm}d_{c_3} < d_m k_4 K_{lb}$ and $b_1 b_2 - b_3 < 0$ obtained from xxpp-auto: the y-axes exhibits the steady state for the MSCs and osteoblasts densities, C_m^* and C_b^*. The x-axis correspond to the values of the parameter d_b. Red-solid line (stable), dark-solid line (unstable).

$d_2 = k_{pb}\,(1 - k_{pm}d_{c_3}/d_m k_4 K_{lb})$, and d_3 such that $d_2 < d_3 < d_1$ and d_3 is a root of the polynomial function $b_1 b_2 - d_3$ with respect to d_b.

To demonstrate the stability of E_1, $d_b = 51$ and the other parameters are set to be as the given values from Table 5.1. Since in this case $d_b = 51 > d_1 = 50.2202$. The initial conditions are $C_m(0) = 1000$, $C_b(0) = 1000$, and $c_3(0) = 200$. Figure 4.12 shows the qualitative behaviors for the MSCs, osteoblasts, and the TGF-β densities of E_1. Here, the MSCs maintain a maximum constant density given by its carrying capacity $K_{lm} = 1 \times 10^6$ while the osteoblasts and growth factor densities decays to zero over the time.

The stability of E_2 is demonstrated using the following parameter values: $d_b = 0.1$, since then $d_b = 0.1 < k_{pb}\left(1 - \frac{k_{pm}d_{c_3}}{d_m k_4 K_{lb}}\right) = 0.218$. Figure 4.13 shows the qualitative behaviors of E_2 for the MSCs, osteoblasts, and growth factor. Here, the MSCs density decays to zero over the time, while the osteoblasts and growth factor maintain a constant density.

The following parameter values are used to show the existence of a Hopf-bifurcation for the model (4.13)-(4.15): K_{lm} =10000, $k_{pm} = 0.5$, $d_m = 0.1$, $k_{pb} =$

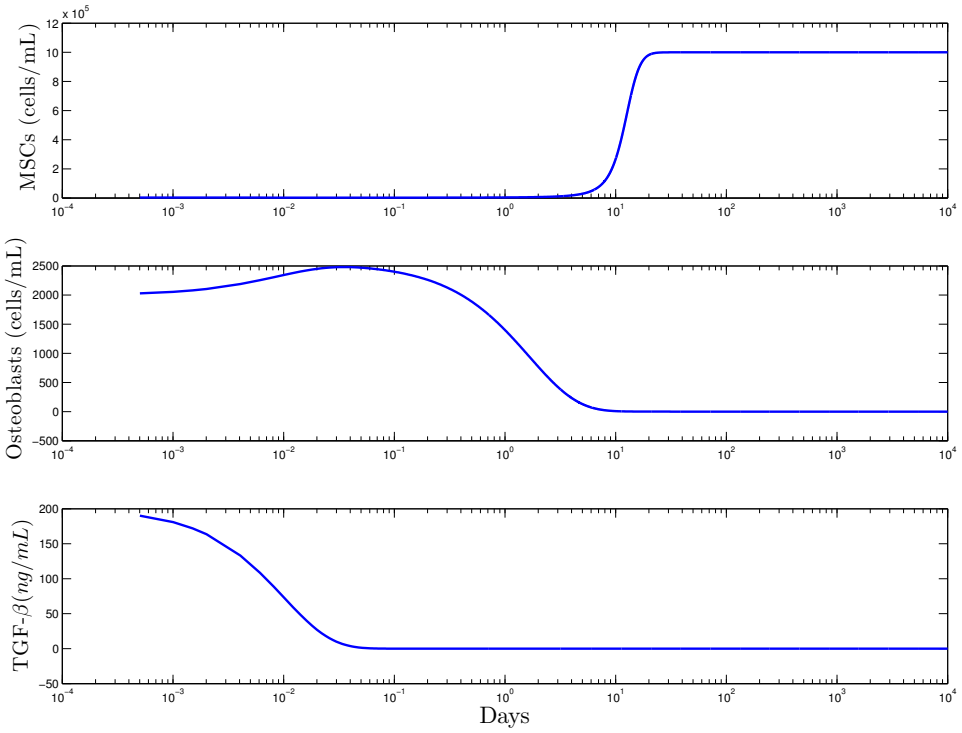

Figure 4.12. Cellular and molecular evolution for E_1.

0.2202, $K_{lb} = 10000$, d_{c_3}=100, k_4=0.05. For this case E_3 has a Hopf-biufurcation at $d_3 = 5.091$, approximately. Figure 4.14 shows how the stability of E_3 changes as the parameter d_b changes around d_3: (a) when $d_b = 5$, the trajectory solution of the system does not converge to E_3, it evolves to a limit cycle (boundary of the figure); (b) when $d_b = 6$, the trajectory solution of the system converges to E_3.

Figure 4.15 shows the numerical solution for E_3, when E_3 is stable: $d_b = 6$, that implies $b_1 b_2 - b_3 < 0$. Here, the MSCs, osteoblasts, and growth factors densities remain constantly over time.

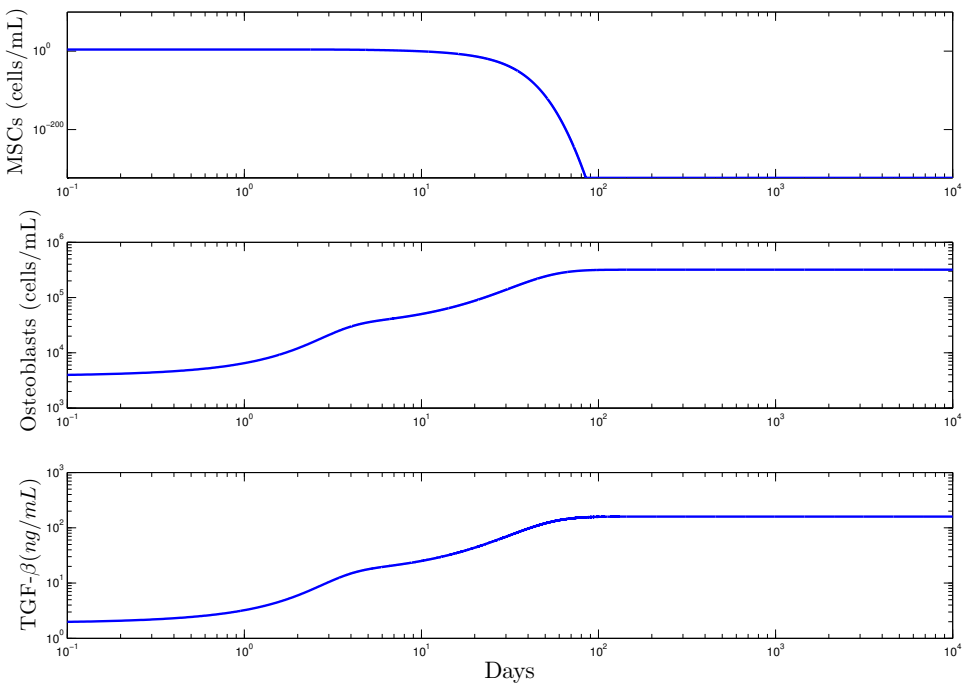

Figure 4.13. Cellular and molecular evolution for E_2.

Figure 4.16 shows the numerical solution for E_3, when E_3 is unstable: $d_b = 5$, that implies $b_1 b_2 - b_3 < 0$. Here, the densities of MSCs, osteoblasts, and growth factors oscillate over time.

4.6 Summary of the Results

In this chapter two new mathematical models was introduced to have a better understanding of the cellular and molecular dynamics occurring during the inflammatory and repair phases of bone fracture healing process. The presented Model (4.1)-(4.12) is a model extension of the model developed in (3.1)-(3.10). Where the transforming growth factors and the chondrocytes were incorporated to in the new model. This extension leads a more realistic model by taking into account the growth

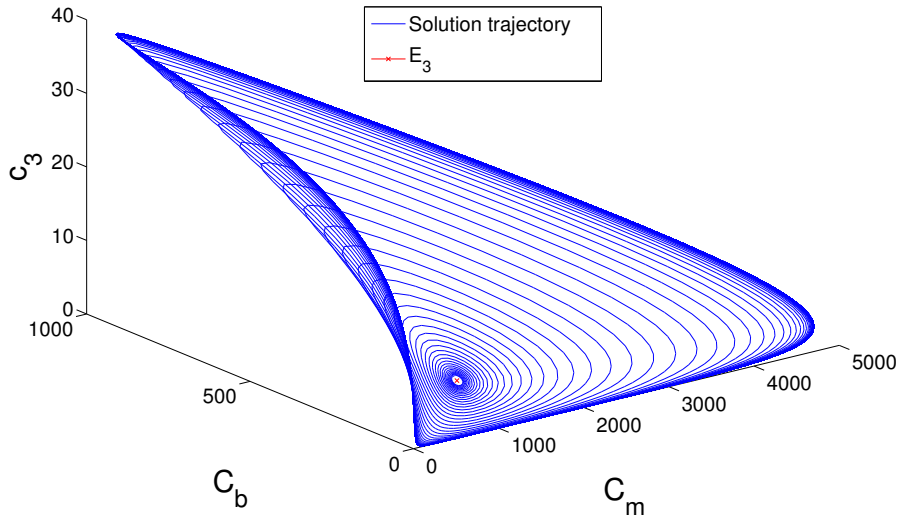

(a) $d_b = 4$

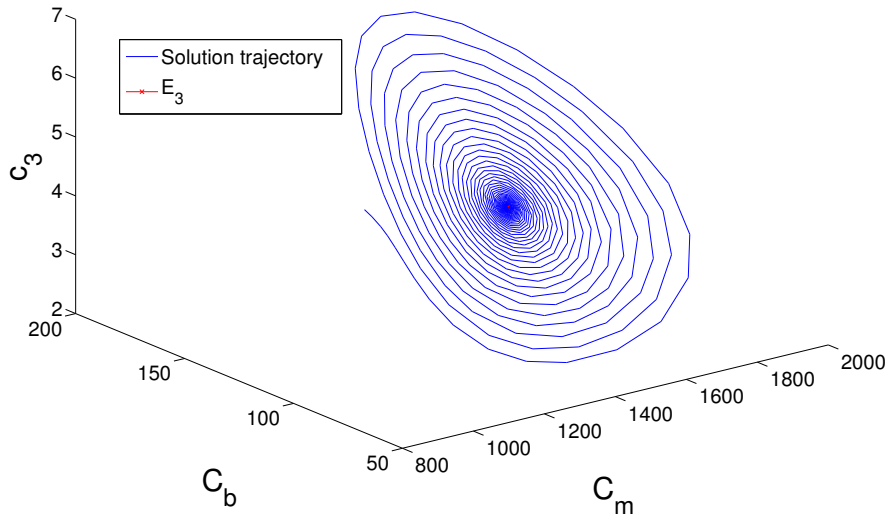

(b) $d_b = 6$

Figure 4.14. Solution trajectories in a neighborhood of E_3 for two different values of d_b: 4, 6.

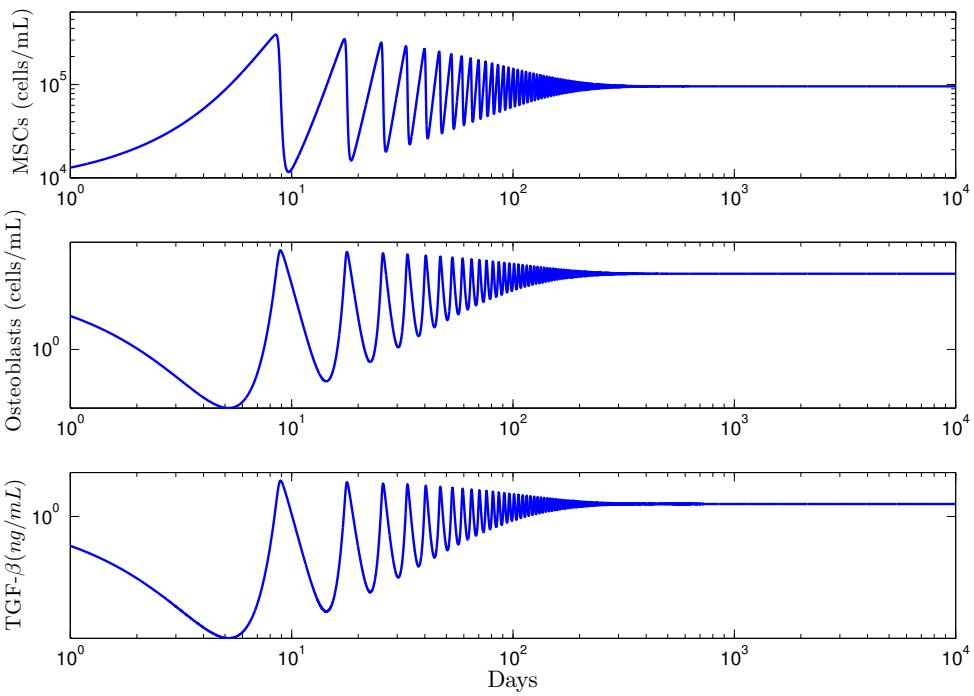

Figure 4.15. Cellular and molecular evolution for E_3, when E_3 is stable: $b_1b_2 - b_3 > 0$, $d_b = 6$, from 0 to 10000 days.

factor stimuli in the MSCs differentiation, and also to separately model the molecular production by the different types of cells. Particularly, the three main molecular production given by the immune cells: the pro- and anti-inflammatory cytokines, and growth factors was carefully modeled. Hence, allowing to gain a greater degree of understanding of the immune system functions during the bone fracture healing process.

The quality analysis of the model showed that the incorporation of c_3 and C_c is a more realistic model, as several new equilibria of the bone fracture healing were found. The set of equilibria of the new model, Model (4.1)-(4.1), includes the equilibria obtained in the two previous models, Models (2.1)-(2.1) and (3.1)-(3.1), and other

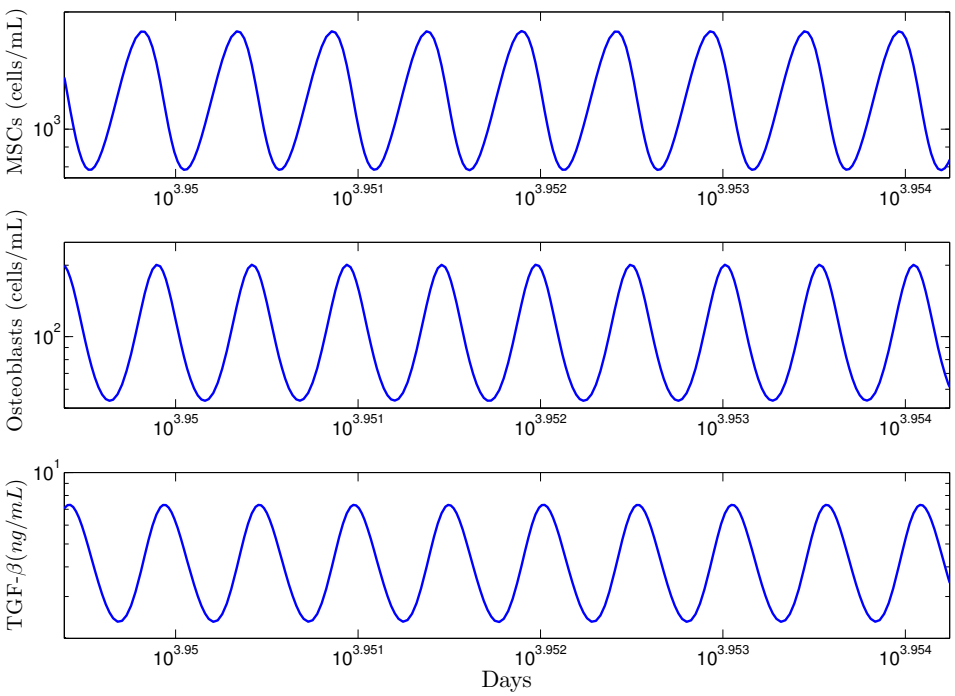

Figure 4.16. Cellular and molecular evolution for E_3, when E_3 is unstable: $d_b = 4$, $b_1 b_2 - b_3 < 0$, from 8900 to 9000 days.

steady-states that captures the endochondral and osteogenic ossification outcomes: E_2, E_3, E_7, E_9, E_{10}. These new equilibria represent nonunion or delayed union, since in all these cases, the osteoclasts fail to completely remove the fibrocartilage. Furthermore, base on the qualitative analyzes of the new model, to observe a successful healing outcome, that is given by the equilibrium E_8, it requires not only the stability conditions founded in the previous model, but also it requires a minimal concentration of growth factor to secure the successful repair. Therefore, to observe a successful healing outcome, E_8, three conditions must be satisfied: (1) the differentiation rate of the MSCs into the osteoblasts is bigger than the osteoblast proliferation rate, i.e., $d_m > k_{pb}$, (2) the apoptotic rate of the chondrocytes is bigger than the chondrocyte

proliferation rate, i.e., $d_c > k_{pc}$, (3) the growth factor production rate over the growth factor degradation rate is bigger than the half saturation of the growth factor, i.e., $k_4 C_b^*/d_{c_3} > a_{33}$, and (4) the growth factor concentration is above to the concentration quantity: $\max\{a_{mb}k_{pm}/(d_m - k_{pm}), a_{cb}k_{pc}/(d_c - k_{pc})\}$. These mathematical condition finding confirm the numerical results provided in [2], where the authors hypothesized that there is a minimal concentration of growth factors to secure the healing of a broken bone.

Furthermore, a new model was introduced, Model (4.13)-(4.15) to have a better understanding of the regulatory effect of the growth factors during the MSCs differentiation. Model (4.13)-(4.15) is a model reduction of Model (4.13)-(4.15) and the model introduced in [2], where only the interaction among the MSCs, osteoblasts, and growth factors are taking into account. The mathematical analysis of Model (4.13)-(4.15) exhibited that the stability of the equilibria, nonunion or delayed union healing outcomes, may change as the parameter values change. These results may justify the different pathological outcomes of bone fracture healing process, where unsuccessful and chronic bone healing are observed. Therefore, the stability conditions of each outcome of the new model can be used to biologically explain why the fracture healing fails, and to design therapeutic interventions to stimulate or accelerate the healing process.

Similar numerical results were also obtained when the administration of growth factors and cytokines are implemented to promote the repair of a broken bone. The administration of anti-inflammatory cytokines and growth factors fails to accelerate the healing process in simple fractures, while it accelerates the healing process in moderate fractures depending on the molecular concentrations, and always improves the healing process in severe fractures. Furthermore, the numerical results suggested

that the administration of growth factors is the most promising therapeutic treatments to enhance bone formation.

CHAPTER 5

CONCLUSION AND FUTURE WORK

Several mathematical and computational models have been recently developed for modeling the bone fracture healing process. However, none of them have considered the immune system functions during the healing process [13, 32]. In this work, new mathematical models were introduced that carefully incorporate the immune system role in bone fracture healing. The models were used to study the regulatory effects of the immune system in order to gain a greater degree of understanding of the bone fracture healing process.

First, the incorporation of the immune system in the models leads to more realistic numerical results, where the evolution of the fibrocartilage and woven bone correlates with the experimental data, see Chapter 4. Second, if the immune cells do not participate in the bone fracture healing process, the healing process evolves into nonunion or delayed union, Chapter 4; such findings have also been supported by several experimental results [29, 47, 49]. In addition, in Chapter 1, it was found that deregulation on the immune system functions leads to nonunion or delayed unions. Furthermore, more fibrocartilage is produced and less bone tissue is synthesized when the immune cells lose their capabilities to engulf debris or when the immune cells deliver high concentration of pro-inflammatory cytokines. In Chapters 2 and 3, it was found that the immune system strongly regulates the evolution of the bone fracture healing through delivered molecular factors, such as the pro- and anti-inflammatory cytokines, and growth factors. The numerical simulations revealed that in small fractures, the immune system does not need additional molecular stimuli

to accelerate the healing process. Indeed, if anti-inflammatory or growth factor drugs are administrated in small fractures, then the drugs negatively affect the progression of the bone healing. However, the administration of anti-inflammatory or growth factor drugs in moderate fractures accelerate the healing process in a dose-dependent manner, and the drugs always improve the healing process in severe fractures or in immune-compromised people. Such results have been also clinically observed when corticosteroids and nonsteroidal anti-inflammatory drugs (NSAIDs), or growth factors drugs are administered in bone fractures [38].

Furthermore, the stability analysis of the model revealed the biological conditions to observe successful healing outcomes. Moreover, the mathematical conditions obtained through the stability analysis of the models confirmed that a minimal concentration of growth factors is needed to secure the healing of a broken bone, Chapter 4. Such result was hypothesized in [2] based on the presented numerical results. In addition, the presented stability analysis revealed conditions on the model parameter values that lead to a successful healing outcome evolving into a nonunion.

Therefore, based on the model findings, the immune system is a main factor that determines the successful outcomes of bone fracture repair. Furthermore, the concentration of debris must be carefully considered when administration of anti-inflammatory and growth factor drugs are implemented to enhance the fracture healing process. In addition, the immune system potentially promotes bone fracture healing in severe and immune-compromised individuals through the delivered anti-inflammatory and growth factors.

The presented mathematical models can also be easily adapted to represent other therapeutic approaches, such as the administration of different tyeps of drugs, suggesting a variety of possible ways to guide clinical experiments and bone tissue engineering strategies.

Future research directions include modifications of the models by incorporating additional molecular and cellular interactions, and processes during the inflammatory and repair phases of fracture healing, such as macrophages and MSCs migration due to cytokine stimuli, and the incorporation of the osteoclasts. Another research direction is the incorporation of the bone remodeling phase of the healing process, which begins at the end of the repair phase and continues long after fracture union. There are different factors that affect the bone remodeling, including other bone cells, such as osteoclasts, osteocytes, progenitor cells, and other sources of cytokines [2, 24, 12]. Therefore, capturing the long-term dynamics of bone fracture healing requires combining the current model for the inflammatory and repair phases of the process with other mathematical models that are specifically developed for the bone remodeling phase of the healing process. This presents a challenging new research direction in the pursuit to better understand the bone fracture healing process and the development of new treatment strategies.

APPENDIX

In this appendix the parameter values used in the presented models are defined and described. Table 5.1, summarizes the baseline parameter values and units for the numerical simulations. These values are estimated in a qualitative manner from data in other studies [39, 40, 63, 2, 24, 27, 55]. Some of those from [27, 55] were also rescaled to account for the different mathematical expressions of the proliferation and differentiation rates of the tissue cells. All parameter values are based on murine experiments with healthy mice having a moderate fracture (a broken bone with a gap size less than 3mm) [2, 24]. However, the bone fracture healing process for humans involves the same cells, cytokines, and qualitative dynamics, differing only in the number of cells, concentrations, and the length of time it takes for a full recovery [20].

All simulations are obtained by using the adaptive MATLAB solver `ode23s` and are initiated with densities of debris, macrophages, MSCs, chondrocytes, and osteoblasts set to $D(0) = 5 \times 10^7$, $M_0(0) = 0$, $M_1(0) = 0$, $M_2(0) = 0$, $C_m(0) = 0$, $C_c(0) = 0$, $C_b(0) = 0$, respectively, and the molecular initial concentrations are set to $c_1(0) = 0$, $c_2(0) = 0$, $c_3(0) = 20$, which represent the densities profiles observed some minutes after a fracture occurs [2]. Some of the Parameter values given in [55, 27, 2, 39, 59] were also re-scaled to account for the different mathematical expressions of the model's variables.

The following parameter values are used for Model (2.1)-(2.7): $\Omega_1 = \{k_0 = 8.5\times10^{-6}; k_1 = 8.3\times10^{-6}, d_{c_1} = 12.79; k_d = 13; a_{ed} = 4.71\times10^6; k_{max} = 0.015; M_{max} = 1 \times 10^6; d_M = 0.121; k_m = 0.0015; K_{lm} = 1 \times 10^6; k_{pm} = 0.5; a_{pm} = \sqrt{10}; a_{pm1} =$

$13; d_m = 1; a_{mb1} = 0.1; k_{pb} = 0.2202; a_{pb} = 10; d_b = 0.15; K_{lb} = 1 \times 10^6; p_{cs} = 3 \times 10^{-7}; q_{cd1} = 3 \times 10^{-7}; q_{cd2} = 0.8 \times 10^{-7}; p_{bs} = 5 \times 10^{-8}; q_{bd} = 5 \times 10^{-8}\}$

Table 5.1. Parameter descriptions and units.

Parameter	Description	Range of values	Reference
k_d	Macrophages phagocytic rate	$3 - 48/day$	[39, 34]
a_{ed}	Half-saturation of debris	4.71×10^6 $cells/mL$	[39]
k_{max}	Maximal migration rate	$0.015 - 0.1$ $/day$	[63, 57]
M_{max}	Maximal macrophages density	$6 \times 10^5 - 1 \times 10^6 cells/mL$	[34, 40]
k_{01}	Activation rate of M_1	$0.55 - 0.611$ $/day$	[63, 59]
k_{02}	Activation rate of M_0 to M_2	$0.0843 - 0.3$ $/day$	[59]
k_{12}	Transition rate from M_1 to M_2	$0.083 - 0.075$ $/day$	[63, 59]
k_{21}	Transition rate from M_2 to M_1	$0.005 - 0.05/$ day	[59]
d_0	Emigration rate of M_0	$0.156 - 0.02$ $/day$	[63, 59]
d_1	Emigration rate of M_1	$0.121 - 0.2$ $/day$	[59, 63, 39]
d_2	Emigration rate of M_2	$0.163 - 0.2$ $/day$	[59, 39, 63]
k_0	Secretion rate of c_1 by debris	$5 \times 10^{-7} - 8.5 \times 10^{-6}$ $ng/cells/day$	[39]
k_1	Secretion rate of c_1 by M_1 macrophages	8.3×10^{-6} $ng/cells/day$	[39]
k_2	Secretion rate of c_2 by M_2 macrophages	3.72×10^{-6} $ng/cells/day$	[39]
k_3	Secretion rate of c_2 by MSCs	$7 \times 10^{-7} - 8 \times 10^{-6}$ $ng/cells/day$	[27]
d_{c_1}	Decay rate of c_1	$12.79 - 55$ $/day$	[59, 39]
d_{c_2}	Decay rate of c_2	$2.5 - 4.632$ $/day$	[59, 39]
a_{12}	Effectiveness of c_2 inhibition of c_1 synthesis	0.025 ng/mL	[59]
a_{22}	Effectiveness of c_2 inhibition of c_2 synthesis	0.1 ng/mL	[59]
a_{pm}	Effectiveness of c_1 inhibition of C_m proliferation	3.162 ng/mL	[27, 3]
a_{mb_1}	Effectiveness of c_1 inhibition of C_m differentiation	0.1 ng/mL	[27, 21]
a_{01}	Half-saturation of c_1 to activate M_1	0.01 ng/mL	[59]
a_{02}	Half-saturation of c_2 to activate M_2	0.005 ng/mL	[59]
a_{pb}	Effectiveness of c_1 inhibition of C_b proliferation	10 ng/mL	[27, 30]
a_{pm_1}	Constant enhancement of c_1 to C_m proliferation	13 ng/mL	[27, 3]
k_{pm}	Proliferation rate of C_m	0.5 $/day$	[27]
d_m	Maximal differentiation rate of C_m to C_b	1 $/day$	[2, 27]
a_{mb_1}	Effectiveness of c_1 inhibition of C_m differentiation into C_b	10 ng/mL	[27, 30]
a_{mc_1}	Effectiveness of c_1 inhibition of C_m differentiation into C_c	10 ng/mL	[2]
a_{mb}	Half saturation of c_3 enhancing C_m differentiation into C_b	10 ng/mL	[2]
a_{mc}	Half saturation of c_3 enhancing C_m differentiation into C_c	10 ng/mL	[2]
a_{cb}	Half saturation of c_3 enhancing necroses of C_c	10 ng/mL	[2]
k_{pb}	Proliferation rate of C_b	0.2202 $/day$	[2, 27]
d_b	Differentiation rate of C_b	0.15 $/day$	[2, 27]
p_{cs}	Fibrocartilage synthesis rate	3×10^{-6} $g/cells/day$	[2, 27]
q_{cd_1}	Fibrocartilage degradation rate	3×10^{-6} $mL/cells/day$	[2, 27]
q_{cd_2}	Fibrocartilage degradation rate by osteoclasts	0.2×10^{-6} $mL/cells/day$	[2, 27]
p_{bs}	Bone tissue synthesis rate	5×10^{-8} $g/cells/day$	[2, 27]
q_{bd}	Bone tissue degradation rate	5×10^{-8} $mL/cells/day$	[2]
K_{lb}	Carrying capacity of C_b	1×10^6 $cells/mL$	[2, 27]
K_{lm}	Carrying capacity of C_m	1×10^6 $cells/mL$	[2, 27]
$D(0)$	Density of necrotic cells	$1 \times 10^6 - 2 \times 10^8$ $cells/mL$	[34, 39, 40]

The following parameter values are used for Model (3.1)-(3.10): $\Omega_2 = \{k_d = 13; a_{ed} = 4.71 \times 10^6; k_{max} = 0.015; M_{max} = 1 \times 10^6; k_{e1} = 1; k_{e2} = 2; k_0 = 8.5 \times 10^{-6}; k1 = 8.3 \times 10^{-4}; d_{c1} = 12.79; K_{lm} = 1.0 \times 10^6; k_{pm} = 0.5; a_{pm} = \sqrt{10}; k_m =$

$0.0015; d_m = 1; a_{mb_1} = 0.1; p_{cs} = 3 \times 10^{-7}; q_{cd1} = 3 \times 10^{-7}; q_{cd2} = 0.8 \times 10^{-7}; p_{bs} = 5 \times 10^{-8}; q_{bd} = 5 \times 10^{-8}; k_{pb} = 0.2202; a_{pb} = 10; d_b = 0.15; K_{lb} = \times 10^6; a_{pm_1} = 13; k_{01} = 0.55; k_{02} = 0.0843; k_{12} = 0.083; k_{21} = 0.005; d_0 = 0.156; d_1 = 0.121; d_2 = 0.163; a_{12} = 0.025; a_{22} = 0.1; a_{01} = 0.01; a_{02} = 0.005; k_2 = 3.72 \times 10^{-4}; k_3 = 3 \times 10^{-5}; k_4 = 0.7 \times 10^{-4}; d_{c2} = 4.632\}$

For Model (4.1)-(4.12) the parameter values defined in Ω_2 and the following parameter values are used: $dmc = 10; dcb = .81; kpc = .8; apc = 3.162; acb1 = .05; acb = 10; amc = 10; amc1 = .05; amb = 10; Klc = 1e6; dc3 = 10; k5 = 7e{-}3; k4 = 4e - 3; k6 = 2e - 3; a33 = 10; k2 = 3.72e - 4; k3 = 3e - 5; dc2 = 4.632.$

The following parameter values are used for Model (4.13)-(4.15): $\Omega_3 = \{k_5 = 0.05; k_{pm} = 0.5; d_{mb} = d_m/a_m b = 0.1; k_{pb} = 0.2202; d_b = 0.15; d_{c3} = 100; K_{lm} = K_{lb} = \times 10^6\}$.

Code for the numerical simulations in the xpp-auto software:

init Cm=0.1 init Cb=0.1 init c3=0.2

par kpm=0.5 dm=1 kpb=0.2202 db=1 dc3=1 kb=3 dCm/dt=kpm*Cm*(1-Cm)-dm*Cm*c3

dCb/dt=kpb*Cb*(1-Cb)+dm*Cm*c3-db*Cb

dc3/dt=kb*Cb-dc3*c3

@ total=5000,dt=.5, xlo=0, xhi=2, ylo=0.0, yhi=10, zlo=0.0, zhi=10,

bound=8000, maxstor=100000, yp=p, dsmin=1e-5, dsmax=0.002, ds=-.0001, parmin=.000, parmax=.004, autoxmin=0,

autoymin=0, autoymax=60, nmax=50000, npr=1000, ntst=30,

dsmin=1e-5, dsmax=0.002, ds=-.0001, parmin=0.0, parmax=5, autoxmin=0.0 @autoxmax=5, autoymin=0, autoymax=5,

nmax=50000, npr=1000 @ EPSU=.0000001, EPSS=.0000001,

EPSL=.0000001

REFERENCES

[1] Guillermo Arango Duque and Albert Descoteaux. Macrophage cytokines: involvement in immunity and infectious diseases. *Frontiers in immunology*, 5:491, 2014.

[2] Alicia Bailon-Plaza and Marjolein CH Van Der Meulen. A mathematical framework to study the effects of growth factor influences on fracture healing. *Journal of Theoretical Biology*, 212(2):191–209, 2001.

[3] Angela P Bastidas-Coral, Astrid D Bakker, Behrouz Zandieh-Doulabi, Cornelis J Kleverlaan, Nathalie Bravenboer, Tim Forouzanfar, and Jenneke Klein-Nulend. Cytokines tnf-α, il-6, il-17f, and il-4 differentially affect osteogenic differentiation of human adipose stem cells. *Stem Cells International*, 2016, 2016.

[4] Lena Batoon, Susan Marie Millard, Liza Jane Raggatt, and Allison Robyn Pettit. Osteomacs and bone regeneration. *Current Osteoporosis Reports*, 15(4):385–395, 2017.

[5] Wayne A Border and Nancy A Noble. Transforming growth factor β in tissue fibrosis. *New England Journal of Medicine*, 331(19):1286–1292, 1994.

[6] Scott P Bruder, David J Fink, and Arnold I Caplan. Mesenchymal stem cells in bone development, bone repair, and skeletal regenaration therapy. *Journal of cellular biochemistry*, 56(3):283–294, 1994.

[7] Aurélie Carlier, Liesbet Geris, Nick van Gastel, Geert Carmeliet, and Hans Van Oosterwyck. Oxygen as a critical determinant of bone fracture healing—a multiscale model. *Journal of theoretical biology*, 365:247–264, 2015.

[8] Jean-Marc Cavaillon. Pro-versus anti-inflammatory cytokines: myth or reality. *Cellular and molecular biology (Noisy-le-Grand, France)*, 47(4):695–702, 2001.

[9] James K Chan, Graeme E Glass, Adel Ersek, Andrew Freidin, Garry A Williams, Kate Gowers, Ana I Espirito Santo, Rosemary Jeffery, William R Otto, Richard Poulsom, et al. Low-dose tnf augments fracture healing in normal and osteoporotic bone by up-regulating the innate immune response. *EMBO molecular medicine*, page e201404487, 2015.

[10] Eunkyung Chung and Youngsook Son. Crosstalk between mesenchymal stem cells and macrophages in tissue repair. *Tissue Engineering and Regenerative Medicine*, 11(6):431–438, 2014.

[11] Rozalia Dimitriou, Eleftherios Tsiridis, and Peter V Giannoudis. Current concepts of molecular aspects of bone healing. *Injury*, 36(12):1392–1404, 2005.

[12] M Doblaré, JM Garcıa, and MJ Gómez. Modelling bone tissue fracture and healing: a review. *Engineering Fracture Mechanics*, 71(13):1809–1840, 2004.

[13] LF Echeverri, MA Herrero, JM Lopez, and G Oleaga. Early stages of bone fracture healing: formation of a fibrin–collagen scaffold in the fracture hematoma. *Bulletin of mathematical biology*, 77(1):156–183, 2015.

[14] Thomas A Einhorn. The science of fracture healing. *Journal of orthopaedic trauma*, 19(10):S4–S6, 2005.

[15] Thomas A Einhorn and Louis C Gerstenfeld. Fracture healing: mechanisms and interventions. *Nature Reviews Rheumatology*, 11(1):45, 2015.

[16] MS Gaston and AHRW Simpson. Inhibition of fracture healing. *Bone & Joint Journal*, 89(12):1553–1560, 2007.

[17] Louis C Gerstenfeld, Cory M Edgar, Sanjeev Kakar, Kimberly A Jacobsen, and Thomas A Einhorn. Osteogenic growth factors and cytokines and their role in bone repair. pages 17–45, 2007.

[18] Mohammad S Ghiasi, Jason Chen, Ashkan Vaziri, Edward K Rodriguez, and Ara Nazarian. Bone fracture healing in mechanobiological modeling: A review of principles and methods. *Bone Reports*, 2017.

[19] E Gibon, F Loi, Luis A Córdova, J Pajarinen, T Lin, L Lu, A Nabeshima, Z Yao, and Stuart B Goodman. Aging affects bone marrow macrophage polarization: relevance to bone healing. *Regenerative engineering and translational medicine*, 2(2):98–104, 2016.

[20] Emmanuel Gibon, Laura Y Lu, Karthik Nathan, and Stuart B Goodman. Inflammation, ageing, and bone regeneration. *Journal of orthopaedic translation*, 10:28–35, 2017.

[21] Linda Gilbert, Xiaofei He, Paul Farmer, Scott Boden, Mirek Kozlowski, Janet Rubin, and Mark S Nanes. Inhibition of osteoblast differentiation by tumor necrosis factor-α 1. *Endocrinology*, 141(11):3956–3964, 2000.

[22] Enrique Gómez-Barrena, Philippe Rosset, Daniel Lozano, Julien Stanovici, Christian Ermthaller, and Florian Gerbhard. Bone fracture healing: cell therapy in delayed unions and nonunions. *Bone*, 70:93–101, 2015.

[23] Florian Hoegel, Ahmed Abdulazim, Peter Augat, and Volker Buehren. Quantification of reaming debris at the fracture gap of diaphyseal a2 and a3 fractures after reamed intramedullary nailing of the sheep tibia. *European Journal of Trauma and Emergency Surgery*, 34(6):587–591, 2008.

[24] Hanna Isaksson. Recent advances in mechanobiological modeling of bone regeneration. *Mechanics Research Communications*, 42:22–31, 2012.

[25] Paola Italiani and Diana Boraschi. From monocytes to m1/m2 macrophages: phenotypical vs. functional differentiation. *Frontiers in immunology*, 5, 2014.

[26] Michael E Joyce, Anita B Roberts, Michael B Sporn, and Mark E Bolander. Transforming growth factor-beta and the initiation of chondrogenesis and os-

teogenesis in the rat femur. *The Journal of cell biology*, 110(6):2195–2207, 1990.

[27] H V Kojouharov, I Trejo, and B M Chen-Charpentier. Modeling the effects of inflammation in bone fracture healing. *AIP Conference Proceedings*, 1895(1):020005, 2017.

[28] Svetlana V Komarova, Robert J Smith, S Jeffrey Dixon, Stephen M Sims, and Lindi M Wahl. Mathematical model predicts a critical role for osteoclast autocrine regulation in the control of bone remodeling. *Bone*, 33(2):206–215, 2003.

[29] Tracy K Kovach, Abhijit S Dighe, Peter I Lobo, and Quanjun Cui. Interactions between mscs and immune cells: implications for bone healing. *Journal of immunology research*, 2015, 2015.

[30] DC Lacey, PJ Simmons, SE Graves, and JA Hamilton. Proinflammatory cytokines inhibit osteogenic differentiation from stem cells: implications for bone repair during inflammation. *Osteoarthritis and Cartilage*, 17(6):735–742, 2009.

[31] Florence Loi, Luis A Córdova, Jukka Pajarinen, Tzu-hua Lin, Zhenyu Yao, and Stuart B Goodman. Inflammation, fracture and bone repair. *Bone*, 86:119–130, 2016.

[32] Yanfei Lu and Tomasz Lekszycki. Modeling of an initial stage of bone fracture healing. *Continuum Mechanics and Thermodynamics*, 27(4-5):851, 2015.

[33] Alberto Mantovani, Silvano Sozzani, Massimo Locati, Paola Allavena, and Antonio Sica. Macrophage polarization: tumor-associated macrophages as a paradigm for polarized m2 mononuclear phagocytes. *Trends in immunology*, 23(11):549–555, 2002.

[34] Athanasius FM Marée, Mitsuhiro Komba, Cheryl Dyck, Marek Labkecki, Diane T Finegood, and Leah Edelstein-Keshet. Quantifying macrophage defects in type 1 diabetes. *Journal of theoretical biology*, 233(4):533–551, 2005.

[35] Richard Marsell and Thomas A Einhorn. The biology of fracture healing. *Injury*, 42(6):551–555, 2011.

[36] Brian McKibbin. The biology of fracture healing in long bones. In *J Bone Joint Surg [Br.* Citeseer, 1978.

[37] Pedro Moreo, José Manuel García-Aznar, and Manuel Doblaré. Bone ingrowth on the surface of endosseous implants. part 2: Theoretical and numerical analysis. *Journal of theoretical biology*, 260(1):13–26, 2009.

[38] Paschalia M Mountziaris and Antonios G Mikos. Modulation of the inflammatory response for enhanced bone tissue regeneration. *Tissue Engineering Part B: Reviews*, 14(2):179–186, 2008.

[39] Sridevi Nagaraja, Anders Wallqvist, Jaques Reifman, and Alexander Y Mitrophanov. Computational approach to characterize causative factors and molecular indicators of chronic wound inflammation. *The Journal of Immunology*, 192(4):1824–1834, 2014.

[40] SIMON L Newman, JANET E Henson, and PETER M Henson. Phagocytosis of senescent neutrophils by human monocyte-derived macrophages and rabbit inflammatory macrophages. *Journal of Experimental Medicine*, 156(2):430–442, 1982.

[41] Bilal Osta, Giulia Benedetti, and Pierre Miossec. Classical and paradoxical effects of tnf-α on bone homeostasis. *Frontiers in immunology*, 5:48, 2014.

[42] Sarah P Otto and Troy Day. *A biologist's guide to mathematical modeling in ecology and evolution*. Princeton University Press, 2011.

[43] Jukka Pajarinen, Tzuhua Lin, Emmanuel Gibon, Yusuke Kohno, Masahiro Maruyama, Karthik Nathan, Laura Lu, Zhenyu Yao, and Stuart B Goodman. Mesenchymal stem cell-macrophage crosstalk and bone healing. *Biomaterials*, 2018.

[44] Timothy T Roberts and Andrew J Rosenbaum. Bone grafts, bone substitutes and orthobiologics: the bridge between basic science and clinical advancements in fracture healing. *Organogenesis*, 8(4):114–124, 2012.

[45] H Schell, GN Duda, A Peters, S Tsitsilonis, KA Johnson, and K Schmidt-Bleek. The haematoma and its role in bone healing. *Journal of experimental orthopaedics*, 4(1):5, 2017.

[46] Aaron Schindeler, Michelle M McDonald, Paul Bokko, and David G Little. Bone remodeling during fracture repair: The cellular picture. In *Seminars in cell & developmental biology*, volume 19, pages 459–466. Elsevier, 2008.

[47] Claudia Schlundt, Thaqif El Khassawna, Alessandro Serra, Anke Dienelt, Sebastian Wendler, Hanna Schell, Nico van Rooijen, Andreas Radbruch, Richard Lucius, Susanne Hartmann, et al. Macrophages in bone fracture healing: their essential role in endochondral ossification. *Bone*, 106:78–89, 2018.

[48] Claudia Schlundt, Hanna Schell, Stuart B Goodman, Gordana Vunjak-Novakovic, Georg N Duda, and Katharina Schmidt-Bleek. Immune modulation as a therapeutic strategy in bone regeneration. *Journal of experimental orthopaedics*, 2(1):1, 2015.

[49] Katharina Schmidt-Bleek, Brian J Kwee, David J Mooney, and Georg N Duda. Boon and bane of inflammation in bone tissue regeneration and its link with angiogenesis. *Tissue Engineering Part B: Reviews*, 21(4):354–364, 2015.

[50] Charles N Serhan and John Savill. Resolution of inflammation: the beginning programs the end. *Nature immunology*, 6(12):1191–1197, 2005.

[51] Jonathan A Sherratt and JD Murray. Models of epidermal wound healing. *Proc. R. Soc. Lond. B*, 241(1300):29–36, 1990.

[52] Gilbert Strang, Gilbert Strang, Gilbert Strang, and Gilbert Strang. *Introduction to linear algebra*, volume 3. Wellesley-Cambridge Press Wellesley, MA, 1993.

[53] Andrew Stuart and Anthony R Humphries. *Dynamical systems and numerical analysis*, volume 2. Cambridge University Press, 1998.

[54] Filip K Swirski, Ingo Hilgendorf, and Clinton S Robbins. From proliferation to proliferation: monocyte lineage comes full circle. In *Seminars in immunopathology*, volume 36, pages 137–148. Springer, 2014.

[55] Imelda Trejo, Hristo Kojouharov, and Benito Chen-Charpentier. Modeling the macrophage-mediated inflammation involved in the bone fracture healing process. *Mathematical and Computational Applications*, 24(1):12, 2019.

[56] Maria Valenti, Luca Dalle Carbonare, and Monica Mottes. Osteogenic differentiation in healthy and pathological conditions. *International journal of molecular sciences*, 18(1):41, 2017.

[57] Ralph Van Furth, Martina MC Diesselhoff-den Dulk, and Herman Mattie. Quantitative study on the production and kinetics of mononuclear phagocytes during an acute inflammatory reaction. *Journal of experimental medicine*, 138(6):1314–1330, 1973.

[58] Alessio Giai Via, Antonio Frizziero, and Francesco Oliva. Biological properties of mesenchymal stem cells from different sources. *Muscles, Ligaments and Tendons Journal*, 2(3):154, 2012.

[59] Yunji Wang, Tianyi Yang, Yonggang Ma, Ganesh V Halade, Jianqiu Zhang, Merry L Lindsey, and Yu-Fang Jin. Mathematical modeling and stability analysis of macrophage activation in left ventricular remodeling post-myocardial infarction. *BMC genomics*, 13(6):S21, 2012.

[60] Stephen Wiggins. *Introduction to applied nonlinear dynamical systems and chaos*, volume 2. Springer Science & Business Media, 2003.

[61] Andy C Wu, Liza J Raggatt, Kylie A Alexander, and Allison R Pettit. Unraveling macrophage contributions to bone repair. *BoneKEy reports*, 2, 2013.

[62] Mengrui Wu, Guiqian Chen, and Yi-Ping Li. Tgf-β and bmp signaling in osteoblast, skeletal development, and bone formation, homeostasis and disease. *Bone research*, 4:16009, 2016.

[63] Tony Yu. *Design and validation of a mathematical model to describe macrophage dynamics in wound healing*. PhD thesis, Drexel University, 2014.

[64] Ran Zhang, Yi Liang, and Shuxiang Wei. M2 macrophages are closely associated with accelerated clavicle fracture healing in patients with traumatic brain injury: a retrospective cohort study. *Journal of orthopaedic surgery and research*, 13(1):213, 2018.

BIOGRAPHICAL STATEMENT

Imelda Trejo was born in Tasquillo, Hidalgo, Mexico in 1984. She earned her B.S. and M.S. degrees in Applied Mathematics at the Universidad Autónoma del Estado de Hidalgo and at the Centro de Investigación en Matemáticas, Guanajuato, Mexico, in 2008 and 2011, respectively. Her research interests focus on computational and mathematical modeling of biological systems that include cellular and molecular dynamics, tissue regeneration, immune system dynamics, uncertainty quantification, and parametric estimation.